UNIVERSITAT POLITÈCNICA
DE CATALUNYA
BARCELONATECH

Estimation and Control in Energy Harvesting Wireless Communication Networks

Ph.D. Dissertation

Author

Miguel Calvo-Fullana

Advisors

Dr. Javier Matamoros

Dr. Carles Antón-Haro

Barcelona, July 2017

This work was partially supported by the Catalan government under grant SGR2014-1567; the Spanish government under grant TEC2013-44591-P (INTENSYV), and grant PCIN-2013-027 (E-CROPS) in the framework of the ERA-NET CHIST-ERA program.

Abstract

Long thought to be an unattainable ambition, self-sustainable and green-powered wireless networks are rapidly becoming a reality. This is driven by recent hardware improvements in what is known as Energy Harvesting (EH). This technology makes it possible for devices to scavenge energy from the environment, be it from solar, thermal, kinetic or other sources. One area where this idea has shown considerable promise is in Wireless Sensor Networks (WSNs). These networks consist of inexpensive, small and low-power sensors, making them a prime candidate for the deployment of energy harvesting technologies. However, when devices are equipped with these new technologies, the intermittent and random nature of the energy supply makes it necessary to take a new approach to the design of communication policies.

It is the main objective of this dissertation to study, evaluate and solve problems that arise in wireless sensor networks with energy harvesting capabilities. The nature of the problems studied can be grouped into two categories. On one hand, we address problems of estimation, which arise when EH sensors collect measurements of some physical phenomenon. On the other hand, we study problems of control, which emerge when EH sensors are part of a dynamical system.

First, we address the estimation problem in EH-powered wireless sensor networks. We approach the problem in a coded manner, where sensors transit their measurements to a Fusion Center (FC) digitally. We consider a point-to-point sensor-to-FC communication scenario, where the measured sources are time-correlated. We derive the transmission policies minimizing the average reconstruction distortion for both delay-constrained and delay-tolerant scenarios. Next, we study the case in which multiple sensors collaborate in the estimation of a source. In this problem, only a limited number of sensors can transmit simultaneously, due to the reduced number of sensor-to-FC channels. The goal is to jointly design the power allocation and sensor selection policies that minimize the average reconstruction distortion. However, this problem is not convex. To overcome this, we propose two policies, an iterative joint policy that finds a stationary solution of the original problem; and a heuristic separate policy in which the optimal power allocation

is given by a convex optimization problem. Both policies are related to each other in the fact that the latter can be used as an initialization point of the former iterative policy. Further, as an alternative approach to the problem, we have also proposed the use of sparsity-promoting techniques.

Then, we turn our attention to problems of a control nature in energy harvesting communication networks. First, we study the problem of jointly routing and scheduling traffic in a communication network with EH-powered nodes. The routing-scheduling policies proposed act as a generalization the stochastic backpressure policies to energy harvesting communication networks. Specifically, we provide two policies, an easy to compute policy and a randomized policy with improved stability guarantees. Furthermore, we ensure that given sustainable data and energy arrivals, the proposed policies stabilize the data queues over all the network. Finally, we study a more general control problem in which energy harvesting sensors share a wireless medium over which they transmit measurements to their respective controllers. Since the medium is shared, simultaneous transmissions might lead to packet collisions. To overcome this issue, we propose the use of a random access scheduling policy. Furthermore, we show that given sustainable energy and stability requirements, the policies stabilize all the control systems while satisfying the energy harvesting constraints.

Resumen

Consideradas durante mucho tiempo una ambición inalcanzable, las redes inalámbricas auto-sostenibles y de energía renovable se están convirtiendo rápidamente en una realidad. Esto viene impulsado por las recientes mejoras de hardware en lo que se conoce como recolección de energía (*energy harvesting*). Esta tecnología permite a los dispositivos recoger la energía del medio ambiente, ya sea de fuentes solares, térmicas, cinéticas u otras. Un área en la que esta idea se ha mostrado considerablemente prometedora son las redes de sensores inalámbricos. Estas redes consisten en sensores baratos, pequeños y de baja potencia, lo que los convierte en un excelente candidato para el despliegue de tecnologías de recolección de energía. Sin embargo, cuando los dispositivos están equipados con estas nuevas tecnologías, la naturaleza intermitente y aleatoria del suministro de energía hace necesario adoptar un nuevo enfoque para el diseño de las políticas de comunicación.

Es el objetivo principal de esta tesis doctoral estudiar, evaluar y resolver problemas que surgen en redes de sensores inalámbricos con capacidades de recolección de energía. La naturaleza de los problemas estudiados puede agruparse en dos categorías. Por un lado, abordamos problemas de estimación, que surgen cuando los sensores con capacidades de recolección de energía recogen mediciones de algún fenómeno físico. Por otro lado, estudiamos los problemas de control, que surgen cuando los sensores con capacidades de recolección de energía forman parte de un sistema dinámico.

En primer lugar, abordamos el problema de estimación en redes de sensores inalámbricos alimentados con recolección de energía. Enfocamos el problema de una manera codificada, donde los sensores transmiten sus mediciones digitalmente a un centro de fusión. Consideramos un escenario de comunicación punto a punto de sensor a centro de fusión, donde las fuentes medidas están correlacionadas temporalmente. Derivamos las políticas de transmisión que minimizan la distorsión media de reconstrucción tanto para los escenarios con limitación de retardo como con tolerancia al retardo. A continuación, estudiamos el caso en el que múltiples sensores colaboran en la estimación de una fuente. En este problema, sólo un número limitado de sensores puede transmitir simultáneamen-

te, debido al número reducido de canales de sensor a centro de fusión. El objetivo es diseñar de manera conjunta las políticas de asignación de potencia y selección de sensores que minimicen la distorsión media de reconstrucción. Sin embargo, este problema no es convexo. Para superar esto, proponemos dos políticas, una política conjunta iterativa que encuentra una solución estacionaria del problema original; y una política separada heurística en la que la asignación de potencia óptima viene dada por un problema de optimización convexa. Ambas políticas están relacionadas entre sí en el hecho de que ésta última puede ser utilizada como un punto de inicialización de la política iterativa anterior. Además, como un enfoque alternativo al problema, también hemos propuesto el uso de técnicas de promoción de la dispersión.

Más tarde, centramos nuestra atención en los problemas de control en las redes de comunicaciones con recolección de energía. En primer lugar, estudiamos el problema de enrutamiento y planificación conjunta del tráfico en una red de comunicaciones con nodos alimentados por recolección de energía. Las políticas de enrutamiento y planificación que proponemos actúan como una generalización de las políticas de *backpressure* estocásticas para las redes de comunicaciones con recolección de energía. Específicamente, ofrecemos dos políticas, una política fácil de calcular y una política aleatoria con mejores garantías de estabilidad. Además, aseguramos que dadas llegadas de datos y energía factibles, las políticas propuestas estabilizan las colas de datos en toda la red. Finalmente, estudiamos un problema de control más general en el que los sensores con recolección de energía comparten un medio inalámbrico sobre el cual transmiten mediciones a sus respectivos controladores. Dado que el medio es compartido, las transmisiones simultáneas pueden llevar a colisiones de paquetes. Para superar este problema, proponemos el uso de una política de planificación de acceso aleatorio. Además, demostramos que, dadas necesidades de energía y estabilidad factibles, las políticas estabilizan todos los sistemas de control y satisfacen las restricciones impuestas por la recolección de energía.

Resum

Considerades durant molt de temps una ambició inassolible, les xarxes sense fils autosostenibles i d'energia renovable s'estan converting ràpidament en una realitat. Aquest fet ve impulsat per les recents millores de hardware en el que es coneix com recol·lecció d'energia (*energy harvesting*). Aquesta tecnologia permet als dispositius recollir l'energia del medi ambient, ja sigui de fonts solars, tèrmiques, cinètiques o altres. Una àrea en la que aquesta idea s'ha mostrat considerablement prometedora són les xarxes de sensors sense fils. Aquestes xarxes consisteixen en sensors barats, petits i de baixa potència, el que els converteix en un excel·lent candidat per al desplegament de tecnologies de recol·lecció d'energia. No obstant, quan els dispositius estan equipats amb aquestes noves tecnologies, la naturalesa intermitent i aleatòria del subministrament d'energia fa necessari adoptar un nou enfocament per al disseny de les polítiques de comunicació.

És l'objectiu principal d'aquesta tesi doctoral estudiar, avaluar i resoldre problemes que sorgeixen en xarxes de sensors sense fils amb capacitats de recol·lecció d'energia. La naturalesa dels problemes estudiats pot agrupar-se en dues categories. D'una banda, abordem problemes d'estimació, que sorgeixen quan els sensors amb capacitats de recol·lecció d'energia recullen mesuraments d'algun fenomen físic. D'altra banda, estudiem els problemes de control, que sorgeixen quan els sensors amb capacitats de recol·lecció d'energia formen part d'un sistema dinàmic.

En primer lloc, abordem el problema d'estimació en xarxes de sensors sense fils alimentats amb recol·lecció d'energia. Enfoquem el problema d'una manera codificada, on els sensors transmeten els seus mesuraments digitalment a un centre de fusió. Considerem un escenari de comunicació punt a punt de sensor a centre de fusió, on les fonts mesurades estan correlacionades temporalment. Derivem les polítiques de transmissió que minimitzen la distorsió mitjana de reconstrucció tant per als escenaris amb limitació de retard com amb tolerància al retard. A continuació, estudiem el cas en què múltiples sensors col·laboren en l'estimació d'una font. En aquest problema, només un nombre limitat de sensors pot transmetre simultàniament, a causa del nombre reduït de canals de sensor a centre de fusió. L'objectiu és dissenyar de manera conjunta les polítiques

d'assignació de potència i selecció de sensors que minimitzin la distorsió mitjana de reconstrucció. No obstant, aquest problema no és convex. Per superar això, proposem dues polítiques, una política conjunta iterativa que troba una solució estacionària del problema original; i una política separada heurística en què l'assignació de potència òptima ve donada per un problema d'optimització convexa. Les dues polítiques estan relacionades entre si en el fet que aquesta última pot ser utilitzada com un punt d'inicialització de la política iterativa anterior. A més, com un enfocament alternatiu al problema, també hem proposat l'ús de tècniques de promoció de la dispersió.

Més tard, centrem la nostra atenció en els problemes de control en les xarxes de comunicacions amb recol·lecció d'energia. En primer lloc, estudiem el problema d'encaminament i planificació conjunta del trànsit en una xarxa de comunicacions amb nodes alimentats per recol·lecció d'energia. Les polítiques d'encaminament i planificació que proposem actuen com una generalització de les polítiques de *backpressure* estocàstiques per a les xarxes de comunicacions amb recol·lecció d'energia. Específicament, oferim dues polítiques, una política fàcil de calcular i una política aleatòria amb millors garanties d'estabilitat. A més, assegurem que donades arribades de dades i energia factibles, les polítiques propostes estabilitzen les cues de dades en tota la xarxa. Finalment, estudiem un problema de control més general en el qual els sensors amb recol·lecció d'energia comparteixen un mitjà sense fils sobre el qual transmeten mesuraments als seus respectius controladors. Atès que el mitjà és compartit, les transmissions simultànies poden dur a col·lisions de paquets. Per superar aquest problema, proposem l'ús d'una política de planificació d'accés aleatori. A més, demostrem que, donades necessitats d'energia i estabilitat factibles, les polítiques estabilitzen tots els sistemes de control i satisfan les restriccions imposades per la recol·lecció d'energia.

Acknowledgements

It is quite difficult to come to terms with the realization that three years have already gone by since I started to work in this Ph.D. thesis. The end of it, which I once thought to be in the distant future, is now very close. As I finish this document, I would like to devote the last written lines to remember the people who have made this journey possible and, above all, truly enjoyable.

First of all, I must express my most sincere gratitude to my advisors Javier Matamoros and Carles Antón-Haro. Their guidance, comments, suggestions and constructive criticism have been essential to the successful development of this thesis, as well as my improvements as a researcher. At the same time, I am also grateful to Alejandro Ribeiro. During my four-month stay in Philadelphia, he welcomed me to his research group at the University of Pennsylvania with the same dedication that he shows to his own students. For this, and many other things, I am sincerely thankful.

Further, I would like to extend my gratitude to Prof. Antonio Pascual Iserte, Prof. Antonio G. Marques and Prof. Geert Leus for agreeing to serve in this thesis' committee. My gratitude also extends to Prof. Davide Dardari for reviewing this thesis, and together with Dr. Miquel Payaró, for fulfilling the role of substitute members of the committee.

During these last years I have been fortunate enough to spend many hours interacting with the people from CTTC, UPC and Penn. To avoid the risk of turning this section into an endless list of names, I will simply thank all of them. All our interactions, in and outside our respective institutions, have delighted me greatly, both at a professional and a personal level. Also, I cannot forget that some of these interactions have resulted in friendships that I greatly cherish. In the same vein, I could not forget the rest of my friends. All of our shared moments have made the ups and downs of being a Ph.D. student a much more enjoyable experience.

Last but not least, I must also express how deeply indebted I am to my family. Ever since I was young, they have provided me with all their love and support. A large part of this thesis belongs to them.

Miguel Calvo Fullana, Barcelona, May 2017

List of Acronyms

BP	Backpressure
DMC	Discrete Memoryless Channel
DP	Dynamic Programming
EH	Energy Harvesting
ESO	Ergodic Stochastic Optimization
FC	Fusion Center
GSM	Global System for Mobile Communications
i.i.d.	Independent and Identically Distributed
IoT	Internet of Things
JSS-EH	Joint Sensor Selection and Power Allocation with Energy Harvesting
KKT	Karush-Kuhn-Tucker
LHS	Left Hand Side
LQG	Linear-Quadratic-Gaussian
MAC	Multiple Access Channel
MDP	Markov Decision Process
MM	Majorization-Minimization
MMSE	Minimum Mean Squared Error
MSE	Mean Squared Error
pdf	Probability Density Function
RF	Radio Frequency
RFID	Radio Frequency IDentification
RHS	Right Hand Side
SBP	Stochastic Backpressure

SBP-EH	Stochastic Backpressure with Energy Harvesting
SNR	Signal to Noise Ratio
SS-EH	Separate Sensor Selection and Power Allocation with Energy Harvesting
SSBP	Stochastic Soft Backpressure
SSBP-EH	Stochastic Soft Backpressure with Energy Harvesting
SSS-EH	Sparse Sensor Selection and Power Allocation with Energy Harvesting
SWIPT	Simultaneous Wireless Information and Power Transfer
WLAN	Wireless Local Area Network
WPT	Wireless Power Transfer
w.r.t.	With Respect To
WSN	Wireless Sensor Network

Notation

x	A scalar.
$\mathbf{x}$	A column vector.
$\mathbf{X}$	A matrix.
$\mathcal{X}$	A set.
$\mathbb{R}$	The set of real numbers.
$\mathbb{R}^n$	The set of real n vectors.
$\mathbb{R}^{m \times n}$	The set of real $m \times n$ matrices.
$\mathbf{relint}\, \mathcal{X}$	Relative interior of set $\mathcal{X}$.
$\mathbf{dom}\, f$	Domain of function f.
$\lvert\mathcal{X}\rvert$	Cardinality of set $\mathcal{X}$.
$\lVert \cdot \rVert$	Norm.
$(\cdot)^T$	Transpose operator.
$\operatorname{tr} \mathbf{X}$	Trace of matrix $\mathbf{X}$.
$\operatorname{diag}(\mathbf{x})$	Matrix with the entries of vector $\mathbf{x}$ in its diagonal.
$\mathbf{X}^{-1}$	Inverse of matrix $\mathbf{X}$.
$\mathbf{I}$	Identity matrix.
max	Maximum.
min	Minimum.
sup	Supremum.
inf	Infimum.
log	Logarithm.
lim	Limit.
arg	Argument.

$\triangleq$	Defined as.
$\approx$	Approximately equal.
$\nabla_{\mathbf{x}} f(\mathbf{x})$	Gradient of function f with respect to $\mathbf{x}$.
$\frac{\partial f(\mathbf{x})}{\partial x_i}$	Partial derivative of function f with respect to x_i.
$[\cdot]^+$	Projection to the interval $[0, \infty]$, i.e., $[\cdot]^+ = \max\{0, \cdot\}$.
$[\cdot]_a^b$	Projection to the interval $[a, b]$, i.e., $[\cdot]_a^b = \min\{\max\{a, \cdot\}, b\}$.
$\mathbb{I}(\cdot)$	Indicator function.
$\Pr(\cdot)$	Probability.
$\mathbb{E}[\cdot]$	Expected value.
$H(\cdot)$	Entropy.
$I(\cdot;\cdot)$	Mutual information.
$\sim$	Distributed according to.
$\mathcal{N}(\boldsymbol{\mu}, \boldsymbol{\Sigma})$	Real Gaussian distributed vector with mean $\boldsymbol{\mu}$ and covariance matrix $\boldsymbol{\Sigma}$.

Contents

List of Figures

Chapter 1

Introduction

1.1 Motivation

Usually, wireless communication devices are equipped with batteries acting as their only energy supply. Even though these batteries might be rechargeable, the wireless nature of such communication devices means that they tend to lack access to a wired energy source from which to easily recharge them. However, in recent years, attention has turned to advances in technologies that make it possible to gather energy from the environment. This technology, *energy harvesting*, has emerged as capable of overcoming (or, at least, alleviating) some of the limitations imposed by traditional battery operation. Devices powered by energy harvesting are capable of acquiring energy from a varied array of natural sources, with the most common being solar, thermal, or vibrational sources. Not only that, even man-made sources, such as Radio Frequency (RF) signals can be exploited by energy harvesting technologies to obtain energy.

An area where this technology has shown much promise is in wireless sensor networks. These networks are composed of sensor nodes which are usually powered by batteries. However, due to their nature, WSNs are sometimes deployed in remote and difficult to access locations. This makes it very difficult for the devices to have access to the power grid in order to have their batteries recharged. Besides, the process of replacing the batteries can be very expensive and difficult. Additionally, with the current micro-manufacturing technology allowing for small, ultra-low power wireless sensors, wireless sensor networks pose an excellent deployment scenario for energy harvesting technologies. Given the wide availability of energy sources coupled with the small energy needs of sensors, it is expected that EH-powered nodes could extend their lifetime considerably. This is to say, they could even operate perpetually, until hardware failure. Also, recently emerging concepts such as the Internet of Things (IoT) envision massive deployment of wireless sensors. It is expected that energy harvesting technologies will play a major role in enabling this vision.

The hardware and circuit design aspects of energy harvesting technologies have long been studied. However, when dealing with the design of communication policies, previous efforts have been in the design of energy efficient policies, focused on reducing the power consumption of the wireless nodes. While this is a sensible approach for battery powered systems, the random nature of the energy harvesting process introduces fundamental changes in the communication system, leaving previous policies inefficient. Hence, the emergence of wireless networks equipped with energy harvesting technologies represents a paradigm shift in the way that communication problems are treated.

The need to design EH-aware communication policies poses several research questions. Specifically, we aim to investigate some of the issues that arise when dealing with problems of estimation and control in communication networks powered by energy harvesting. Consider a system of EH-powered sensors acquiring some type of measurements which they must transmit to a fusion center for further processing. What is the optimal power allocation for transmission if our goal is to minimize the reconstruction distortion? If the measurements are obtained from a time-correlated source, how does correlation affect the transmission policies? Can we allow some delay in the reconstruction to better exploit the intermittency of the energy supply? Now, if the estimation is done with multiple sensors which share a wireless medium of limited bandwidth, how do we select which sensors are allowed to transmit at each time? Additionally, all this information needs to be delivered to its destination. This might require the routing and scheduling of data traffic. How can we design policies that ensure that the data queues are stable when the energy supply itself is subject to randomness? And, what if the sensors are measuring any kind of dynamical system. Can we give some guarantees on the stability of the system when control policies rely on the measurements collected and transmitted by an energy harvesting device? These are some of the questions that this dissertation aims to answer.

1.2 Outline of the Thesis

As discussed earlier, in this dissertation we study wireless sensor networks powered by energy harvesting. Specifically, our focus lies on issues related to estimation and control in the energy harvesting scenario. Broadly speaking, the contribution of this thesis can be split in two parts. The first part (Chapters 4 and 5) is devoted to estimation problems, while the second part (Chapters 6 and 7) studies control problems. In more detail, this document is organized as follows.

In Chapter 2, we provide the reader with some background knowledge on the state of the art of energy harvesting technologies. Specifically, we review the sources from which energy can be harvested and how they are modeled. Also, we survey the communication aspects of wireless devices powered by energy harvesting. Notably, we review the

information-theoretical foundations as well as the current advances in both offline and online transmission policies.

In Chapter 3, we review a number of important mathematical concepts over which much of the work of this thesis is built. Specifically, we review convex optimization, non-convex optimization and ergodic stochastic optimization.

We begin the contributions of this dissertation in Chapter 4. We start by considering the estimation of a phenomenon which is correlated over time. More formally, we consider a *point-to-point* communication scenario between a sensor node and a fusion center. The sensor node is powered by energy harvesting and obtains measurements from a series of time-correlated sources. In this scenario, we aim to find coded transmission policies which minimize the average reconstruction distortion at the fusion center. Due to correlation, the transmission policies leverage on the previously encoded sources as side information. We derive these policies for both a delay-constrained case (in which sources must be reconstructed at the next time slot) and a delay-tolerant scenario (where a certain time lag is allowed in the reconstruction of sources). We take an offline approach to the problem and pose it in a convex optimization framework. The optimal policies can be computed by the proposed iterative algorithm, which consists of a coupling between a two-directional waterfilling (for power allocation) and a reverse waterfilling (for rate allocation). Furthermore, we also provide an online myopic form of these policies, for which its offline counterpart serves as a benchmark.

Chapter 5 extends some of the ideas of the previous chapter to the case of *multiple* sensor nodes. Specifically, we consider a scenario in which multiple EH-powered sensors acquire different measurements of the same source and want to transmit them to a fusion center. Due to the limited number of available sensor-to-FC channels, a decision on which sensors should transmit must be made at each time slot. Additionally, the sensors must design their power allocation policy. Our goal is to jointly derive the sensor selection and power allocation policies which minimize the average reconstruction distortion of the source at the fusion center. Unfortunately, we show that this problem is not convex. Instead, we propose two suboptimal offline policies. First, we provide a *joint* sensor selection and power allocation scheme, based on an iterative majorization-minimization procedure which allows us to find a locally optimal solution of the original non-convex problem. Then, we also propose a *separate* sensor selection and power allocation policy. In this separate policy, we propose a heuristic sensor selection policy which takes into account the energy harvesting process. Then, given this selection, the optimal power allocation can be computed as the solution to a convex optimization problem. Furthermore, the separate sensor selection and power allocation policy can be used as an initialization point of the iterative algorithm of the joint policy, which then in turn, improves on the separate policy. Also, as in the previous chapter, we provide the online myopic form of these policies. Further, we also study an alternative approach to the problem, based in

promoting sparsity in the power allocation.

In Chapter 6 we turn our attention to some control aspects of energy harvesting networks. Specifically, in this chapter we investigate the problem of routing and scheduling traffic in an energy harvesting communication network. Each node in the network independently generates data packets to be delivered to some other node in the network and nodes must collaborate to ensure that data packets are delivered to their destination. To solve this problem, we propose routing-scheduling policies which act as a generalization of the well-known backpressure family of algorithms for EH-powered networks. To do this, we leverage on stochastic subgradient methods on the dual domain. Specifically, we propose two distinct policies: (i) a straightforward policy where the routing-scheduling decision is taken by the comparison of a node's and its neighbors' Lagrange multipliers; and (ii) a policy given by a randomized decision. Instead of a direct comparison between a node's and its neighbors' Lagrange multipliers, this second policy equalizes the differences between multipliers by means of an inverse waterfilling. This results in a routing-scheduling probability mass function over which the node samples to take its decision. This second policy results in a faster convergence speed. Furthermore, we show that given sustainable packet and energy arrival processes, both policies stabilize the data queues over all the network. And, hence, such stabilization can be regarded as a control problem.

In Chapter 7 we investigate networked control systems in a more general manner. Specifically, we study a scenario in which multiple EH-powered sensor nodes must transmit measurements to their respective controllers in order to stabilize their dynamical system. This transmission occurs over a shared wireless medium. Due to this, collisions might occur if sensors transmit simultaneously. Under these conditions, our goal is to design transmission policies capable of stabilizing all the control loops subject to the constraints imposed by the energy harvesting process. Since each control loop might have a different control performance requirement, we propose the use of a control performance abstraction which translates the average control requirements into probabilities of successful transmission in a random access communication scheme. Then, leveraging on dual subgradient methods, we propose a policy satisfying these probabilities of successful transmission.

Finally, in Chapter 8 we conclude this thesis by providing a summary and final remarks on the main results of this work. Also, we outline and discuss some possible lines of future work.

1.3 Contribution

The research presented in this dissertation has also been disseminated through the following publications [1–11].

Chapter 4

- M. Calvo-Fullana, J. Matamoros, and C. Antón-Haro, "Reconstruction of Correlated Sources with Energy Harvesting Constraints in Delay-constrained and Delay-tolerant Communication Scenarios," *IEEE Transactions on Wireless Communications*, vol. 16, no. 3, pp. 1975-1986, March 2017.

- M. Calvo-Fullana, J. Matamoros, and C. Antón-Haro, "Reconstruction of Correlated Sources with Energy Harvesting Constraints," in Proceedings of *European Wireless (EW)*, Budapest, Hungary, May 2015.

Chapter 5

- M. Calvo-Fullana, J. Matamoros, and C. Antón-Haro, "Sensor Selection and Power Allocation Strategies for Energy Harvesting Wireless Sensor Networks," *IEEE Journal on Selected Areas in Communications*, vol. 34, no. 12, pp. 3685-3695, December 2016.

- M. Calvo-Fullana, J. Matamoros, and C. Antón-Haro, "Decentralized Sparsity-Promoting Sensor Selection in Energy Harvesting Wireless Sensor Networks," in Proceedings of *European Signal Processing Conference (EUSIPCO)*, Budapest, Hungary, August 2016.

- M. Calvo-Fullana, J. Matamoros, C. Antón-Haro, and Sophie M. Fosson, "Sparsity-promoting Sensor Selection with Energy Harvesting Constraints," in Proceedings of *International Conference on Acoustics, Speech and Signal Processing (ICASSP)*, Shanghai, China, March 2016.

- M. Calvo-Fullana, J. Matamoros, and C. Antón-Haro, "Sensor Selection in Energy Harvesting Wireless Sensor Networks," in Proceedings of *IEEE Global Conference on Signal and Information Processing (GlobalSIP)*, Orlando, USA, December 2015. **Best Paper Award**.

Chapter 6

- M. Calvo-Fullana, C. Antón-Haro, J. Matamoros, and A. Ribeiro, "Stochastic Routing and Scheduling Policies for Energy Harvesting Communication Networks," to be submitted, 2017.

- M. Calvo-Fullana, J. Matamoros, C. Antón-Haro, and A. Ribeiro, "Stochastic Backpressure in Energy Harvesting Networks," in Proceedings of *International Conference on Acoustics, Speech and Signal Processing (ICASSP)*, New Orleans, USA, March 2017.

Chapter 7

- M. Calvo-Fullana, C. Antón-Haro, J. Matamoros, and A. Ribeiro, "Random Access Communication for Wireless Control Systems with Energy Harvesting Sensors," in preparation, 2017.
- M. Calvo-Fullana, C. Antón-Haro, J. Matamoros, and A. Ribeiro, "Random Access Policies for Wireless Networked Control Systems with Energy Harvesting Sensors," in Proceedings of *American Control Conference (ACC)*, Seattle, USA, May 2017.

Other contributions not included in this dissertation

- J. Matamoros, M. Calvo-Fullana, and C. Antón-Haro, "On the impact of correlated sampling processes in WSNs with Energy-neutral operation," in Proceedings of *IEEE International Conference on Communications (ICC)*, London, UK, June 2015. **Best Paper Award**.

Chapter 2

State of the Art in Energy Harvesting Technologies

In this section, we provide an overview of the current state of the art in energy harvesting technologies. Specially, we focus on wireless communication systems powered by energy harvesting. As discussed earlier in the introduction, batteries alone are not capable of coping with the demands of current devices. Consequently, the attention has turned to energy harvesting as a way to extend the lifetime of wireless devices.

2.1 Sources and Models for Energy Harvesting

The first step to EH-powered systems is to have an energy source providing an adequate supply of energy. Scavenging energy from sources like water and wind goes back in time to structures like water wheels and windmills. Nowadays, solar farms, wind farms and hydroelectric plants form the main bulk of renewable energy generation. These tend to be very large installations meant to supply energy to the power grid in a sustainable manner. However, as advances in microelectronics allowed for the manufacturing of small and power efficient devices, interest arose to also use energy harvesting to power those devices. In this case, due to their low-power nature, the range of energy harvesting sources available is considerably larger. In Table 2.1 we provide an overview of a variety of energy sources and their associated power densities. Also, we discuss some of these sources in the following.

- **Light.** By using photovoltaic cells, photons can be converted into electricity. The efficiency of this process depends on the materials used for the construction of the photovoltaic cells, with usual efficiency values around $5 - 30\%$. When deployed outside with direct solar illumination, photovoltaic cells have a power density of around 100 $\mathrm{mW/cm^2}$. This makes the sun an excellent source for energy harvesting.

Energy source	**Power density**
Acoustic Noise [12]	0.003 $\mu W/cm^3$ at 75 dB 0.96 $\mu W/cm^3$ at 100 dB
Temperature Variation [13]	10 $\mu W/cm^3$
Ambient Radio Frequency [14]	< 1 $\mu W/cm^2$
Ambient Light [15]	100 mW/cm^2 (Direct sun) 100 $\mu W/cm^2$ (Illuminated office)
Thermoelectric [16]	60 $\mu W/cm^2$
Vibrational Microgenerators [17]	4 $\mu W/cm^3$ (Human motion, Hz) 800 $\mu W/cm^3$ (Machines, kHz)
Vibrations (Piezoelectric) [18]	200 $\mu W/cm^3$
Ambient Airflow [19]	1 $\mu W/cm^2$
Push buttons [20]	50 $\mu J/N$
Hand generators [21]	30 W/kg
Heel strike [22]	7 W/cm^2

Table 2.1: Power density of several energy harvesting sources [23].

When deployed indoors, the available illumination levels tend to be smaller, with resulting power densities around 100 $\mu W/cm^2$. Altogether, photovoltaic cells are a well developed and mature technology.

- **Radio frequency.** With the extensive amount of radio signals in today's world, the harvesting of RF waveforms to obtain energy is a possibility. The most common sources being Global System for Mobile Communications (GSM) and Wireless Local Area Network (WLAN) signals. However, power densities tend to be very small, less than 1 $\mu W/cm^2$, making it difficult to harvest enough energy for practical applications. A more promising idea is the concept of Wireless Power Transfer (WPT) [24], where a dedicated RF source transmits for the sole purpose of being harvested as energy. Recently, there has also been considerable interest in the idea of transmitting both information and power, a concept known as Simultaneous Wireless Information and Power Transfer (SWIPT) [25]. A practical example of WPT are Radio Frequency IDentification (RFID) tags, which wirelessly receive their required amount of energy, which can be as low as 1 μW. On a more general note, at a transmission power of 100 mW and 20 cm of separation, harvested values of 1.5 mW have been reported [26]. And, in [27], for the same 100 mW of transmission power, 200 μW were harvested at a distance of 2 m.

- **Thermoelectric.** By heat transfer, objects or environments that present a difference in temperature offer the opportunity to generate power. A classical example of this is any of the widely used heat engines throughout history. More interesting

however, is the Seebeck effect, which states that when two junctions made of two dissimilar conductors are kept at different temperatures, an open circuit voltage develops between them [15]. Thermoelectric devices exploiting the Seebeck effect can be used to harvest energy in human body applications. At an ambient temperature of 22 °C, a thermal gradient of 15 °C can be converted to energy with an an efficiency around 0.8%. The resulting power density is around 15 $\mu W/cm^2$ [28]. Practical uses of thermoelectric energy harvesting in human body applications can be found, for example, to power a wristwatch by the small thermal gradient provided by the human body heat over ambient temperature. On another note, for industrial applications with a much higher thermal gradient, power densities of 60 $\mu W/cm^2$ have been reported [16].

- **Vibrational and mechanical.** Vibrational and mechanical stimuli are widely available. In order to convert them into energy, the most common transduction mechanism are piezoelectric, or electromagnetic. The former exploits the piezoelectric effect, by which some materials generate an electric charge under mechanical stress. When piezoelectrics are coupled with vibrating structures, they can generate up to around 200 $\mu W/cm^3$ [18]. Besides, electromagnetic transducers tend to be found in vibrational microgenerators. These systems are based on the interaction between moving magnets and coils. They exploit vibrations, with power levels ranging from 4 $\mu W/cm^3$ (typical human motion, a motion of 5 mm at 1 Hz) up to 800 $\mu W/cm^3$ (machine motion, a motion of 2 nm at 2.5 kHz) [17]. Another significant source of mechanical power is human input in various forms. Examples of this are pushing, shaking or pulling to power devices (e.g., typical examples of this use of human sources are self-winding wristwatches or shake-powered flashlights). For example, the available power in a walking person's heel strike is 7 W/cm^2 (70 kg at 1 Hz), with demonstrated systems harvesting around $250 - 700$ mW out of it [22].

In oder to design systems powered by energy harvesting, it is important to have an accurate characterization of the energy harvested from the sources. In this regard, considerable attention has been given in the literature to this issue, with light energy sources being the most researched ones. Models for solar power in outdoor scenarios have been studied in [29], with a focus on wireless sensor networks. Similarly, the authors in [30] improve solar source models with the inclusion of weather forecasts. In [31], the authors propose a model that adapts to seasonal variations in sunlight and diurnal cycles. Furthermore, in [32] the authors developed an indoor light model. With respect to other types of sources, a wind model has been studied in [31], while a mechanical energy model related to human motion (such as, walking, running and cycling), has been considered in [33].

In a more general sense, the energy harvesting process can be modeled as a discrete-time stochastic process. This is convenient, for instance, in order to design EH-aware communication policies. The stochastic process can be characterized either statistically or from samples of real harvested energy measurements. For tractability, some specific stochastic processes have been considered in the literature. For example, the authors in [34] consider an stationary Markov chain and the authors in [35] extend those results to a non-stationary Markov model.

2.2 Wireless Networks Powered by Energy Harvesting

While the hardware and modeling aspects of energy harvesting have been researched for a long time, the study of wireless communication systems powered by energy harvesting is more recent. When powered by energy harvesting, the random nature of the energy supply introduces fundamental changes in how wireless communication problems need to be addressed. In this section, we provide an overview of recent results in energy harvesting wireless communication[1]. First, we discuss how the introduction of energy harvesting alters the communication problem from an information-theoretic perspective. Then, we review the transmission policies found in the literature. For the latter, there are two distinct approaches, *offline* transmission policies and *online* transmission policies. Offline policies are derived under non-causal knowledge of the energy harvesting process by the transmitter. That is, they assume the knowledge of present, past and future energy arrivals and their magnitudes. For tractability reasons, these strategies are widely used to derive upper bounds on the performance of the system. On the contrary, online policies assume only a causal knowledge of the energy harvesting process (even though, statistical knowledge is also acceptable). Hence, they are more realistic and applicable to real systems.

2.2.1 Information-theoretic Approaches

When dealing with EH-powered communication, some information-theoretic questions require some thought. Mainly, the study of the channel capacity under the consideration that energy harvesting constrains the transmission has received considerable attention. In general, energy harvesting can be modeled as a discrete stochastic process. Hence, the use of energy harvesting introduces a new energy queue in the system. The canonical model for energy harvesting communication systems is shown in Figure 2.1.

In the classical Additive White Gaussian Noise (AWGN) channel with unit-variance Gaussian noise, the capacity is given by the well-known expression $C = \frac{1}{2}\log(1+P)$,

[1] We refer the reader to references [36] and [37] for a more detailed overview.

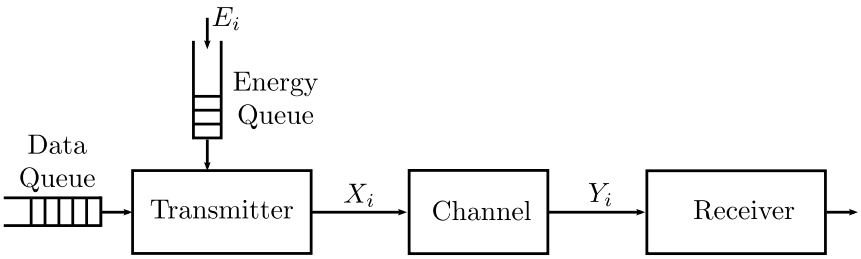

Figure 2.1: Wireless communication model powered by energy harvesting.

where P is the average power constraining the transmitted codewords X_i, that is

$$\frac{1}{2}\sum_{i=1}^{n} X_i^2 \leq P, \tag{2.1}$$

for n very large. In the case of an energy harvesting system, let us consider the energy harvesting process E_i as a stationary and ergodic random process with average arrival rate $\mathbb{E}[E_i] = P$. In order to transmit a codeword, a sufficient amount of energy must have been harvested and stored first. The resulting constraints are called the *energy causality constraints*, given by

$$\sum_{i=1}^{k} X_i^2 \leq \sum_{i=1}^{k} E_i, \quad k = 1, \ldots, n. \tag{2.2}$$

That is, for each channel use, the cumulative energy spent cannot exceed the cumulative harvested energy. Consequently, transmission decisions made in a given channel use also affect all future channel uses. For each time instant, additional constraints stem from the battery state. We define a battery state B_i, with evolution given by

$$B_{i+1} = \left[B_i - X_i^2 + E_i\right]_0^{B_{\max}}, \tag{2.3}$$

where $B_{\max}$ corresponds to the battery capacity. Hence, the battery state B_i is a random process correlated over time even when the energy arrivals are independent and identically distributed (i.i.d.). Then, the instantaneous transmission constraints are simply given by $X_i^2 \leq B_i$.

Due to this, the study of the capacity of the energy harvesting channel is an intricate problem for which some preliminary results can be found in the literature. The most tractable case to tackle is that of *infinite* battery capacity, i.e., $B_{\max} = \infty$. For this case, and the AWGN channel, the authors in [38] derive two schemes capable of asymptotically achieving the classical AWGN channel capacity. These results have been extended in [39] and [40] to include the Multiple Access Channel (MAC).

The other extreme case entails the lack of battery, i.e., $B_{\max} = 0$. In this case, the instantaneous constraints are given by $X_i^2 \leq E_i$, that is, just depending on the energy harvested at the current time instant. This condition can be used to account for systems

that become active when they receive energy (e.g., those who store energy in supercapacitors), which they immediately consume to transmit, and become inactive again. This case has been studied by the authors in [41], where they derive the capacity for this scenario and provide a coding scheme to achieve it. The resulting capacity is related to the capacity of the amplitude-constrained AWGN channel [42]. The constraints, however, are not deterministic and constant, but time-varying and stochastic. As expected, the capacity is significantly lower than that of the $B_{\max} = \infty$ case. Complementarily, the extension to the MAC channel has been studied in [43].

Results for a *finite* battery are much more elusive. For a unit battery size, $B_{\max} = 1$, the authors in [44] study the capacity over a binary noiseless channel. They derive the channel capacity by showing that the noiseless binary channel with a unit battery can be equivalently modeled as a timing channel [45]. For the more general case of batteries of an arbitrary size, the authors in [46] conjecture an expression for the capacity, and compute it numerically. Also, in [47], the authors provide for the AWGN channel with finite battery size, an approximate capacity expression with a guarantee on the approximation gap.

2.2.2 Design of Offline Transmission Policies

A common preliminary assumption when designing transmission policies is the assumption of non-causal knowledge of the time-varying system variables (channel state, energy and data arrivals). Usually, this simplifies the problem, allowing it to be cast into a convex optimization framework. As discussed earlier, typically, the performance of such offline policies is used as a benchmark for the performance of online ones.

We start by discussing *point-to-point* communication scenarios. Under the assumption of an infinite size battery and communication over a AWGN channel, the authors in [48], derive the power allocation policy which minimizes the transmission completion time. Since minimizing the transmission completion time given a number of bits is equivalent to maximizing the number of bits given a duration, this problem is equivalent to throughput maximization. These results are then extended to the case of finite battery capacity by the authors in [49]. Both policies can be analyzed by means of the cumulative curve methodology introduced in [50]. These results show that the optimal power allocation policy must be piecewise linear and due to the concavity of the power-rate function, power allocation is kept as constant as possible subject to the energy harvesting constraints and battery overflow conditions. Battery imperfections have also been considered in [51], where the authors study the case in which the battery suffers energy leakage over time. This modifies the resulting power allocation policy due to the change in the cumulative energy profile. The authors in [52] have considered the fading channel, where they also introduce the directional waterfilling algorithm. This algorithm allows to solve the KKT conditions associated to the optimization problem and acts as a gen-

eralized version of the waterfilling algorithm under energy harvesting constraints. Its behavior is similar to that of a waterfilling algorithm, however, right-permeable walls are placed at energy arrival times, restricting the direction of the water flow and representing the causality constraints imposed by the energy harvesting process. These results are further extended in [53], in which the authors consider processing costs, where energy is not only spent in transmission but also for transmission circuitry. They derive the throughput maximizing power allocation under this scenario, which is given by a directional glue-pouring algorithm. The optimal policy results into a bursty transmission due to the effect of the processing cost.

Multiuser scenarios have also been extensively analyzed. The two-user *broadcast channel* with an infinite battery capacity transmitter has been studied in [54]. The authors derive the optimal transmit power allocation policy, which follows the same structure as in the point-to-point scenario. However, the authors show that there exists a cut-off power level, where only the power above this level is allocated to the weaker user. These results are then generalized in [55] to the broadcast channel with an arbitrary number of users and finite battery capacity. For this case, a similar structure of multiple cut-off powers is identified. The two-user *Multiple Access Channel* (MAC), has been studied in [56]. The authors assume a battery of infinite capacity and characterize, by means of an energy harvesting version of the generalized iterative waterfilling algorithm [57], the transmission policies which maximize the departure region of the transmitters. These results are then extended in [58] to the finite battery case for an arbitrary number of transmitters. The resulting transmission policy can be computed by a generalization of the iterative waterfilling algorithm [59] to the energy harvesting case. This results in a dynamic waterfilling algorithm, the waterlevels of which varies with the battery level. The two-user Gaussian *interference channel* has been considered in [60], where the authors provide sum-rate optimal transmission policies. The two-hop full duplex *relay channel* has been studied in [61]. The scenario studied consists on a source and relay terminal, powered by energy harvesting. The authors show that the optimal policy can be computed independently between source and relay, where the source maximizes its throughput with respect to its energy supply only. Likewise, the relay maximizes its throughput with respect to the data received from the source and its energy supply. These results are then generalized to the half-duplex case in [62].

2.2.3 Design of Online Transmission Policies

In practice, the assumptions of non-causal knowledge of the energy harvesting and data arrival processes used in offline transmission policies are rarely realistic. In this section, we consider transmission policies that drop this assumption and merely need *causal* knowledge of the processes.

Due to the coupling in time of the energy causality constraints, online energy har-

vesting problems can be cast as stochastic control problems. Usually, the transmitter attempts to maximize a certain expected outcome, but due to the energy causality constraints, their decision at any time affects all future decisions. The optimal solution to this problem can be found by using standard Dynamic Programming (DP) tools. However, due to the time-coupled nature of the problem, the computational complexity grows rapidly with the state space. This means that finding the optimal solution incurs a high computational cost, making these policies impractical.

In order to render the online problem solvable many authors have casted into a Markov Decision Process (MDP) framework. Each state of the system has a set of actions (idle, transmit) and transitions depend on events (harvested energy). Then, a policy is designed such that decisions are taken in order to maximize a given reward. Under this framework, state transitions satisfy the Markov property, which makes the resulting state space sufficiently manageable. Under perfect knowledge of the battery state, [63] studies for the MDP framework, the optimal online transmission policy, where the reward function is given by an importance value assigned to packets. These results are then extended to the case of a time-correlated energy supply in [64]. In some cases, perfect knowledge of the battery state is difficult to obtain, this is studied in [65], where the resulting system model is given by a partially observable Markov decision process. In [66] these results are extended to the case of time-correlated energy supply.

Chapter 3

Mathematical Preliminaries

In this section we aim to provide the reader with an overview of some important mathematical concepts that are used throughout this thesis. We focus on concepts related to optimization theory, namely, convex optimization, non-convex optimization and ergodic stochastic optimization. These are the most important tools used to solve the problems tackled in this thesis. Since these are vast fields of knowledge, it is our intent to present only the most relevant parts of the subject matter. Hence, we refer the reader to classical texts such as [67] and [68] for a more in-depth discussion.

3.1 Convex Optimization

Convex optimization deals with a specific subclass of optimization problems, that is, *convex* problems. Due to their convexity, these problems have certain characteristics that make them deserving of independent study from a more general class of optimization problems. Their main singularity being that local optimality and global optimality are equivalent. While, in general, convex optimization problems have no analytical solution, there exist efficient algorithms for computing their solutions. This means that this type of problems can be solved numerically with high reliability and efficiency. Convex optimization problems are very common, arising in a vast number of disciplines and scenarios, such as statistics, signal processing, communications and control systems, among others. Convex optimization is a well studied subject, even though it is still one of very active research. In the following, we present a brief summary of its foundations[1].

[1] Hereinafter, we present a summary based on Chapters 2 to 5 in [67].

3.1.1 Convexity

Definition 3.1. A set $\mathcal{C}$ is *convex* if the line segment between any two points in $\mathcal{C}$ lies in $\mathcal{C}$, i.e., if for any $x_1, x_2 \in \mathcal{C}$ and any θ with $0 \leq \theta \leq 1$, we have

$$\theta x_1 + (1 - \theta) x_2 \in \mathcal{C}. \tag{3.1}$$

Essentially, this means that a set is convex if the line between any two points inside the set lies inside the set.

Definition 3.2. A function $f : \mathbb{R}^n \to \mathbb{R}$ is convex if $\mathbf{dom}\, f$ is a *convex* set and if for all x, $y \in \mathbf{dom}\, f$ and θ with $0 \leq \theta \leq 1$, we have

$$f\left(\theta \mathbf{x} + (1 - \theta)\, \mathbf{y}\right) \leq \theta f\left(\mathbf{x}\right) + (1 - \theta)\, f\left(\mathbf{y}\right). \tag{3.2}$$

When dealing with functions, we have a similar interpretation as in sets. Geometrically, this means that for a convex function, any line between $(\mathbf{x}, f(\mathbf{x}))$ and $(\mathbf{y}, f(\mathbf{y}))$ must lie above the graph. Also, we refer to any function that satisfies (3.2) with strict inequality for $\mathbf{x} \neq \mathbf{y}$ and $0 \leq \theta \leq 1$ as *strictly convex*. Furthermore, we say that a function f is *concave* if $-f$ is convex. Likewise, we that a function f is *strictly concave* if $-f$ is strictly convex.

Definition 3.3. The *epigraph* of a function $f : \mathbb{R}^n \to \mathbb{R}$ is defined as

$$\mathbf{epi}\, f = \{(\mathbf{x}, t) \mid \mathbf{x} \in \mathbf{dom}\, f, f(\mathbf{x}) \leq t\}. \tag{3.3}$$

The epigraph allows to establish a relationship between convex sets and convex functions. Namely, a function is convex if and only if its epigraph is a convex set. Now, we establish the conditions that allow us to identify convexity.

Proposition 3.4 (First-order conditions)**.** *Suppose f is differentiable. Then f is convex if and only if* $\mathbf{dom}\, f$ *is convex and*

$$f\left(\mathbf{y}\right) \geq f\left(\mathbf{x}\right) + \nabla f\left(\mathbf{x}\right)^T \left(\mathbf{y} - \mathbf{x}\right). \tag{3.4}$$

The right hand side term of this inequality corresponds to the first-order Taylor approximation of the function f near $\mathbf{x}$. The inequality shows that for convex functions, the first-order Taylor approximation acts as a global lower bound of the function. This is one of the most important properties of convex functions. From this inequality, we can conclude that if $\nabla f\left(\mathbf{x}\right) = \mathbf{0}$, then $\mathbf{x}$ is a global minimizer of f, i.e. $f\left(\mathbf{y}\right) \geq f\left(\mathbf{x}\right)$ for all $\mathbf{y} \in \mathbf{dom}\, f$.

Proposition 3.5 (Second-order conditions)**.** *Assume that f is twice differentiable, that is, its Hessian or second derivative $\nabla^2 f$ exists at each point in* $\mathbf{dom}\, f$*, which is open. Then f is convex if and only if* $\mathbf{dom}\, f$ *is convex and its Hessian is positive semidefinite: for all $x \in \mathbf{dom}\, f$,*

$$\nabla^2 f\left(\mathbf{x}\right) \geq 0. \tag{3.5}$$

Geometrically, this condition corresponds to the requirement that the function have upward curvature at $\mathbf{x}$.

3.1.2 Convex Optimization Problems

Definition 3.6. An *optimization problem* can be written in general form as

$$\underset{\mathbf{x}}{\text{minimize}} \quad f_0(\mathbf{x}) \tag{3.6a}$$

$$\text{subject to} \quad f_i(\mathbf{x}) \leq 0, \quad i = 1, \ldots, m \tag{3.6b}$$

$$h_i(\mathbf{x}) = 0, \quad i = 1, \ldots, p \tag{3.6c}$$

where $\mathbf{x} \in \mathbb{R}^n$ is the *optimization variable*, $f_0 : \mathbb{R}^n \to \mathbb{R}$ is the *objective function*, $f_i : \mathbb{R}^n \to \mathbb{R}$ are the *inequality constraint functions*, and $h_i : \mathbb{R}^n \to \mathbb{R}$ are the *equality constraint functions*. The inequalities $f_i(\mathbf{x}) \leq 0$ are called the *inequality constraints*, and the equations $h_i(\mathbf{x}) = 0$ are called the *equality constraints*.

Definition 3.7. The optimization problem (3.6) is a *convex optimization problem* if the objective function $f_0(\mathbf{x})$ is convex, the inequality constraint functions functions $f_i(\mathbf{x}), i = 1, \ldots, m$ are convex and the equality constraint functions $h_i(\mathbf{x}), i = 1, \ldots, p$ are affine.

By convention, we express problems in the minimization form. With a slight abuse of notation, we will also refer to *concave maximization problems* as convex optimization problems. A maximization problem can be solved under this convention by the simple minimization of the $-f_0(\mathbf{x})$ objective function.

Definition 3.8. The set of points for which the objective and all constraint functions are defined, is called the *domain* of the optimization problem, and is given by

$$\mathcal{D} = \bigcap_{i=0}^{m} \mathbf{dom}\, f_i \cap \bigcap_{i=1}^{p} \mathbf{dom}\, h_i. \tag{3.7}$$

In the case of a convex optimization problem, the domain is convex.

Definition 3.9. A point $\mathbf{x} \in \mathcal{D}$ is called *feasible* if it satisfies $f_i(\mathbf{x}) \leq 0$ for $i = 1, \ldots, m$ and $h_i(\mathbf{x}) = 0$ for $i = 1, \ldots, p$.

Definition 3.10. The *optimal value* $p^\star$ of the optimization problem is given by

$$p^\star = \inf \{ f_0(\mathbf{x}) \mid f_0(\mathbf{x}) \leq 0, i = 1, \ldots, m, h_i(\mathbf{x}) = 0, i = 1, \ldots, p \}. \tag{3.8}$$

Furthermore, we say $\mathbf{x}^\star$ is an *optimal point*, if $\mathbf{x}^\star$ is feasible and $f_0(\mathbf{x}^\star) = p^\star$.

Definition 3.11. We say a feasible point $\mathbf{x}$ is locally optimal if there is an $R > 0$ such that

$$f_0(\mathbf{x}) = \inf \{ f_0(\mathbf{z}) \mid f_i(\mathbf{z}) \leq 0, i = 1, \ldots, m, h_i(\mathbf{z}) = 0, i = 1, \ldots, p, \|\mathbf{z} - \mathbf{x}\|_2 \leq R \}. \tag{3.9}$$

This is to say that a locally optimal point minimizes f_0 over nearby feasible points.

3.1.3 Duality

Definition 3.12. The *Lagrangian* $\mathcal{L} : \mathbb{R}^n \times \mathbb{R}^m \times \mathbb{R}^p \to \mathbb{R}$ of optimization problem (3.6) is defined as

$$\mathcal{L}(\mathbf{x}, \boldsymbol{\lambda}, \boldsymbol{\nu}) = f_0(\mathbf{x}) + \sum_{i=1}^{m} \lambda_i f_i(\mathbf{x}) + \sum_{i=1}^{p} \nu_i h_i(\mathbf{x}), \tag{3.10}$$

where λ_i is referred as the *Lagrange multiplier* associated to constraint $f_i(\mathbf{x}) \leq 0$ and ν_i as the Lagrange multiplier associated to constraint $h_i(\mathbf{x}) = 0$. The vectors $\boldsymbol{\lambda}, \boldsymbol{\nu}$ are the *Lagrange multiplier vectors*, also called the *dual variables* of the optimization problem.

Definition 3.13. The *Lagrange dual function* $g : \mathbb{R}^m \times \mathbb{R}^p \to \mathbb{R}$ is defined as

$$g(\boldsymbol{\lambda}, \boldsymbol{\nu}) = \inf_{\mathbf{x} \in \mathcal{D}} \mathcal{L}(\mathbf{x}, \boldsymbol{\lambda}, \boldsymbol{\nu}) = \inf_{\mathbf{x} \in \mathcal{D}} \left(f_0(\mathbf{x}) + \sum_{i=1}^{m} \lambda_i f_i(\mathbf{x}) + \sum_{i=1}^{p} \nu_i h_i(\mathbf{x}). \right) \tag{3.11}$$

Furthermore, we denote any pair $(\boldsymbol{\lambda}, \boldsymbol{\nu})$ with $\boldsymbol{\lambda} \geq 0$ and $(\boldsymbol{\lambda}, \boldsymbol{\nu}) \in \mathbf{dom}\, g$ as *dual feasible*.

An important thing to notice is that since the dual function $g(\boldsymbol{\lambda}, \boldsymbol{\nu})$ is given by the pointwise infimum of a family of affine functions, it is concave even when the original problem is not convex.

Proposition 3.14 (Lower bound on optimal value)**.** *The dual function gives a lower bound on the optimal value $p^\star$, for any $\boldsymbol{\lambda} \geq 0$ and $\boldsymbol{\nu}$ we have*

$$g(\boldsymbol{\lambda}, \boldsymbol{\nu}) \leq p^\star. \tag{3.12}$$

Since for each pair $(\boldsymbol{\lambda}, \boldsymbol{\nu})$ with $\boldsymbol{\lambda} \geq 0$, the dual function provides a lower bound on the optimal value $p^\star$, one might want to obtain the best lower bound possible. This is the dual problem.

Definition 3.15. The *Lagrange dual problem* is given by

$$\underset{\boldsymbol{\lambda}, \boldsymbol{\nu}}{\text{maximize}} \quad g(\boldsymbol{\lambda}, \boldsymbol{\nu}) \tag{3.13a}$$

$$\text{subject to} \quad \boldsymbol{\lambda} \geq 0 \tag{3.13b}$$

$$\tag{3.13c}$$

We denote by $d^\star$ the optimal value of the Lagrange dual problem. As previously said, the Lagrange dual problem allows us to find the best lower bound possible. Furthermore, since the dual function is concave, the Lagrange dual problem is a convex optimization problem even when the original problem (3.6) is not convex.

Proposition 3.16 (Duality gap)**.** *We have the inequality*

$$d^\star \leq p^\star, \tag{3.14}$$

this property is called weak duality *and we refer to the difference $p^\star - d^\star$ as the* duality gap*. If $p^\star = d^\star$ we say that* strong duality *holds.*

In general, strong duality does not hold. When the primal problem is a convex optimization problem, usually (but not always), strong duality holds. There exist several results that establish conditions under which strong duality holds. These conditions are called *constraint qualifications*. One important constraint qualification under which strong duality holds is *Slater's condition*.

Proposition 3.17 (Slater's condition)**.** *There exists an* $\mathbf{x} \in \mathbf{relint}\,\mathcal{D}$ *such that*

$$f_i(\mathbf{x}) < 0, i = 1, \ldots, m \tag{3.15}$$

and

$$h_i(\mathbf{x}) = 0, i = 1, \ldots, p. \tag{3.16}$$

Furthermore, a point satisfying these conditions is called an strictly feasible *point.*

Slater's condition not only implies strong duality for convex problems. It also implies the existence of a dual feasible pair $(\boldsymbol{\lambda}^\star, \boldsymbol{\nu}^\star)$ with $g(\boldsymbol{\lambda}^\star, \boldsymbol{\nu}^\star) = p^\star = d^\star$.

3.1.4 Optimality Conditions

Proposition 3.18 (Karush-Kuhn-Tucker conditions)**.** *Assume the functions* $f_0, \ldots, f_m$ *and* $h_1, \ldots, h_p$ *are differentiable and let* $\mathbf{x}^\star$ *and* $(\boldsymbol{\lambda}^\star, \boldsymbol{\nu}^\star)$ *be any primal and dual optimal points with zero duality gap. Then the following Karush-Kuhn-Tucker (KKT) conditions must be satisfied,*

$$f_i(\mathbf{x}^\star) \leq 0, \quad i = 1, \ldots, m \tag{3.17}$$

$$h_i(\mathbf{x}^\star) = 0, \quad i = 1, \ldots, p \tag{3.18}$$

$$\lambda_i^\star \geq 0, \quad i = 1, \ldots, m \tag{3.19}$$

$$\lambda_i^\star f_i(\mathbf{x}^\star) = 0, \quad i = 1, \ldots, m \tag{3.20}$$

$$\nabla f_0(\mathbf{x}^\star) + \sum_{i=1}^{m} \lambda_i^\star \nabla f_i(\mathbf{x}^\star) + \sum_{i=1}^{p} \nu_i^\star \nabla h_i(\mathbf{x}^\star) = 0 \tag{3.21}$$

The Karush-Kuhn-Tucker (KKT) conditions say that any pair of primal and dual optimal points must satisfy these conditions. Furthermore, if the optimization problem is convex, then the KKT conditions are necessary and sufficient for optimality. While these conditions give us the requirements for optimality. they can rarely be solved analytically. Instead, we usually resort to iterative algorithms to find solutions satisfying the KKT conditions.

3.2 Non-convex Optimization

When the optimization problem is not convex, there are in general no effective methods for solving the problem. As a whole, we can subdivide the approach taken in two subfields, *global optimization* and *local optimization*.

In *global* optimization, the aim is to find the solution which minimizes the objective function over all feasible points. However, due to the lack of convexity, the worst-case complexity of these methods grows exponentially with the problem size. Nonetheless, in practice one hopes that the method is faster. However, these situations are far from typical. The computational cost is therefore very high and such methods are usually only justified when the value of finding the true global solution is very high. For example, in the verification of safety-critical systems.

Another approach is local optimization. In this case, a compromise is made to find a *locally* optimal solution, meaning a solution that minimizes the objective over nearby feasible points. However, this does not guarantee that the solution is globally optimal. These methods tend to be faster and they are widely used when the goal is to find a good enough solution and not necessarily the best one. These types of methods are highly dependent on the initialization point, which ultimately determines the solution to which the method converges. A common way to choose the initial point is by a simple randomization. And sometimes, to obtain a good initial guess, a *convex relaxation* of the non-convex problem is solved, in which the non-convex parts of the problem are replaced by looser, but convex ones.

Next, we focus on the Majorization-Minimization (MM) algorithm, a simple yet effective method that is widely used to find *locally* optimal solutions to non-convex optimization problems.

3.2.1 Majorization-Minimization Algorithm

The Majorization-Minimization algorithm [69] , also known as Minorization-Maximization algorithm when dealing with maximization problems, is an optimization procedure used to iteratively solve problems that are too difficult to solve directly. In the case of non-convex problems, the MM algorithm aims at solving a sequence of convex problems that lead to a locally optimal solution of the original non-convex one. The MM algorithm has been shown to be very useful, for example, for high-dimensional problems that otherwise would be difficult to solve. The method relies on the concept of majorization.

Definition 3.19. A function $g : \mathbb{R}^n \times \mathbb{R}^n \to \mathbb{R}$ is said to *majorize* a function $f : \mathbb{R}^n \to \mathbb{R}$ at the point $\mathbf{x}_k$ if

$$f(\mathbf{x}_k) = g(\mathbf{x}_k, \mathbf{x}_k) \tag{3.22}$$

$$f(\mathbf{x}) \leq g(\mathbf{x}, \mathbf{x}_k), \quad \mathbf{x} \neq \mathbf{x}_k \tag{3.23}$$

This is to say that the surface $g(\mathbf{x}, \mathbf{x}_k)$ lies over the surface $f(\mathbf{x})$ and is tangent to it at the point $\mathbf{x} = \mathbf{x}_k$. Then, the MM algorithm consists on the iterative minimization of a surrogate majorizer of the original non-convex function. We have illustrated this process in Figure 3.1. The point $\mathbf{x}_k$ corresponds to the current iterate of the MM algorithm, and

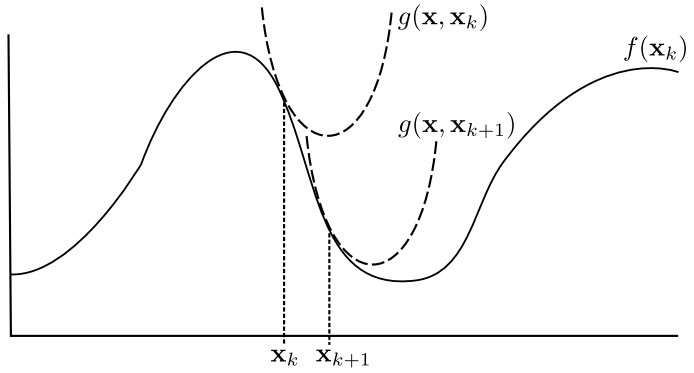

Figure 3.1: Majorization-Minimization algorithm.

a sequence $\{\mathbf{x}_k\}$ of iterates is generated by the update

$$\mathbf{x}_{k+1} := \arg\min_{\mathbf{x}\in\mathcal{X}} g(\mathbf{x}, \mathbf{x}_k), \tag{3.24}$$

where $\mathcal{X}$ is a convex set. Since the update $\mathbf{x}_{k+1}$ minimizes the majorizer function $g(\mathbf{x}, \mathbf{x}_k)$, it follows that $g(\mathbf{x}_{k+1}, \mathbf{x}_k) \leq g(\mathbf{x}_k, \mathbf{x}_k)$. Then, the resulting iterates satisfy the following inequality

$$\begin{aligned} f(\mathbf{x}_{k+1}) &= g(\mathbf{x}_{k+1}, \mathbf{x}_k) + f(\mathbf{x}_{k+1}) - g(\mathbf{x}_{k+1}, \mathbf{x}_k) \\ &\leq g(\mathbf{x}_k, \mathbf{x}_k) + f(\mathbf{x}_k) - g(\mathbf{x}_k, \mathbf{x}_k) \\ &= f(\mathbf{x}_k). \end{aligned} \tag{3.25}$$

Hence, the MM procedure forces $f(\mathbf{x}_{k+1}) \leq f(\mathbf{x}_k)$ and the iterate sequence $\{\mathbf{x}_k\}$ can be shown, under mild conditions, to converge to a local minimizer to the original non-convex function. Then, in practice, the problem is usually to find an appropriate majorizer of the non-convex function.

3.3 Ergodic Stochastic Optimization

In this section, we present an overview of the Ergodic Stochastic Optimization (ESO) algorithm introduced in [70]. This algorithm is used to solve optimization problems involving random variables and where the optimality criteria is given by long term averages. Such conditions commonly arise in the optimization of resource allocation problems in wireless communications [71, 72], signal processing [73] and many other areas. In order to solve such problems in a strictly *online* manner, the ESO algorithm resorts to a stochastic approximation of the Lagrangian function. In this way, the algorithm does not need to know the probability distribution function of the random variable, but only its current realization. Then, a subgradient method in the dual domain is used, where the step size is kept constant in order to have an online and adaptive algorithm. From

the solution in the dual domain, the primal iterates are then recovered and their ergodic averages can be shown to converge almost surely to the optimal solution.

More formally, consider a problem involving a time-varying state $\mathbf{h}(t)$ which has a probability distribution function $m(\mathbf{h})$, a resource allocation function $\mathbf{p}(t)$ and an ergodic variable $\mathbf{x} := \lim_{t\to\infty} \frac{1}{t} \sum_{u=1}^{t} \mathbf{x}(u)$ which constrains the system. This is described by the following optimization problem

$$\begin{aligned} \underset{\substack{\mathbf{x}\in\mathcal{X},\\ \{m(\mathbf{p}(\mathbf{h})):\mathbf{p}(\mathbf{h})\in\mathcal{P}(\mathbf{h})\}}}{\text{maximize}} \quad & f_0\left(\mathbf{x}\right) && \text{(3.26a)} \\ \text{subject to} \quad & \mathbf{x} \leq \mathbb{E}_h\left[\mathbb{E}_{m(\mathbf{p}(\mathbf{h}))}\left[f_1(\mathbf{p}(\mathbf{h}),\mathbf{h})\right]\right], && \text{(3.26b)} \\ & f_2(\mathbf{x}) \geq \mathbf{0}, && \text{(3.26c)} \end{aligned}$$

where the maximization of the concave objective function $f_0\left(\mathbf{x}\right)$ is with respect to the ergodic averages $\mathbf{x}$ and the pdf of the resource allocation $m(\mathbf{p}(\mathbf{h}))$. The constraints $\mathbf{x} \in \mathcal{X}$ and $\{m(\mathbf{p}(\mathbf{h})) : \mathbf{p}(\mathbf{h}) \in \mathcal{P}(\mathbf{h})\}$ are left implicit in order to model constraints satisfied for all time instants. The convex set $\mathcal{X}$ constrains the ergodic variable $\mathbf{x}$, while the set $\mathcal{P}(\mathbf{h})$ constrains the resource allocation $\mathbf{p}(\mathbf{h})$ and does not need to be convex. The explicit constraints in the system are given by a concave function $f_2(\mathbf{x})$ and a function $f_1(\mathbf{p}(\mathbf{h}),\mathbf{h})$ which is parametrized by the random state $\mathbf{h}$ and does not need to be concave with respect to the resource allocation $\mathbf{p}(\mathbf{h})$. Due to the definition of ergodic limits $\mathbf{x} := \lim_{t\to\infty} \frac{1}{t} \sum_{u=1}^{t} \mathbf{x}(u)$, constraint (3.26b) and (3.26c) are equivalent to the long term constraints

$$\lim_{t\to\infty} \frac{1}{t} \sum_{u=1}^{t} \mathbf{x}(u) \leq \lim_{t\to\infty} \frac{1}{t} \sum_{u=1}^{t} f_1(\mathbf{p}(u),\mathbf{h}(u)), \tag{3.27}$$

$$f_2\left(\lim_{t\to\infty} \frac{1}{t} \sum_{u=1}^{t} \mathbf{x}(u)\right) \geq \mathbf{0}. \tag{3.28}$$

Due to the inclusion of the pdf $m(\mathbf{p}(\mathbf{h}))$, the problem in the primal domain consists of an infinite number of primal variables, which makes it difficult to solve. On the contrary, the dual problem has a finite number of variables, making it much more tractable. To this end, consider the Lagrangian of the optimization problem (3.26), given by

$$\mathcal{L}(\mathbf{x}, m(\mathbf{p}(\mathbf{h})), \boldsymbol{\lambda}) = f_0\left(\mathbf{x}\right) + \boldsymbol{\lambda}_1^T \left(\mathbb{E}_h\left[\mathbb{E}_{m(\mathbf{p}(\mathbf{h}))}\left[f_1(\mathbf{p}(\mathbf{h});\mathbf{h})\right]\right] - \mathbf{x}\right) + \boldsymbol{\lambda}_2^T f_2(\mathbf{x}),, \tag{3.29}$$

where $\boldsymbol{\lambda}_1$ are the Lagrange multipliers associated to constraint (3.26b) and $\boldsymbol{\lambda}_2$ the Lagrange multipliers associated to constraint (3.26c). Also, for compactness we have collected both multipliers in the variable $\boldsymbol{\lambda} := [\boldsymbol{\lambda}_1^T, \boldsymbol{\lambda}_2^T]^T$. The ESO algorithm takes a stochastic approximation of the Lagrangian (3.29), consisting in the substitution of the random variable $\mathbf{h}$ for its instantaneous value $\mathbf{h}(t)$. Then, it solves the problem in a primal-dual sense by means of a subgradient method. The resulting steps of the ESO algorithm can be summarized as follows

1. **Primal Iteration.** Given multipliers $\boldsymbol{\lambda}(t)$, find the primal variables $\mathbf{x}(t) \in \mathcal{X}$ and $\mathbf{p}(t) \in \mathcal{P}(\mathbf{h}(t))$ such that

$$\mathbf{x}(t) := \arg\max_{\mathbf{x}\in\mathcal{X}} \left\{ f_0(\mathbf{x}) - \boldsymbol{\lambda}_1^T(t)\mathbf{x} + \boldsymbol{\lambda}_2^T(t) f_2(\mathbf{x}) \right\} \tag{3.30}$$

$$\mathbf{p}(t) := \arg\max_{\mathbf{p}(\mathbf{h}(t))\in\mathcal{P}(\mathbf{h}(t))} \left\{ \boldsymbol{\lambda}_1^T(t) f_1(\mathbf{p}(\mathbf{h}(t)), \mathbf{h}(t)) \right\} \tag{3.31}$$

2. **Dual Stochastic Subgradients.** Define the stochastic subgradient $\hat{\mathbf{s}}(t) = \hat{\mathbf{s}}(\mathbf{h}(t), \boldsymbol{\lambda}(t)) = [\hat{\mathbf{s}}_1^T(t), \hat{\mathbf{s}}_2^T(t)]^T$ of the dual function given by

$$\hat{\mathbf{s}}_1(t) := f_1(\mathbf{p}(t), \mathbf{h}(t)) - \mathbf{x}(t), \tag{3.32}$$

$$\hat{\mathbf{s}}_2(t) := f_2(\mathbf{x}(t)). \tag{3.33}$$

3. **Dual Iteration.** Update in the dual domain with a predetermined step size ϵ along the direction $-\hat{\mathbf{s}}(t)$

$$\boldsymbol{\lambda}(t+1) := [\boldsymbol{\lambda}(t) - \epsilon\hat{\mathbf{s}}(t)]^+ = \begin{bmatrix} \boldsymbol{\lambda}_1(t) - \epsilon\left(f_1(\mathbf{p}(t), \mathbf{h}(t)) - \mathbf{x}(t)\right) \\ \boldsymbol{\lambda}_2(t) - \epsilon f_2(\mathbf{x}(t)) \end{bmatrix}^+. \tag{3.34}$$

Usually, when solving an optimization problem such as (3.26), the goal is to find optimal variables $\mathbf{x}^\star$ and $m^\star(\mathbf{p}(\mathbf{h}))$, where $f_0(\mathbf{x}^\star)$ is maximized while also satisfying the problem constraints (3.26b) and(3.26c). Since the ESO is an online algorithm with ergodic constraints, the aim is slightly different. Our objective is to find iterates $\{\mathbf{x}(t)\}_{t=1}^\infty$ and $\{\mathbf{p}(t)\}_{t=1}^\infty$ that satisfy constraints (3.26b) and (3.26c) over a sufficiently long period of time (as shown by the equivalent constraints (3.27) and (3.28)). While, at the same time, maintaining a sufficiently small optimality gap. Specifically, the guarantees provided by the ESO algorithm are outlined in the following theorem.

Theorem 3.20. *Consider the optimization problem previously defined and sequences $\{\mathbf{x}(t)\}_{t=1}^\infty$ and $\{\mathbf{p}(t)\}_{t=1}^\infty$ generated by the ESO algorithm defined previously. Let $\mathbb{E}[\|\hat{\mathbf{s}}(t)\|^2 \mid \boldsymbol{\lambda}(t)] \leq \hat{S}^2$ be a bound on the second moment of the norm of the stochastic subgradients $\hat{\mathbf{s}}(t)$ and assume that there exists strictly feasible $\mathbf{x}_0 \in \mathcal{X}$ and $m_0(\mathbf{p}(\mathbf{h}))$ such that $\mathbb{E}_h\left[\mathbb{E}_{m_0(\mathbf{p}(\mathbf{h}))}\left[f_1(\mathbf{p}(\mathbf{h}); \mathbf{h})\right]\right] - \mathbf{x}_0 > C$ and $f_2(\mathbf{x}) > C$ for some strictly positive constant $C > 0$. Then*

1. **Almost sure feasibility.** *Sequences $\{\mathbf{x}(t)\}_{t=1}^\infty$ and $\{\mathbf{p}(t)\}_{t=1}^\infty$ are feasible with probability 1, i.e.,*

$$\lim_{t\to\infty} \frac{1}{t}\sum_{u=1}^{t} \mathbf{x}(u) \leq \lim_{t\to\infty} \frac{1}{t}\sum_{u=1}^{t} f_1(\mathbf{p}(u); \mathbf{h}(u)), \quad \textit{a.s.} \tag{3.35}$$

$$f_2\left(\lim_{t\to\infty} \frac{1}{t}\sum_{u=1}^{t} \mathbf{x}(u)\right) \geq \mathbf{0}, \quad \textit{a.s.} \tag{3.36}$$

2. **Almost sure near optimality.** *The ergodic average of* $f_0(\mathbf{x}(t))$ *almost surely converges to a value with optimality gap smaller than* $\epsilon\hat{S}^2/2$*, i.e.,*

$$f_0\left(\mathbf{x}^\star\right) - f_0\left(\lim_{t\to\infty}\frac{1}{t}\sum_{u=1}^{t}\mathbf{x}(u)\right) \leq \frac{\epsilon\hat{S}^2}{2}. \tag{3.37}$$

From these guarantees, we can draw some final remarks. First, note that the optimality gap can be made arbitrarily small by the choice of step size ϵ. Furthermore, the ergodic limit $\mathbf{x} := \lim_{t\to\infty}\frac{1}{t}\sum_{u=1}^{t}\mathbf{x}(u)$ of the solution provided by the ESO algorithm satisfies the constraints of the optimization problem with probability 1. Also, when finding the solution to the problem, note that the optimal resource allocation distribution $m^\star(\mathbf{p}(\mathbf{h}))$ is not directly computed by the ESO algorithm. Instead, the algorithm generates samples of $\mathbf{p}(t)$ from a distribution that asymptotically approximates $m^\star(\mathbf{p}(\mathbf{h}))$.

Chapter 4

Reconstruction of Correlated Sources

In this chapter, we investigate the reconstruction of time-correlated sources in a point-to-point communications scenario comprising an energy harvesting sensor and a fusion center. Our goal is to minimize the average distortion in the reconstructed observations by using data from previously encoded sources as side information. First, we analyze a delay-constrained scenario, where the sources must be reconstructed before the next time slot. We formulate the problem in a convex optimization framework and derive the optimal transmission (i.e., power and rate allocation) policy. To solve this problem, we propose an iterative algorithm based on the subgradient method. Interestingly, the solution to the problem consists of a coupling between a two-dimensional directional waterfilling algorithm (for power allocation) and a reverse waterfilling algorithm (for rate allocation). Then we find a more general solution to this problem in a delay-tolerant scenario where the time horizon for source reconstruction is extended to multiple time slots. Finally, we provide some numerical results that illustrate the impact of delay and correlation in the power and rate allocation policies, and in the resulting reconstruction distortion. We also discuss the performance gap exhibited by a heuristic *online* policy derived from the optimal (offline) one.

4.1 Introduction

A number of works address the problem of source reconstruction and estimation in wireless sensor network contexts. For uncoded transmissions, [74] investigates a number of energy-related aspects in a context of wireless sensor networks for parameter estimation. As for the coded case, in [75] the authors generalize Wyner-Ziv's source coding strategies with side information [76] to tree-structured sensor networks. Several aspects of source and channel coding have been analyzed in *energy harvesting* scenarios. A point-to-point

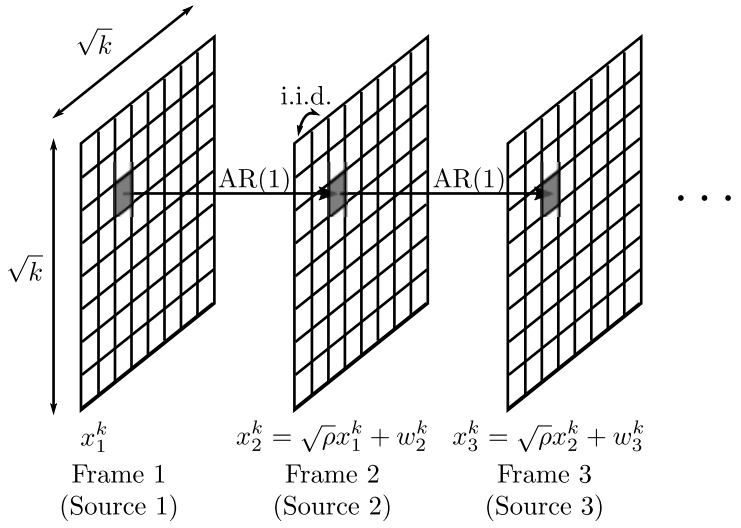

Figure 4.1: Temporal and spatial correlation models in video coding.

case was studied in [77], where rate-distortion allocation is optimized for stationary energy arrivals under data queue stability. These results were extended in [78] to the case of *finite* energy and data buffers. Besides, the multi-hop scenario was studied in [79] with *correlated* sources and *distributed* source coding. From a finite-horizon point of view, in [80] the problem of minimizing the reconstruction distortion of a Gaussian source is considered.

4.1.1 Contribution

In this chapter, we investigate the reconstruction of time-correlated sources in a point-to-point communications scenario. As in [48, 51, 55, 80] we assume that energy arrivals are non-causally known, thus taking an *offline* optimization approach to the problem. Hence, the solution turns out to be a benchmark against which *any* online policy can be compared (we also propose one heuristic online policy). The introduction of temporal correlation in the sources is particularly relevant for video coding applications [81] since, in this case, images (i.e., sources) in consecutive frames are clearly correlated. Video source coding has been widely investigated in the literature [82–84]. In [82] the authors model video signals as a sequence of time-correlated (correlation given by a first-order auto-regressive process) spatially independent and identically distributed Gaussian processes (namely, frames). Such correlation model, which we adopt in this work, is illustrated in Fig. 4.1. Still, more general correlation models are also available [84]. In other works [83], the authors analyze the impact of a *delay-tolerant* reconstruction of the correlated source. Those studies, however, were conducted in scenarios without energy harvesting. Our work goes one step beyond and incorporates energy harvesting constraints (in the sensor node) in the source coding process itself. Consequently, the

closed-form expressions that we derive for the power and rate allocation policies explicitly take correlation into account. In this respect, we generalize the results of [80] to the correlated case. In this more general setting and in contrast to previous works, we further leverage on side information-aware coding strategies for WSNs [75] to exploit correlation. First, we study the *delay-constrained* case in which the source must be reconstructed at the FC before the next time slot. Then we generalize our study to the delay-tolerant case, where the time horizon for source reconstruction is extended to multiple time slots. For both cases, we derive the optimal transmission policy which minimizes the average reconstruction distortion at the destination. Our policy reverts to that of [80] for uncorrelated sources, and to that of [48] for the uncorrelated and delay-constrained case. In order to compute this rate and power allocation policy, we propose an iterative algorithm based on the subgradient method [68]. Interestingly, we show that the procedure encompasses the interaction between a two-directional directional waterfiling and a reverse waterfilling [85, Chapter 10] schemes. Finally, we provide extensive numerical results which illustrate the impact of correlation and delay in the transmit policy and the resulting reconstruction distortion.

The remainder of this chapter is organized as follows. In Section 4.2 we introduce the system model and provide details on the encoding process. In Section 4.3, we address the distortion minimization problem for the delay-constrained case. We formulate the problem as a convex program and derive the optimal power and rate allocation policy. In order to compute this resulting transmission policy, we propose in Section 4.3.3 an iterative algorithm based on the subgradient method. Next, in Section 4.4 we generalize the problem (and the solution) to the delay-tolerant case. We provide numerical results in Section 4.5, where the effect of correlation as well as delay on the transmit policy and the resulting distortion are assessed. Finally, Section 4.6 closes the chapter by providing some concluding remarks.

4.2 System Model

Consider the point-to-point communications scenario depicted in Fig. 4.2 which comprises one Energy Harvesting (EH) sensor and one Fusion Center (FC). We adopt a slotted transmission model, with K denoting the total number of time slots. The sensor measures a time-varying phenomenon of interest which, in the sequel, we model by multiple correlated and memoryless Gaussian wide-sense stationary sources (see rationale in the preceding section). Specifically, each source models the phenomenon in a given time slot. In the k-th time slot, the sensor node (i) collects a *large* number of independent and identically distributed (i.i.d.) samples from the k-th source; and (ii) encodes those measurements. The encoded data is then transmitted to the FC in d consecutive time slots.

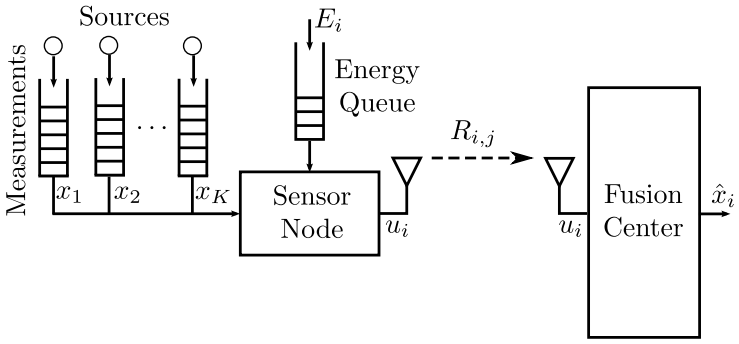

Figure 4.2: System Model.

In this work, we consider both delay-constrained ($d = 1$) and delay-tolerant ($d > 1$) communication scenarios. Clearly, in delay-tolerant scenarios the encoded data transmitted in a given time slot corresponds to multiple sources, as Figure 4.3 illustrates. Let $R_{i,j}$ denote the average transmission rate assigned to the encoded samples of the j-th source in the i-th time slot. Necessarily, the sum-rate in the i-th time slot is upper bounded by the channel capacity[1], namely,

$$\sum_{j=i-d+1}^{i} R_{i,j} \leq \log\left(1 + |h_i|^2 p_i\right), \qquad i = 1, \ldots, K, \tag{4.1}$$

with $|h_i|^2$ and p_i standing for the channel gain and average transmit power in time slot i, respectively (channel noise is assumed to be Gaussian-distributed, with zero-mean and unit variance). The n i.i.d. samples collected by the sensor node from the i-th source will be denoted in the sequel by $\{x_i^k\}_{k=1}^n$. Such samples, we assume, are correlated over time slots through a first-order autoregressive process. Hence, for the k-th sample from the i-th source we have that

$$x_i^k = \sqrt{\rho} x_{i-1}^k + w_i^k, \qquad \begin{matrix} k = 1, \ldots, n, \\ i = 1, \ldots, K, \end{matrix} \tag{4.2}$$

with $\rho = \mathbb{E}\left[x_i^k x_{i-1}^k\right]$ denoting the correlation coefficient, and w_i^k standing for an i.i.d. zero-mean Gaussian random variable with variance $\sigma_w^2 = (1-\rho)\sigma_x^2$.

As for the underlying energy harvesting process, we model it as a counting process [48, 49] with packet energy arrivals of E_i Joules at the beginning of time slot i. For simplicity, we assume that energy can be stored in a rechargeable battery of infinite capacity. By considering transmit power as the only energy cost, any transmission (power allocation) policy $\{p_i\}$ at the sensor node must satisfy the following energy causality

[1]For the ease of notation, we let the number of channel uses to be equal to the number of samples collected in a given time slot. This number, in turn, is assumed to be large enough to satisfy Shannon's source coding theorem.

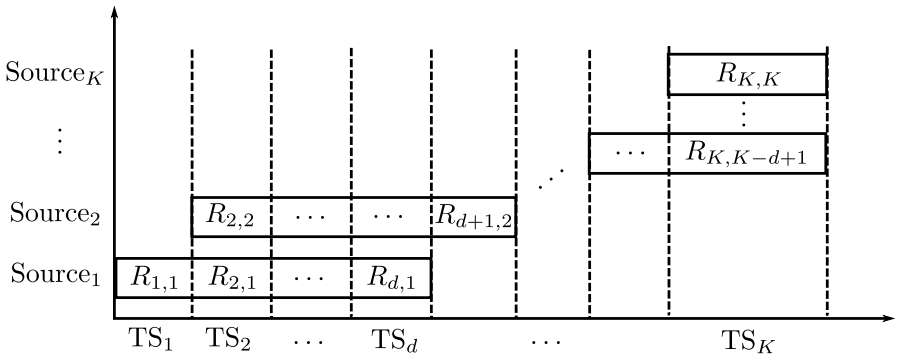

Figure 4.3: Simultaneous transmission of source measurements.

constraint:

$$T_s \sum_{j=1}^{i} p_j \leq \sum_{j=1}^{i} E_j, \qquad i = 1, \ldots, K, \tag{4.3}$$

where T_s denotes the duration of the time slot which, in the sequel, we normalize (i.e., $T_s = 1$).

Remark 4.1. There exist more sophisticated power consumption models encompassing non-ideal circuit power consumption effects [86] or the impact of processing power [87] (See also references [88] and [89] for more insight into these matters). In this work, for simplicity, we restrict ourselves to *transmit* power consumption. Nonetheless, the proposed model easily adapts to a constant circuit power consumption. Any model of the form $T_s \sum_{j=1}^{i} p_j + T_s \sum_{j=1}^{i} P_i^c \leq \sum_{j=1}^{i} E_j$, with P_i^c being the circuit power consumption at the i-th time slot, can be rewritten as $T_s \sum_{j=1}^{i} p_j \leq \sum_{j=1}^{i} \bar{E}_j$, where we have defined a new energy harvesting process as $\bar{E}_i = E_i - T_s P_i^c$. Using this new energy harvesting process, the proposed framework can be used to obtain policies adapted to a constant circuit power consumption.

Our goal is to reconstruct at the FC the sequence of measurements $\{x_i^k\}_{k=1}^n$ of each source in up to d time slots since they were collected. Due to the continuous-valued nature of the sources and the rate constraint (4.1), the reconstructed measurements $\{\hat{x}_i^k\}_{k=1}^n$ will be unavoidably subject to some distortion. Such distortion will be characterized by a Mean Squared Error (MSE) metric:

$$D_i = \frac{1}{n} \sum_{k=1}^{n} \left(x_i^k - \hat{x}_i^k \right)^2, \qquad i = 1, \ldots, K. \tag{4.4}$$

4.2.1 Source Coding and Distortion

Hereinafter, we assume separability of source and channel coding at the sensor node. Hence, $\{x_i^k\}_{k=1}^n$ can be first encoded into a length-n codeword (with a sufficiently large

n) given by $\{u_i^k\}_{k=1}^n$. This process, as in [90], can be modeled as

$$u_i = x_i + z_i, \qquad i = 1, \ldots, K, \tag{4.5}$$

where z_i denotes i.i.d. zero-mean Gaussian random noise of variance $\sigma_{z_i}^2$, which plays the role of encoding noise (the sample index has been omitted here for brevity). We know that, in order to decode the received data, the FC will exploit the available side information (i.e., all the preceding u_i). Hence, the sum of the (average) encoding rates per sample for the i-th source over the d consecutive time slots must satisfy [85]

$$\sum_{j=i}^{i+d-1} R_{j,i} \geq I(x_i; u_i | u_1, \ldots, u_{i-1}), \quad i = 1, \ldots, K, \tag{4.6}$$

where $I(\cdot;\cdot|\cdot)$ stands for the conditional mutual information. From (4.5), this last expression can be rewritten as

$$\begin{aligned} I(x_i; u_i | u_1, \ldots, u_{i-1}) =& H\left(u_i | u_1, \ldots, u_{i-1}\right) - H\left(u_i | u_1, \ldots, u_{i-1}, x_i\right) \\ =& \log\left(1 + \frac{\sigma^2_{x_i|u_1,\ldots,u_{i-1}}}{\sigma^2_{z_i}}\right), \end{aligned} \tag{4.7}$$

with $H(\cdot|\cdot)$ standing for the conditional entropy and $\sigma^2_{x_i|u_1,\ldots,u_{i-1}}$ for the conditional variance of the i-th observation given all the previous data available at the FC. Hence, by taking equality in (4.6), the variance of the encoding noise reads

$$\sigma^2_{z_i} = \frac{\sigma^2_{x_i|u_1,\ldots,u_{i-1}}}{\mathrm{e}^{\sum_{j=i}^{i+d-1} R_{j,i}} - 1}. \tag{4.8}$$

In each time slot, the FC produces an optimal Minimum Mean Squared Error (MMSE) estimate of the observations which, as discussed earlier, exploits all the preceding u_i, namely

$$\hat{x}_i = \mathbb{E}\left[x_i | u_1, \ldots, u_i\right], \qquad i = 1, \ldots, K. \tag{4.9}$$

The distortion in the reconstruction of x_i thus reads:

$$D_i = \sigma^2_{x_i|u_1,\ldots,u_i}, \tag{4.10}$$

which, in turn, can be expressed as[2] (see Appendix 4.7, for a detailed derivation)

$$D_i = \sigma_x^2 \left((1-\rho) \sum_{j=2}^{i} \rho^{i-j} \mathrm{e}^{-\sum_{k=j}^{i} \sum_{l=k}^{k+d-1} R_{l,k}} + \rho^{i-1} \mathrm{e}^{-\sum_{k=1}^{i} \sum_{l=k}^{k+d-1} R_{l,k}} \right). \tag{4.11}$$

[2] With some abuse of notation, in the summation interval we write $k+d-1$. Still, we restrict such summations to the valid range of timeslot values, namely, $\max\{k+d-1, K\}$.

4.3 Minimization of the Average Distortion: The Delay-Constrained Scenario

Here, samples must be encoded, transmitted and reconstructed before the next time slot starts (i.e., $d = 1$). The particularization of the channel capacity constraint (4.1) thus reads

$$R_i \leq \log\left(1 + |h_i|^2 p_i\right), \tag{4.12}$$

where R_i stands for the transmission rate which is assigned to the i-th source in the i-th time slot *only* (i.e., no summation of rates over subsequent time slots). Likewise, the rate-distortion constraint (4.6) can be particularized to

$$R_i \geq I(x_i; u_i | u_1, \ldots, u_{i-1}), \tag{4.13}$$

From all the above, the reconstruction distortion in (4.11) simplifies to

$$D_i = \sigma_x^2 \left((1-\rho) \sum_{j=2}^{i} \rho^{i-j} \mathrm{e}^{-\sum_{k=j}^{i} R_k} + \rho^{i-1} \mathrm{e}^{-\sum_{k=1}^{i} R_k} \right). \tag{4.14}$$

Our goal is to find the optimal power $\{p_i\}$ and rate $\{R_i\}$ allocation that minimize the average distortion given by (4.14) subject to the energy causality constraint of (4.3) and the capacity constraint of (4.1). Unfortunately, due to the coupling (over time slots) of the rates in the exponential terms of (4.14), this optimization problem cannot be solved analytically. To circumvent this, we define the *cumulative rates* r_{ij} as $r_{ij} \triangleq \sum_{k=j}^{i} R_k$, for $i = 1, \ldots, K, j = 1, \ldots, i$. By doing so, the optimization problem can be posed as:

$$\underset{\{p_i\},\{R_i\},\{r_{ij}\}}{\text{minimize}} \quad \frac{\sigma_x^2}{K} \sum_{i=1}^{K} \left((1-\rho) \sum_{j=2}^{i} \rho^{i-j} \mathrm{e}^{-r_{ij}} + \rho^{i-1} \mathrm{e}^{-r_{i1}} \right) \tag{4.15a}$$

$$\text{subject to} \quad r_{ij} = \sum_{k=j}^{i} R_k, \quad i = 1, \ldots, K, j = 1, \ldots, i \tag{4.15b}$$

$$R_i \leq \log\left(1 + |h_i|^2 p_i\right), \quad i = 1, \ldots, K, \tag{4.15c}$$

$$\sum_{j=1}^{i} p_j \leq \sum_{j=1}^{i} E_j, \quad i = 1, \ldots, K, \tag{4.15d}$$

$$p_i \geq 0, \quad i = 1, \ldots, K, \tag{4.15e}$$

$$R_i \geq 0, \quad i = 1, \ldots, K, \tag{4.15f}$$

$$r_{ij} \geq 0, \quad i = 1, \ldots, K, j = 1, \ldots, i \tag{4.15g}$$

where the optimization is with respect to variables $\{p_i\}$, $\{R_i\}$ and, also, $\{r_{ij}\}$ (this follows from the introduction of the additional constraint (4.15b) associated to the definition of cumulative rates). Since the objective function (4.15a) is convex and the

constraints (4.15b)-(4.15g) define a convex feasible set, the optimization problem (4.15) is convex and, thus, has a global solution [67]. By satisfying the Karush-Kuhn-Tucker (KKT) conditions, we identify the necessary and sufficient conditions for optimality. The Lagrangian of (4.15) reads

$$\begin{aligned}\mathcal{L} = &\frac{\sigma_x^2}{K}\sum_{i=1}^{K}\left((1-\rho)\sum_{j=2}^{i}\rho^{i-j}\mathrm{e}^{-r_{ij}} + \rho^{i-1}\mathrm{e}^{-r_{i1}}\right)\\ &+\sum_{i=1}^{K}\sum_{j=1}^{i}\lambda_{ij}\left(r_{ij}-\sum_{k=j}^{i}R_k\right)\\ &+\sum_{i=1}^{K}\mu_i\left(R_i-\log\left(1+|h_i|^2p_i\right)\right)\\ &+\sum_{i=1}^{K}\beta_i\left(\sum_{j=1}^{i}p_j-\sum_{j=1}^{i}E_j\right)\\ &-\sum_{i=1}^{K}\eta_i p_i-\sum_{i=1}^{K}\phi_i R_i-\sum_{i=1}^{K}\sum_{j=1}^{i}\delta_i r_{ij},\end{aligned} \tag{4.16}$$

where $\{\mu_i\} \geq 0$, $\{\beta_i\} \geq 0$, $\{\eta_i\} \geq 0$, $\{\phi_i\} \geq 0$, $\{\delta_{ij}\} \geq 0$ and $\{\lambda_{ij}\}$ stand for the corresponding Lagrange multipliers. The additional complementary slackness conditions are given by

$$\mu_i\left(R_i-\log\left(1+|h_i|^2p_i\right)\right)=0, \quad \forall i, \tag{4.17}$$

$$\beta_i\left(\sum_{j=1}^{i}p_j-\sum_{j=1}^{i}E_j\right)=0, \quad \forall i, \tag{4.18}$$

$$\eta_i p_i = 0, \quad \forall i, \tag{4.19}$$

$$\phi_i R_i = 0, \quad \forall i, \tag{4.20}$$

$$\delta_i r_{ij} = 0, \quad \forall i,j. \tag{4.21}$$

Finally, by taking the derivative of the Lagrangian with respect to p_i, R_i, r_{ij} and letting them be equal to zero we the set of stationarity conditions follow, namely,

$$\frac{\partial\mathcal{L}}{\partial p_i} = -\frac{\mu_i|h_i|^2}{1+|h_i|^2p_i}+\sum_{j=i}^{K}\beta_j-\eta_i=0, \tag{4.22}$$

$$\frac{\partial\mathcal{L}}{\partial R_i} = -\sum_{k=i}^{K}\sum_{j=1}^{i}\lambda_{kj}+\mu_i-\phi_i=0, \tag{4.23}$$

$$\frac{\partial\mathcal{L}}{\partial r_{ij}} = \begin{cases}-\frac{\sigma_x^2}{K}\rho^{i-j}\mathrm{e}^{-r_{ij}}+\lambda_{ij}-\delta_{ij}=0, & \text{if } j=1,\\ -\frac{\sigma_x^2}{K}(1-\rho)\rho^{i-j}\mathrm{e}^{-r_{ij}}+\lambda_{ij}-\delta_{ij}=0, & \text{if } j\neq 1.\end{cases} \tag{4.24}$$

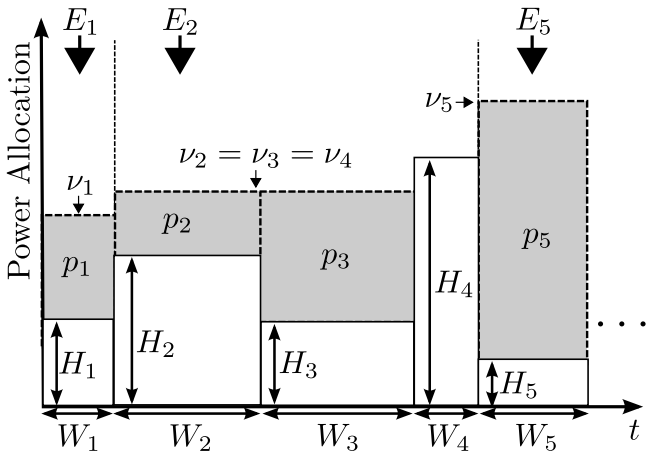

(a) Two-dimensional directional waterfilling.

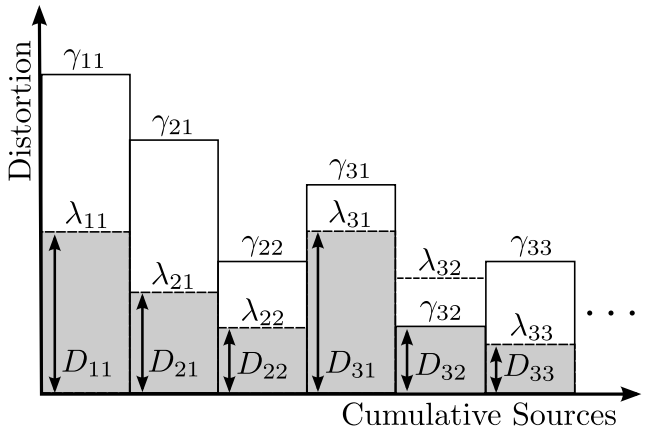

(b) Reverse waterfilling with multiple waterlevels.

Figure 4.4: Optimal power and cumulative rate allocation.

4.3.1 Optimal Power Allocation

From the stationarity conditions on p_i (4.22) and R_i (4.23), and the slackness conditions of (4.21), the optimal power allocation follows:

$$p_i^\star = \left[\frac{\sum_{k=i}^{K} \sum_{j=1}^{i} \lambda_{kj}}{\sum_{j=i}^{K} \beta_j} - \frac{1}{|h_i|^2} \right]^+, \qquad i = 1, \ldots, K, \tag{4.25}$$

This solution can be interpreted as a two-dimensional directional waterfilling, as shown in Fig. 4.4(a). For each time slot i, we have a rectangle of solid material of width $W_i \triangleq \sum_{k=i}^{K} \sum_{j=1}^{i} \lambda_{kj}$ and height $H_i \triangleq 1/\left(|h_i|^2 \sum_{k=i}^{K} \sum_{j=1}^{i} \lambda_{kj}\right)$. Right-permeable taps are placed in time slots with energy arrivals. Water is consequently poured up to a waterlevel $\nu_i \triangleq 1/\sum_{j=i}^{K} \beta_j$. The resulting power allocation corresponds to the area of water above the solid rectangle.

4.3.2 Optimal Rate Allocation

Next, by solving (4.24) for r_{ij}, and taking into account the corresponding slackness conditions, the optimal cumulative rate allocation can be written as

$$r_{ij}^{\star} = \begin{cases} \left[\log\left(\dfrac{\frac{1}{K}\sigma_x^2\rho^{i-j}}{\lambda_{ij}}\right)\right]^+, & \text{if } j=1, \\ \left[\log\left(\dfrac{\frac{1}{K}\sigma_x^2\left(1-\rho\right)\rho^{i-j}}{\lambda_{ij}}\right)\right]^+, & \text{if } j\neq 1. \end{cases} \tag{4.26}$$

From this last expression, it becomes apparent that, necessarily, $\{\lambda_{ij}\} > 0$. Hence, from (4.23), we have that $\{\mu_i\} > 0$ too. This implies that constraint (4.15c) is satisfied with equality. Moreover, expression (4.26) can be readily interpreted in terms of a *reverse* waterfilling solution for the reconstruction of parallel Gaussian sources [85, Chapter 10]. To see that, we define

$$\gamma_{ij} = \begin{cases} \frac{1}{K}\sigma_x^2\rho^{i-j}, & \text{if } j=1, \\ \frac{1}{K}\sigma_x^2\left(1-\rho\right)\rho^{i-j}, & \text{if } j\neq 1, \end{cases} \tag{4.27}$$

and

$$D_{ij} = \begin{cases} \lambda_{ij}, & \text{if } \lambda_{ij} < \gamma_{ij}, \\ \gamma_{ij}, & \text{if } \lambda_{ij} \geq \gamma_{ij}. \end{cases} \tag{4.28}$$

Bearing the above in mind, equation (4.26) can be rewritten as

$$r_{ij}^{\star} = \left[\log\left(\frac{\gamma_{ij}}{D_{ij}}\right)\right]^+. \tag{4.29}$$

As Figure 4.4(b) illustrates, this solution mimics that of a rate-distortion allocation problem for parallel Gaussian sources. However, here the allocated rates $r_{ij}^{\star}$ (and sources) are *cumulative* rather than *individual*; and the reverse water level given by λ_{ij} is not constant. Besides, the numerator in the argument of (4.29) does not only depend on the variance of the sources σ_x^2 but also on the correlation coefficient ρ, as (4.27) evidences.

Finally, by replacing (4.29) in (4.14), the optimal distortion for the reconstruction of the i-th source reads

$$D_i^{\star} = \sum_{j=1}^{i} D_{ij}. \tag{4.30}$$

that is, it can be computed as the sum of the distortions associated to the corresponding cumulative rates.

4.3.3 Optimization Algorithm

As discussed in the previous section, the optimal power (4.25) and cumulative rate (4.26) allocation are coupled by the Lagrange multipliers λ_{ij}. Further, one can easily prove

Algorithm 4.1 Optimal power and rate allocation for the delay-constrained case.

1: **Initialize:** $\{\lambda_{ij}^{(t)}\} := 0$.
2: **Step 1:** For all i, allocate power.
3: $p_i^{(t+1)} := \left[\dfrac{\sum_{k=i}^{K} \sum_{j=1}^{i} \lambda_{kj}^{(t)}}{\sum_{j=i}^{K} \beta_j} - \dfrac{1}{|h_i|^2} \right]^+$
4: **Step 2:** For all i, j, cumulative rate allocation.
5: $r_{ij}^{(t+1)} := \left[\log \left(\dfrac{\gamma_{ij}}{\lambda_{ij}^{(t)}} \right) \right]^+$
6: **Step 3:** For all i, j, update multiplier.
7: $\lambda_{ij}^{(t+1)} := \left[\lambda_{ij}^{(t)} + \alpha \left(r_{ij}^{(t+1)} - \sum_{k=j}^{i} \log \left(1 + |h_k|^2 p_k^{(t+1)} \right) \right) \right]$
8: **Step 4:** Go to Step 1 until stopping criteria is met.

that problem (4.15) satisfies Slater's condition, and therefore, strong duality holds [67]. Since in these conditions the duality gap is zero, we propose to solve the corresponding *dual* problem in order to determine the *primal* solution (power and rates) in which we are interested. To that aim, we resort to the subgradient method [68] on which basis the solution to the dual problem, $\{\lambda_{ij}\}$, can be iteratively found (convergence can be guaranteed under some mild conditions). Specifically, in the t-th iteration, the Lagrange multipliers are updated as follows[3]:

$$\lambda_{ij}^{(t+1)} := \left[\lambda_{ij}^{(t)} + \alpha \left(r_{ij}^{(t+1)} - \sum_{k=j}^{i} \log \left(1 + |h_k|^2 p_k^{(t+1)} \right) \right) \right], \tag{4.31}$$

with α standing for the corresponding step size. In Algorithm 4.1, we summarize the proposed procedure to solve the power and cumulative rate allocation problem.

The algorithm corresponds to a a subgradient ascent on the dual function. Hence, it has a convergence rate of the order of $\mathcal{O}(1/\sqrt{t})$ [91, Chapter 8.2]. Moreover, for a node, a single iteration of the algorithm will be of the order of $\mathcal{O}(K \log K)$, as it is a form of waterfilling. Namely, sorting takes $\mathcal{O}(K \log K)$ operations, while each waterfilling operation takes $\mathcal{O}(K)$ operations and there are at most $\mathcal{O}(\log K)$ waterfillings to be done, since we can compute a binary search between the water bins.

[3]Here, we use extended-value definitions for all functions [67], thus taking $+\infty$ values outside their respective domain.

4.4 Minimization of the Average Distortion: The Delay-Tolerant Scenario

Here, we address the more general case in which data is allowed to be transmitted and reconstructed within $d > 1$ time slots after samples are collect and encoded. Again, to render the problem solvable, we define the *cumulative rates* as

$$r_{ij} \triangleq \sum_{k=j}^{i} \sum_{l=k}^{k+d-1} R_{l,k} \quad \text{for } i = 1, \ldots, K, j = 1, \ldots, i. \tag{4.32}$$

In delay-tolerant scenarios, each time slot conveys data from up to d different sources (see Fig. 4.3). Hence, the number of unknowns ($\{R_{i,j}\}$), $Kd - d(d-1)/2$ in total, exceeds the number of equations given by the capacity constraints (4.1), K in total. Consequently, the system of equations becomes underdetermined. This means that, even if a unique solution exists when optimizing on the *cumulative* rates r_{ij} (as we discuss next), there exist *multiple* solutions for the *individual* rates. Thus, we propose to solve the optimization problem in terms of cumulative rates (only), and then define some criteria to select one solution in terms of individual rates (this will be further elaborated in Section 4.5 ahead).

To start with, we need to rewrite not only (i) the objective function given by (4.11); but, also, (ii) the set of constraints, in terms of cumulative rates. The latter can be accomplished by expressing the cumulative rates in the following recursive form:

$$r_{ij} \triangleq \begin{cases} \sum_{k=j}^{i} r_{kk}, & \text{if } j \neq i \\ \sum_{k=j}^{j+d-1} R_{k,j}, & \text{if } j = i \end{cases} \tag{4.33}$$

for $i = 1, \ldots, K, j = 1, \ldots, i$, and then resorting to Fourier-Motzkin elimination [92]. Further, we prove that the system obtained by Fourier-Motzkin elimination is equivalent.

$$\left\{ \begin{array}{r} r_{ii} = \sum_{j=i}^{i+d-1} R_{j,i}, \\ i = 1, \ldots, K \\ \sum_{j=i-d+1}^{i} R_{i,j} \leq \log\left(1 + |h_i|^2 p_i\right), \\ i = 1, \ldots, K \\ R_{i,j} \geq 0, \\ i = 1, \ldots, K, j = i-d+1, \ldots, i \end{array} \right\} \equiv \left\{ \begin{array}{r} r_{ij} = \sum_{k=j}^{i} r_{kk}, \\ i = 1, \ldots, K, j = 1, \ldots, i-1 \\ r_{ij} \leq \sum_{k=j}^{d+i-1} \log\left(1 + |h_k|^2 p_k\right), \\ i = 1, \ldots, K, j = 1, \ldots, i \\ r_{ij} \geq 0, \\ i = 1, \ldots, K, j = 1, \ldots, i \end{array} \right\} \tag{4.34}$$

Proposition 4.2. *The systems of inequalities in* (4.34) *are equivalent when solving optimization problem* (4.35)*. That is, the set of variables* $\{p_i\}$,$\{R_{i,j}\}$ *and* $\{r_{ij}\}$ *satisfy*

the constraints on the left hand side of (4.34) *if and only if they satisfy the constraints on the right hand side of* (4.34).

Proof. See Appendix 4.8. ■

Finally, in order to pose the optimization problem, it suffices to include the corresponding *energy harvesting* constraints of (4.3) too, namely

$$\underset{\{p_i\},\{r_{ij}\}}{\text{minimize}} \quad \frac{\sigma_x^2}{K}\sum_{i=1}^{K}\left((1-\rho)\sum_{j=2}^{i}\rho^{i-j}\mathrm{e}^{-r_{ij}}+\rho^{i-1}\mathrm{e}^{-r_{i1}}\right) \tag{4.35a}$$

$$\text{subject to} \quad r_{ij}=\sum_{k=j}^{i} r_{kk}, i=1,\ldots,K, j=1,\ldots,i-1 \tag{4.35b}$$

$$r_{ij}\leq \sum_{k=j}^{d+i-1}\log\left(1+|h_k|^2p_k\right), i=1,\ldots,K, j=1,\ldots,i \tag{4.35c}$$

$$\sum_{j=1}^{i}p_j\leq\sum_{j=1}^{i}E_j, \quad i=1,\ldots,K, \tag{4.35d}$$

$$p_i\geq 0, \quad i=1,\ldots,K, \tag{4.35e}$$

$$r_{ij}\geq 0, \quad i=1,\ldots,K, j=1,\ldots,i \tag{4.35f}$$

where, clearly, the optimization is now with respect to variables $\{p_i\}$ and $\{r_{ij}\}$. Differently from Section 4.3, constraint (4.35b) guarantees, on the one hand, that the cumulative rates satisfy definition (4.33). On the other, constraint (4.35c) enforces the cumulative rates to satisfy the per time slot channel capacity constraint.

The optimization problem (4.35) is convex and can be solved in closed-form by (i) computing the Lagrangian function:

$$\begin{aligned}\mathcal{L}=&\frac{\sigma_x^2}{K}\sum_{i=1}^{K}\left((1-\rho)\sum_{j=2}^{i}\rho^{i-j}\mathrm{e}^{-r_{ij}}+\rho^{i-1}\mathrm{e}^{-r_{i1}}\right)\\&+\sum_{i=1}^{K}\sum_{j=1}^{i}\mu_{ij}\left(r_{ij}-\sum_{k=j}^{i}r_{kk}\right)\\&+\sum_{i=1}^{K}\sum_{j=1}^{i}\lambda_{ij}\left(r_{ij}-\sum_{k=j}^{d+i-1}\log\left(1+|h_i|^2p_i\right)\right)\\&+\sum_{i=1}^{K}\beta_i\left(\sum_{j=1}^{i}p_j-\sum_{j=1}^{i}E_j\right)\\&-\sum_{i=1}^{K}\eta_ip_i-\sum_{i=1}^{K}\sum_{j=1}^{i}\delta_{ij}r_{ij}.\end{aligned} \tag{4.36}$$

with $\{\lambda_{ij}\} \geq 0$, $\{\beta_i\} \geq 0$, $\{\eta_i\} \geq 0$, $\{\delta_i\} \geq 0$; and $\{\mu_{ij}\}$ standing for the corresponding Lagrangian multipliers; and (ii) satisfying the Karush-Kuhn-Tucker (KKT) conditions that follow from the Lagrangian. Along the lines of Section 4.3, the optimal power allocation reads,

$$p_i^\star = \left[\frac{\sum\limits_{k=i-d+1}^{K} \sum\limits_{l=1}^{k} \lambda_{kl}}{\sum\limits_{j=i}^{K} \beta_j} - \frac{1}{|h_i|^2} \right]^+, \quad i = 1, \ldots, K. \tag{4.37}$$

The optimal power allocation for the (more general) delay-tolerant scenario admits again a two-dimensional directional waterfilling interpretation. Differently from the delay-constrained scenario, the width and height of the solid rectangle, namely $W_i \triangleq \sum_{k=i-d+1}^{K} \sum_{l=1}^{k} \lambda_{kl}$ and $H_i \triangleq 1/\left(|h_i|^2 \sum_{k=i-d+1}^{K} \sum_{l=1}^{k} \lambda_{kl}\right)$, have an explicit dependence on d, the maximum latency[4].

Along the lines of the preceding section, the optimal cumulative rates for the delay-constrained scenario follow:

$$r_{ij}^\star = \left[\log\left(\frac{\gamma_{ij}}{\lambda_{ij} + \bar{\mu}_{ij}} \right) \right]^+. \tag{4.38}$$

where we have defined

$$\bar{\mu}_{ij} = \begin{cases} -\sum\limits_{k=i}^{K} \sum\limits_{\substack{l=1 \\ l \neq k}}^{i} \mu_{kl}, & \text{if } i = j, \\ \mu_{ij}, & \text{if } i \neq j. \end{cases} \tag{4.39}$$

and γ_{ij} is given by (4.27). Again, this solution can be interpreted in terms of a classical reverse waterfilling scheme.

As in Section 4.3.3, we solve the corresponding dual problem by resorting to the subgradient method. However, now *both* dual variables λ_{ij} and μ_{ij} must be updated as follows

$$\lambda_{ij}^{(t+1)} := \left[\lambda_{ij}^{(t)} + \alpha_\lambda \left(r_{ij}^{(t+1)} - \sum_{k=j}^{d+i-1} \log\left(1 + |h_k|^2 p_k^{(t+1)}\right) \right) \right]^+, \tag{4.40}$$

$$\mu_{ij}^{(t+1)} := \left[\mu_{ij}^{(t)} + \alpha_\mu \left(r_{ij}^{(t+1)} - \sum_{k=j}^{i} r_{kk}^{(t+1)} \right) \right], \tag{4.41}$$

where α_λ and α_μ denote the corresponding step sizes. Algorithm 4.2 details the proposed procedure to obtain the optimal power and cumulative rate allocation.

4.5 Numerical Results

In this section, we assess the performance of the proposed optimal power and rate allocation schemes. We are particularly interested in analyzing the impact of the correlation

[4] As expected, these expressions simplify to the ones for the delay-constrained scenario for $d = 1$.

Algorithm 4.2 Optimal power and rate allocation for the delay-tolerant case.

1: **Initialize:** $\{\lambda_{ij}^{(t)}\} := 0$, $\{\mu_{ij}^{(t)}\} := 0$.
2: **Step 1:** For all i, allocate power.
3: $$p_i^{(t+1)} := \left[\frac{\sum_{k=i-d+1}^{K} \sum_{l=1}^{k} \lambda_{kl}^{(t)}}{\sum_{j=i}^{K} \beta_j} - \frac{1}{|h_i|^2} \right]^+$$
4: **Step 2:** For all i, j, cumulative rate allocation.
5: $$r_{ij}^{(t+1)} := \left[\log \left(\frac{\gamma_{ij}}{\lambda_{ij}^{(t)} + \bar{\mu}_{ij}^{(t)}} \right) \right]^+$$
6: **Step 3:** For all i, j, update multipliers.
7: $$\lambda_{ij}^{(t+1)} := \left[\lambda_{ij}^{(t)} + \alpha_\lambda \left(r_{ij}^{(t+1)} - \sum_{k=j}^{d+i-1} \log \left(1 + |h_k|^2 p_k^{(t+1)} \right) \right) \right]^+$$
8: $$\mu_{ij}^{(t+1)} := \left[\mu_{ij}^{(t)} + \alpha_\mu \left(r_{ij}^{(t+1)} - \sum_{k=j}^{i} r_{kk}^{(t+1)} \right) \right]$$
9: **Step 4:** Go to Step 1 until stopping criteria is met.

coefficient ρ and the delay d in the resulting transmission policies. For this reason, in all numerical results we have set the channel gains to a (constant) unit value. Unless otherwise stated, the simulation setup considers a system with $K = 10$ time slots and an (arbitrary) energy harvesting profile with energy arrivals given by $E_1 = 0.2$, $E_3 = 0.6$, $E_6 = 0.8$ and $E_7 = 1.4$.

4.5.1 Delay-Constrained Scenario ($d = 1$)

The resulting optimal power allocation policy is shown in Figure 4.5. For uncorrelated sources ($\rho = 0$), the optimal policy turns out to be the well-known geometric solution of [48] and [50]. This corresponds to the tightest string below the cumulative energy harvesting curve connecting the original and the total harvested energy by the end of time slot K. However, as the correlation increases, the harvested energy tends to be spent (i.e., allocated as transmit power) sooner. As a result, in Fig. 4.5 the slope of the energy consumption curves right after new energy arrivals (e.g., in the beginning of time slot 3) increases with ρ. This indicates that, in order to minimize the average distortion, one should encode the observations as accurately as possible when some new energy is made available. This stems from the fact that past observations are used here as side information at the receiver. Intuitively, the earlier an observation is accurately encoded, the more estimates (in subsequent time slots) can benefit from such an increased accuracy. This holds true even at the expense of a reduced (or zero, as in time slot 10, for $\rho = 1$) transmit power being allocated to some subsequent time slots. That is, at the expense of suspending data transmission. All the above is in stark contrast with the uncorrelated case studied in [48] where transmit power is (i) strictly positive for all time

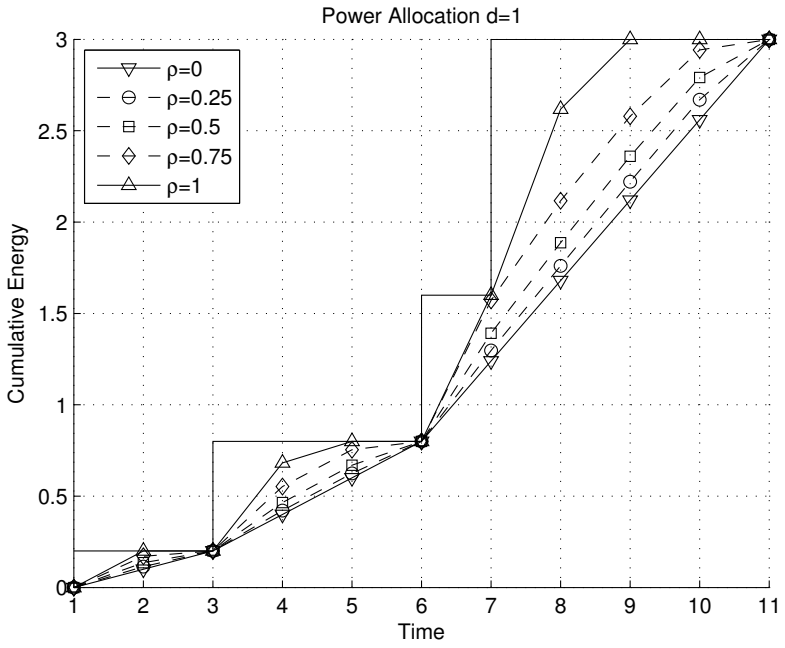

Figure 4.5: Optimal power allocation for $d = 1$ and varying correlation coefficient ρ.

slots and (ii) a monotonically increasing function.

Figure 4.6 depicts the reconstruction distortion for *each* source (and time slot since $d = 1$) associated to the optimal policy. Unsurprisingly, the higher the correlation, the more predictable the sources become and, hence, the lower the distortion (curves are shifted downwards). For correlated sources, however, distortion does not monotonically decrease with time slot index. As discussed in the previous paragraph, this stems from the *anticipated* consumption of the harvested energy for the encoding of previous observations. Consequently, one can observe (i) a substantial decrease of the individual distortion for sources in time slots with energy arrivals (time slots 3, 6, and 7); and (ii) distortion upturns in time slots where the energy harvested so far has been spent or is close to (time slots 2, 5, and 10). Still, the average distortion is lower.

4.5.2 Delay-Tolerant Scenario ($d > 1$)

Figure 4.7 illustrates the impact of delay on the optimal power allocation. Interestingly, as d increases the solution converges to the tightest string below the cumulative energy harvesting curve of [48]. The intuition behind is as follows. To recall, the tightest string solution attempts to maximize the total throughput (rate) for the whole transmission period. To that aim, the sequence of transmit powers (and rates) must be monotonically increasing, that is, transmit power is higher by the end of the transmission period (i.e, last time slot(s)). For $d = 1$, on the contrary, the allocated transmit power (and, thus, rate) is higher in time slots with energy arrivals, and not necessarily in the last one(s).

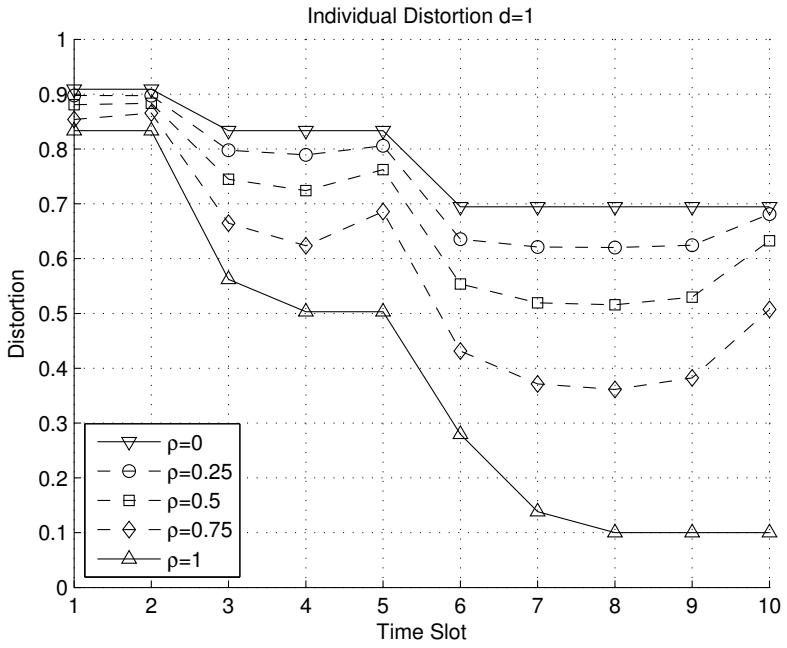

Figure 4.6: Individual distortion for $d = 1$ and varying ρ.

Moreover, the source must be reconstructed *immediately*, that is, after $d = 1$ time slots (assuming the processing time at the FC to be negligible). In other words, there is some *urgency* to allocate power (namely, spend energy). This is in stark contrast with the tightest string solution where higher power and rates can be found at the *end*. Things, however, are radically different when d increases. On the one hand, the deadline by which individual sources must be reconstructed is shifted d time slots towards the *end*. On the other, the rates (and power) needed to encode a specific source can be allocated over *multiple* time slots, rather than just one. Hence, for increasing d the urgency to allocate power decreases and, thus, the way in which power is allocated is more aligned with that of the tightest string solution.

Figure 4.8 depicts the average distortion as a function of delay. Clearly, the average distortion decreases with delay since the higher the delay, the higher the degrees of freedom to allocate transmit power (and, thus, spend energy in a more sensible manner). Unsurprisingly, distortion is lower for higher values of ρ, since the preceding (correlated) sources used as side information at the FC are more informative.

Next, we investigate to what extent our system leverages on the knowledge on source correlation. To that aim, the rate and power allocation policy from [80], which was derived for a scenario with *uncorrelated* sources, is used as a benchmark. Specifically, whereas the source encoding rate depends on $I(x_i; u_i)$ (namely, the mutual information with the *current* source only) the sources at the FC are reconstructed according to (4.9). Our approach, on the contrary, exploits correlation both in the encoding and

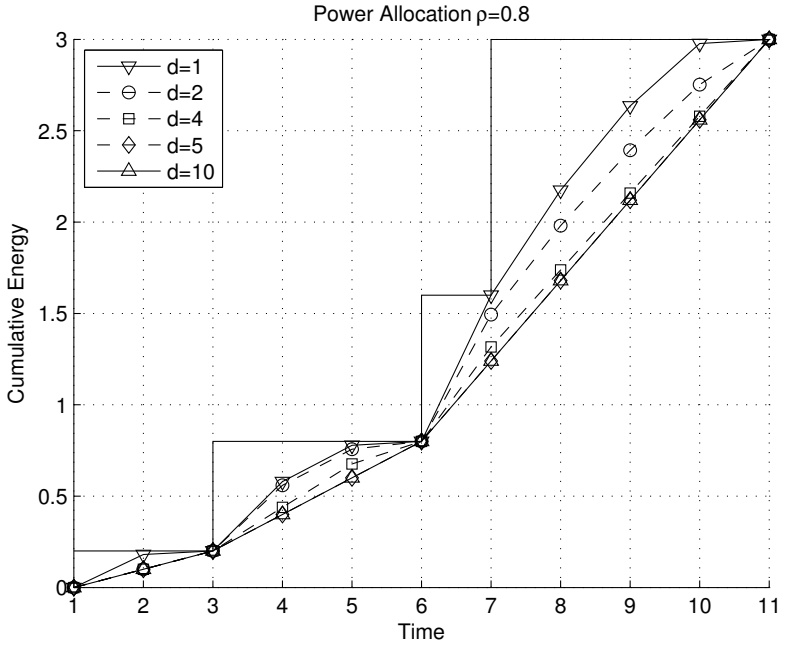

Figure 4.7: Optimal power allocation for $\rho = 0.8$ and varying delay d.

decoding/reconstruction processes. Figure 4.9 shows the normalized reduction (difference) in the average distortion attained by such benchmark and our scheme. For delay-constrained scenarios, the reduction in distortion can be as high 25% for our scheme. For delay-tolerant ones ($d = 10$), reduction can go up to 80%, which is very remarkable.

4.5.3 Comparison with an Online Policy

As discussed earlier, the proposed (offline) transmit power and rate allocation scheme requires *non-causal* knowledge on energy arrivals. Here, instead, we introduce a more realistic *online* version just requiring *causal* knowledge. The offline scheme will be used as a benchmark.

Similar to [52], a *myopic*[5] online policy can be computed as follows. Assume for a moment that, after harvesting some energy in the initial timeslot (i.e., $E_1 > 0$), no additional energy is harvested in subsequent timeslots. Hence, we let $E_2 = \cdots = E_K = 0$ and solve problem (4.35) for $k = 1, \ldots, K$. In the absence of knowledge on future energy arrivals, this is a sensible approach too. After all, distortion would be minimized should no additional energy be actually harvested. And, otherwise, we can react accordingly. Let $k_0 < K$ denote the next timeslot in which some energy is harvested (i.e., $E_{k_0} > 0$). For the preceding timeslots (i.e., $k = 1, \ldots, k_0 - 1$), we force the power and rate allocations computed after the last energy arrival to remain unchanged. Hence, the

[5]More general online policies accounting for different degrees of availability of channel and energy state information can be also be considered (see e.g., [93]).

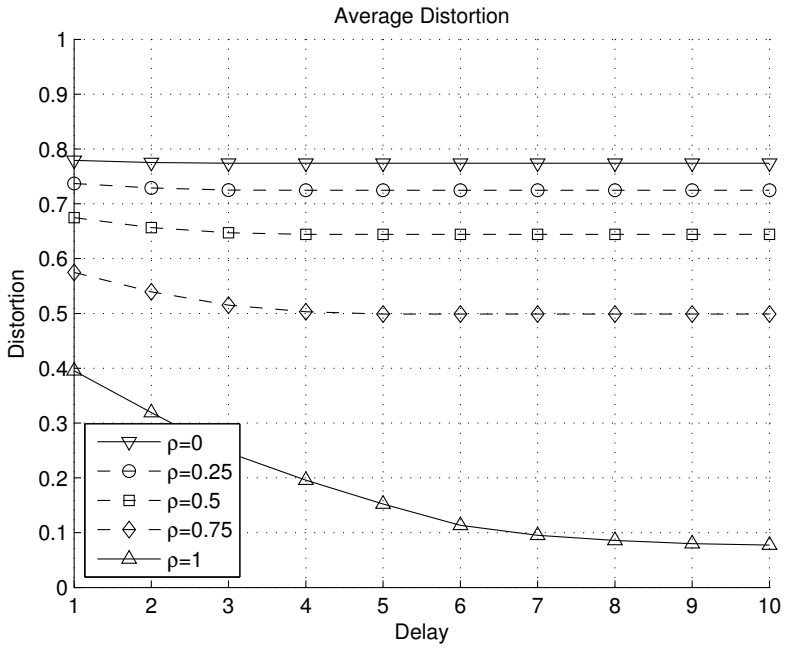

Figure 4.8: Average distortion vs. delay d for varying correlation ρ.

unspent energy in the beginning of timeslot k_0 reads $E_{k_0}^u = \sum_{j=1}^{k_0-1} E_j - \sum_{j=1}^{k_0-1} p_j$. Next, we let $E_{k_0} := E_{k_0}^u + E_{k_0}$ and $E_{k_0+1} = \cdots = E_K = 0$ and, again, solve problem (4.35) for $k = k_0, \ldots, K$. That is, we compute the optimal power and rate allocations for all subsequent timeslots. This procedure is iterated until all energy arrivals have been accounted for.

Of course, no optimality can be claimed for the resulting policy. Still, the interesting property of such scheme is its ability to adjust (re-compute) the remaining power and rate allocations every time that some energy is harvested. By doing so, the additional (and causal) knowledge on energy arrivals is effectively exploited.

Figure 4.10 illustrates the performance of the offline and online policies vs. the intensity rate of energy arrivals (which are modeled as a Poisson process). Unsurprisingly, the distortion of the offline versions turns out to be a lower bound of that attained by online ones. For a given intensity rate, the additional distortion associated to the online version can be regarded as moderate (some 20% at an energy arrival rate equal to 1, $\rho = 0.2$, and $d = 1$). Interestingly, the online version requires a 40% increase of the intensity rate to achieve the same distortion as its offline counterpart (for the same operating point). The distortion gap becomes narrower for delay-tolerant scenarios ($d = 10$) and wider in percentage for scenarios with high correlation (see $\rho = 0.8$ curves) or when the intensity rate increases.

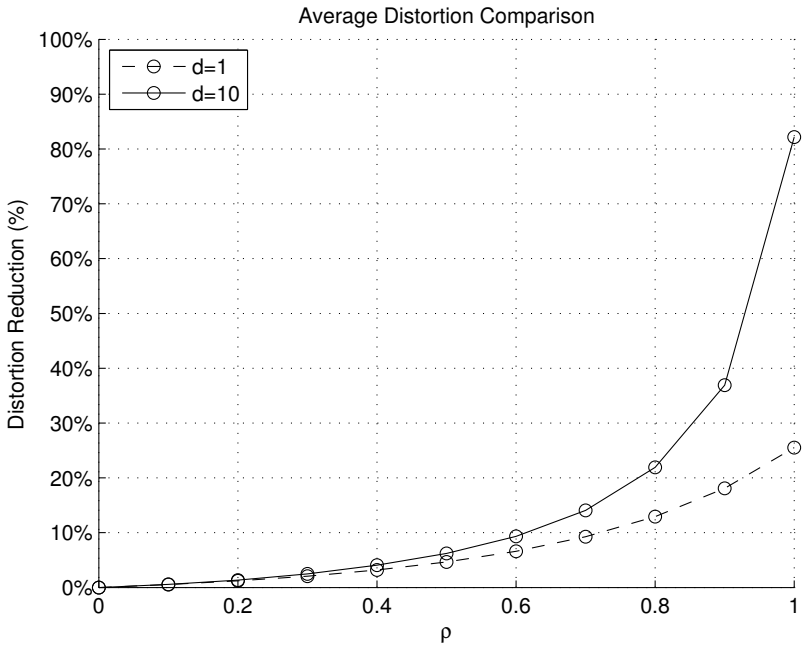

Figure 4.9: Reduction in average distortion.

4.5.4 Convergence

Next, we investigate the convergence properties of the proposed scheme. Specifically, in Figure 4.11 we depict the relative error ε between the average distortion at iteration t and its optimal value, namely, $\varepsilon = \left| D^{\star}_{avg} - D^{(t)}_{avg} \right| / D^{\star}_{avg}$. For the update of the dual variables in (4.31), we have used a time-varying step size[6]. Clearly, convergence is slower for larger d values. This stems from the fact that, for delay-tolerant scenarios, the search space for the solution is larger, as the summation in equation (4.35c) evidences.

4.5.5 Allocation of Individual Rates

As discussed in Section 4.4, for $d > 1$ there exists an infinite number of solutions for the allocation of the *individual* rates (the system of equations is underdetermined). In order to get some insight on how individual rates are allocated, we will select the solution with the lowest 2-norm. This, clearly, penalizes solutions with very large (dissimilar) rates.

After solving the optimization problem (4.35) and determining the optimal cumula-

[6]The step size used is $\alpha^{(t)} = \bar{\alpha}^{(t)} / \|g^{(t)}\|_2$, where $g^{(t)}$ is the corresponding subgradient and $\bar{\alpha} = 1/\sqrt{t}$. This diminishing step size satisfies the convergence conditions given by $\bar{\alpha}^{(t)} \geq 0$, $\lim_{t\to\infty} \bar{\alpha}^{(t)} = 0$ and $\sum_{t=1}^{\infty} \bar{\alpha}^{(t)} = \infty$ [68].

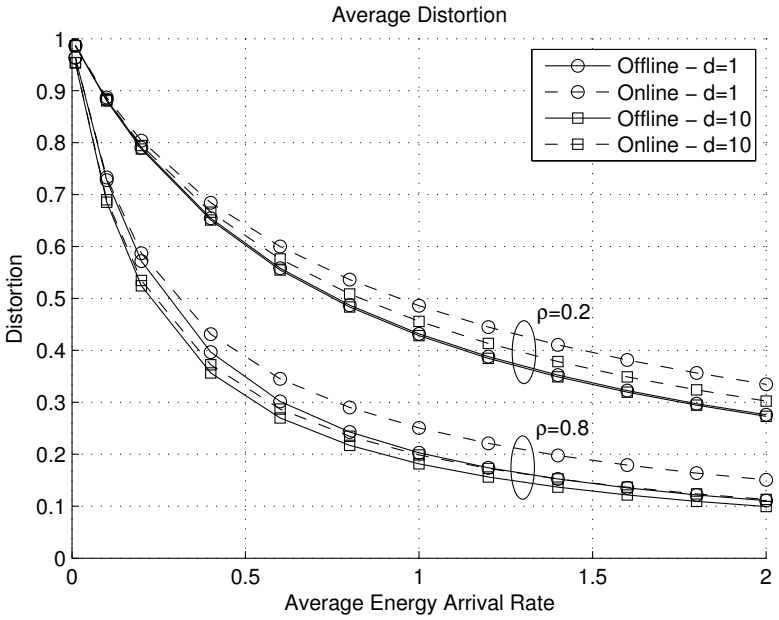

Figure 4.10: Average distortion for the offline and online policies, for low ($\rho = 0.2$) and high ($\rho = 0.8$) correlation, and delay-constrained ($d = 1$) and delay-tolerant ($d = 10$) scenarios.

tive rates $r_{i,j}$, we find the individual rates $R_{i,j}$ by solving:

$$\underset{\{R_{i,j}\}}{\text{minimize}} \quad \left(\sum_{i=1}^{K} \sum_{j=i-d+1}^{i} R_{i,j}^2 \right)^{1/2} \tag{4.42a}$$

$$\text{subject to} \quad r_{ii} = \sum_{j=i}^{i+d-1} R_{j,i}, i = 1, \ldots, K \tag{4.42b}$$

$$\sum_{j=i-d+1}^{i} R_{i,j} \leq \log\left(1 + |h_i|^2 p_i\right), i = 1, \ldots, K \tag{4.42c}$$

$$R_{i,j} \geq 0, i = 1, \ldots, K, j = i - d + 1, \ldots, i \tag{4.42d}$$

To that aim, we need to use r_{ii} and p_i from the solution of the (cumulative) rate and power allocation problem as an input (see first and second inequality constraints in the problem above).

Figure 4.12 shows the allocation of *individual* rates over the d time slots for each source (a different color is used for each source). We consider scenarios with sources exhibiting low ($\rho = 0.2$) and high ($\rho = 0.8$) correlation. Interestingly enough, the higher the correlation, the lower the spread of individual rates over time slots (fewer sources in each time slot). This is consistent with the fact that, as discussed earlier, for low ρ (and $d = 1$) energy tends to be spent sooner. Accordingly, in delay-tolerant scenarios where

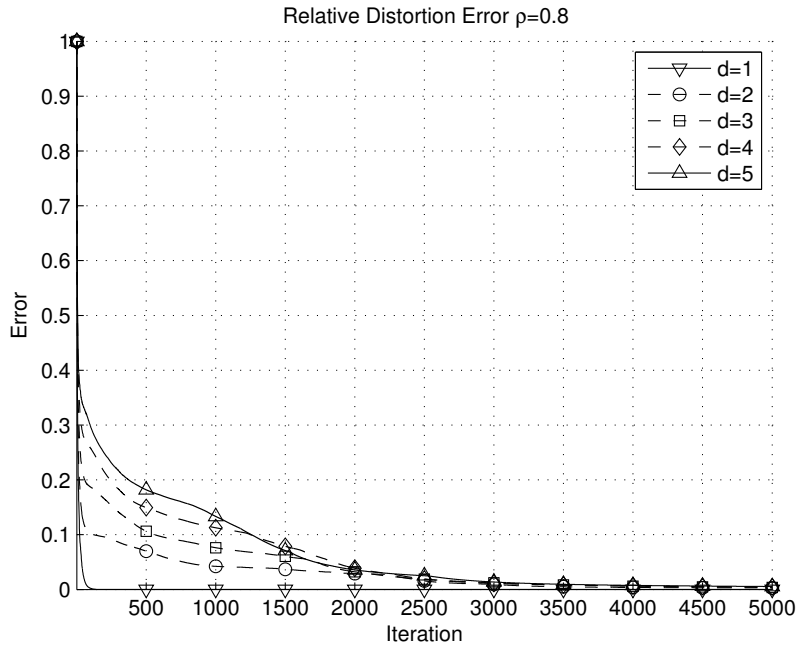

Figure 4.11: Relative distortion error for $\rho = 0.8$ and varying d.

the encoded data is transmitted in a number of time slots, when correlation is high the first time slots are favored.

4.6 Conclusions

In this chapter, we have investigated the impact of source correlation in the design of point-to-point optimal transmission policies with energy harvesting sensors. We have considered both delay-constrained delay-tolerant scenarios. In both cases, our goal was to minimize the average distortion in the decoded (reconstructed) observations by using data from previously encoded sources as side information. We have formulated the problems in a convex optimization framework. Besides, we have proposed an iterative procedure, based on the subgradient method, to solve both problems. Interestingly, the procedure entails the interaction of a directional and reverse waterfilling schemes in each iteration. For the delay-constrained scenario, numerical results revealed that, differently from the uncorrelated case, minimizing the average distortion implies encoding observations as accurately as possible upon energy arrivals. This holds true even if the transmit power allocated to subsequent time slots is lower or, eventually, zero (and, thus, an increase in distortion in such time slots). For the delay-tolerant scenario, we have observed that as delay increases, the power allocation policy converges to the tightest string below the cumulative energy harvesting curve. And, also, that the average distortion decreases. In comparison with other schemes not exploiting correlated sources

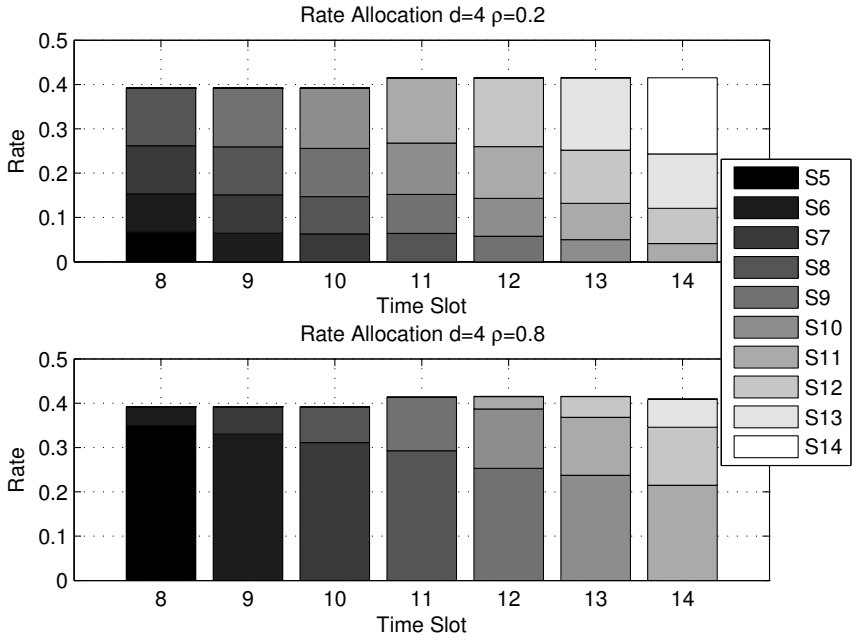

Figure 4.12: Allocation of individual rates for sources with low (top) and high (bottom) correlation ($K = 20$; $d = 4$; energy profile: $E_1 = 0.2$, $E_2 = 1$, $E_4 = 0.6$, $E_6 = 1$, $E_7 = 0.8$, $E_8 = 0.2$, $E_9 = 0.4$, $E_{11} = 1.4$, $E_{13} = 0.6$, $E_{14} = 0.6$, $E_{16} = 0.8$, $E_{17} = 0.2$, $E_{18} = 1$, $E_{19} = 0.2$, and $E_{20} = 0.4$).

as side information, ours attains an average distortion which is substantially lower (with reductions of up to 25% or 80% for $d = 1$ and $d = 10$, respectively. We have also proposed a myopic online policy exhibiting a moderate performance gap (some 20% for low correlation and delay-constrained scenarios) with respect to the offline (optimal) policy. Besides, we have found that the time needed for the algorithm to convergence is higher for delay-tolerant scenarios since the search space is substantially larger there. Finally, we have observed that for delay-tolerant scenarios, the higher the correlation, the lower the spread of individual rates over time slots.

4.7 Appendix: Derivation of the Average Distortion in (4.11)

For compactness, hereinafter we let $R_i \triangleq \sum_{j=i}^{i+d-1} R_{j,i}$ denote the rate assigned to the i-th source over its d time slots; and $D_i = \sigma^2_{x_i|u_1,\ldots,u_i}$ the distortion for the i-th source which can be recursively expressed as [94]:

$$\sigma^2_{x_k|u_1,\ldots,u_k} = \sigma^2_{x_k|u_1,\ldots,u_{k-1}} - \frac{\mathrm{cov}^2(u_k, x_k|u_1,\ldots,u_{k-1})}{\sigma^2_{u_k|u_1,\ldots,u_{k-1}}}. \tag{4.43}$$

We prove by induction that

$$\begin{aligned} D_i &= \sigma_x^2\bigg((1-\rho)\sum_{j=2}^{i}\rho^{i-j}\mathrm{e}^{-\sum_{k=j}^{i}\sum_{l=k}^{k+d-1}R_{l,k}} + \rho^{i-1}\mathrm{e}^{-\sum_{k=1}^{i}\sum_{l=k}^{k+d-1}R_{l,k}}\bigg) \\ &= \sigma_x^2\bigg((1-\rho)\sum_{j=2}^{i}\rho^{i-j}\mathrm{e}^{-\sum_{k=j}^{i}R_k} + \rho^{i-1}\mathrm{e}^{-\sum_{k=1}^{i}R_k}\bigg). \end{aligned} \tag{4.44}$$

We start by showing this expression holds for the base case ($i = 1$). That is

$$D_1 = \sigma^2_{x_1|u_1} = \sigma_x^2 - \frac{\left(\sigma_x^2\right)^2}{\sigma_x^2 + \sigma_{z_1}^2} = \sigma_x^2 - \frac{\left(\sigma_x^2\right)^2}{\sigma_x^2 + \dfrac{\sigma_x^2}{e^{R_1}-1}} = \sigma_x^2 e^{-R_1}, \tag{4.45}$$

which satisfies expression (4.44). For the inductive step, assume expression (4.44) is true for $i = n$. Then consider

$$\begin{aligned} D_{n+1} &= \sigma^2_{x_{n+1}|u_1,\ldots,u_{n+1}} \\ &= \sigma^2_{x_{n+1}|u_1,\ldots,u_n} - \sigma^2_{x_{n+1}|u_1,\ldots,u_n}\left(1-e^{-R_{n+1}}\right) \\ &= \sigma^2_{x_{n+1}|u_1,\ldots,u_n}e^{-R_{n+1}} \\ &= \sigma^2_{\sqrt{\rho}x_n+w_n|u_1,\ldots,u_n}e^{-R_{n+1}} \\ &= \left(\rho\sigma^2_{x_n|u_1,\ldots,u_n} + \sigma^2_{w_n|u_1,\ldots,u_n}\right)e^{-R_{n+1}} \\ &= \left(\rho D_n + \sigma_x^2(1-\rho)\right)e^{-R_{n+1}} = D_n\rho e^{-R_{n+1}} + \sigma_x^2(1-\rho)e^{-R_{n+1}} \end{aligned} \tag{4.46}$$

Then by the induction hypothesis we have

$$\begin{aligned} D_{n+1} = \sigma_x^2\bigg((1-\rho)\sum_{j=2}^{n}\rho^{n-j}\mathrm{e}^{-\sum_{k=j}^{n}R_k} \\ +\rho^{n-1}\mathrm{e}^{-\sum_{k=1}^{n}R_k}\bigg)\rho e^{-R_{n+1}} + \sigma_x^2(1-\rho)e^{-R_{n+1}} \end{aligned} \tag{4.47}$$

and by rearranging terms we have

$$D_{n+1} = \sigma_x^2\bigg((1-\rho)\sum_{j=2}^{n+1}\rho^{n+1-j}\mathrm{e}^{-\sum_{k=j}^{n+1}R_k} + \rho^{n+1-1}\mathrm{e}^{-\sum_{k=1}^{i+1}R_k}\bigg). \tag{4.48}$$

Thus, expression (4.44) holds for $i = n+1$. Therefore, by the principle of induction, expression (4.44) holds for all i.

4.8 Appendix: Proof of Proposition 4.2.

Proof. For notational convenience, let $c_i \triangleq \log(1+|h_i|^2 p_i)$ denote the channel capacity in the i-th timeslot. First, we focus on the direct proof. Assuming that the LHS of (4.34), which is given by the system of inequalities

$$\sum_{j=i}^{i+d-1} R_{j,i} = r_{ii}, \qquad i = 1, \ldots, K, \tag{4.49a}$$

$$\sum_{j=i-d+1}^{i} R_{i,j} \leq c_i, \qquad i = 1, \ldots, K, \tag{4.49b}$$

$$R_{i,j} \geq 0, \qquad i = 1, \ldots, K, j = 1, \ldots, i-d+1, \tag{4.49c}$$

has a solution in terms of individual rates $R_{i,j}$, our goal is to find the system of inequalities in the RHS of (4.34), namely

$$r_{ij} = \sum_{k=j}^{i} r_{kk}, \qquad i = 1, \ldots, K, j = 1, \ldots, i-1, \tag{4.50a}$$

$$r_{ij} \leq \sum_{k=j}^{i+d-1} c_k, \qquad i = 1, \ldots, K, j = 1, \ldots, i, \tag{4.50b}$$

$$r_{ij} \geq 0, \qquad i = 1, \ldots, K, j = 1, \ldots, i. \tag{4.50c}$$

The constraints (4.50a) follow directly from the definition of the cumulative rates (4.33). Constraint (4.50c) is also straightforward since, from its definition in (4.32), the cumulative rates $r_{i,j}$ can be expressed as a summation of *non-negative* (see (4.49c)) individual rates $R_{i,j}$. As for (4.50b), note that from (4.49b) each *non-negative* individual rate can be upper-bounded as follows

$$R_{i,j} \leq c_i, \qquad i = 1, \ldots, K, j = 1, \ldots, i-d+1. \tag{4.51}$$

Next, by direct substitution of the bounds (4.51) into the equalities (4.49a), we have that

$$r_{ii} \leq \sum_{j=i}^{i+d-1} c_j, \qquad i = 1, \ldots, K \tag{4.52}$$

Finally, by substitution of (4.52) into the definition of cumulative rates (4.33), inequality (4.50b) follows.

Consider now the converse. Assume that the RHS of (4.34), which is also given by the system of inequalities (4.50), has a solution in terms of cumulative rates r_{ij}. Then, we want to prove that there exists a non-empty set of individual rates $R_{i,j}$ satisfying the inequalities (4.49) (i.e., the RHS of (4.34) has a solution even if it might not be unique, as discussed earlier). To prove that, we focus on the more restrictive case where we force the capacity constraint (4.49b) to be satisfied with equality. Hence, the first two constraints in (4.50) become:

$$\sum_{j=i}^{i+d-1} R_{j,i} = r_{ii}, \qquad i = 1, \ldots, K \tag{4.53a}$$

$$\sum_{j=i-d+1}^{i} R_{i,j} = c_i, \qquad i = 1, \ldots, K. \tag{4.53b}$$

The system of equations above can be rewritten in matrix form:

$$\mathbf{A}\mathbf{x} = \mathbf{b} \tag{4.54}$$

where we have defined the column vectors $\mathbf{x} \triangleq [R_{1,1}, R_{2,1}, \ldots, R_{K,K}]^T$ and $\mathbf{b} \triangleq [r_{1,1}, \ldots, r_{K,K}, c_1, \ldots, c_K]^T$, and where matrix $\mathbf{A}$ is given by the $\{0, 1\}$ entries yielding the summations in (4.53). Next, we resort to Farkas' lemma:

Lemma 4.3 (Farkas' Lemma [21])**.** *If $\mathbf{A} \in \mathbb{R}^{m \times n}$ and $\mathbf{b} \in \mathbb{R}^m$, then exactly one of the following holds:*

(i) There exists $\mathbf{x} \in \mathbb{R}^n$ such that $\mathbf{A}\mathbf{x} = \mathbf{b}$ and $\mathbf{x} \geq 0$.

(ii) There exists $\mathbf{y} \in \mathbb{R}^m$ such that $\mathbf{y}^T\mathbf{A} \geq 0$ and $\mathbf{y}^T\mathbf{b} < 0$.

where the inequality $\mathbf{x} \geq 0$ is defined element-wise. Clearly, alternative (i) in the Farkas lemma states that, if it holds, a solution to the LHS in terms of individual rates exists. In the next paragraphs, we prove (by contradiction) that alternative (ii) does *not* hold for our problem. To that aim, we start by defining $\mathbf{y} \triangleq [k_{r_{11}}, \ldots, k_{r_{KK}}, k_{c_1}, \ldots, k_{c_K}]^T$. Assume that alternative (ii) holds. To satisfy the condition $\mathbf{y}^T\mathbf{A} \geq 0$, there must exist a nonnegative set of coefficients $k_{r_{ii}}$ and k_{c_i} such that

$$k_{r_{ii}} + k_{c_j} \geq 0, \quad i = 1, \ldots, K, j = i, \ldots, i + d - 1. \tag{4.55}$$

And, condition $\mathbf{y}^T\mathbf{b} < 0$ can be rewritten as

$$\textstyle\sum_{i=1}^{K} k_{r_{ii}} r_{ii} + \sum_{i=1}^{K} k_{c_i} c_i < 0. \tag{4.56}$$

Next, we will check that for any set of valid $k_{r_{ii}}$ and k_{c_j} equation (4.56) does not hold. To that aim, we will determine the lowest possible value of the LHS of (4.56) subject to the inequalities given by (4.55). In other words, we need to solve an optimization (minimization) problem with the LHS of (4.56) playing the role of the objective function and (4.55) as constraints. Since r_{ii} and c_i are nonnegative, this is a linear program. Hence, the solution will lie at the vertex of the feasible region defined by (4.55) [92, Chapter 7]. Since the expressions (4.55) define a convex cone, its only vertex is given by

$$k_{r_{ii}} + k_{c_j} = 0, \quad i = 1, \ldots, K, j = i, \ldots, i + d - 1. \tag{4.57}$$

By recursively analyzing the various equations in (4.57), we conclude that necessarily

$$k \triangleq k_{r_{ii}} = -k_{c_i}, \quad i = 1, \ldots, K. \tag{4.58}$$

That is, except for the sign, all the coefficients are identical. By replacing (4.58) into the LHS of (4.56), the objective function in the optimization problem becomes

$$k \textstyle\sum_{i=1}^{K} r_{ii} - k \sum_{i=1}^{K} c_i. \tag{4.59}$$

From (4.50a) and (4.50b), we have that $\sum_{i=1}^{K} r_{ii} \leq \sum_{i=1}^{K} c_i$. That is, the sum of cumulative rates of all sources is *below or equal to* the channel capacity over all time slots.

However, since the objective function in (4.35) is nonincreasing in all r_{ij}, the optimal solution of (4.35) must satisfy $\sum_{i=1}^{K} r_{ii} = \sum_{i=1}^{K} c_i$ (i.e., with equality). This means that, necessarily, (4.59) is lower bounded by 0, hence, (4.56) does not hold and, in turn, alternative (ii) in the Farkas theorem does not hold either. This concludes the proof. ■

Chapter 5

Sensor Selection and Power Allocation Strategies

In this chapter, we investigate the problem of *jointly* selecting a predefined number of energy harvesting sensors *and* computing the optimal power allocation. The ultimate goal is to minimize the reconstruction distortion at the fusion center. This optimization problem is, unfortunately, non-convex. To circumvent that, we propose two suboptimal strategies: (i) a *joint* sensor selection and power allocation (JSS-EH) scheme that, we prove, is capable of iteratively finding a stationary solution of the original problem from a sequence of surrogate convex problems; and (ii) a *separate* sensor selection and power allocation (SS-EH) scheme, on which basis we can identify a sensible sensor selection and analytically find a power allocation policy by solving a convex problem. We also discuss the interplay between the two strategies. Alternatively, we also propose a sparse sensor selection (SSS-EH) scheme, where we promote sparsity directly in the power allocation vector. Performance in terms of reconstruction distortion, impact of initialization, actual subsets of selected sensors and computed power allocation policies, etc., is assessed by means of computer simulations. To that aim, an EH-agnostic sensor selection strategy, a lower bound on distortion, and an online version of the SS-EH and JSS-EH schemes are derived and used for benchmarking.

5.1 Introduction

Current technological advances make it feasible to deploy inexpensive sensors in *large* numbers. In this context, the problem of optimally selecting a subset of sensors to perform a given task naturally arises. This often stems from resource (e.g., bandwidth), interference level or energy consumption constraints, which make massive sensor to Fusion Center (FC) communications barely recommended or simply not possible. While the aforementioned *sensor selection problem* is combinatorial in nature, Joshi and Boyd

studied in [95] a convex relaxation allowing to (approximately) solve the problem with a reasonable computational cost. Other more recent approaches leverage on the inherent sparsity of the problem. For instance, the authors in [96] investigate—both from centralized and distributed standpoints—strategies aimed to minimize the number of selected sensors subject to a given Mean Square Error (MSE) target. Non-linear measurement models (such as those in source localization and tracking problems) have been considered in [97], also in a sparsity-promoting framework. Further, the sensor selection problem has also been studied in [98] for correlated measurement noise. From an energy efficiency point of view, the authors in [99] used a sparsity-promoting penalty function to discourage the repeated selection of any sensor node in particular (e.g., the most informative ones). By doing so, uneven battery drainage can be prevented. Likewise, the same authors propose in [100] a periodic sensor scheduling strategy which limits the number of times that a sensor can be selected and transmit in a given period of time.

5.1.1 Contribution

In this chapter, we investigate the problem of *jointly* selecting a *predefined* number of energy harvesting sensors and computing the optimal power allocation. The selection is needed due to the reduced number of sensor-to-FC channels. Our goal is to minimize the distortion in the reconstruction of the underlying source at the FC subject to the causality constraints imposed by the EH process. This is in stark contrast with the approaches in e.g., [99] [100] which were EH-agnostic. Unfortunately, the aforementioned optimization problem is not convex. For this reason, we propose *two* suboptimal *offline* strategies. First, the *joint* sensor selection and power allocation (JSS-EH) scheme is capable of finding a stationary solution to the problem on the basis of a Majorization-Minimization (MM) procedure [101]. The MM procedure allows us to identify a sequence of surrogate (and approximate) convex optimization problems that we iteratively solve. As an alternative, we propose a method to *separately* identify a sensible (and EH-aware) sensor selection and the corresponding power allocation policy. By doing so, the power allocation problem for a *given* sensor selection becomes convex. Hereinafter, this is referred to as the *separate* sensor selection and power allocation (SS-EH) scheme. Very interestingly, the corresponding power allocation policy can be analytically derived and, as we discuss, it can be interpreted as a two-dimensional [102] waterfilling solution. Besides, the SS-EH solution turns out to be a suitable initialization to compute in a relatively low number of iterations a *refined* (i.e., with lower distortion) stationary solution to the JSS-EH problem. Furthermore, we derive an *online* version of both schemes and, as an alternative approach to the problem, we also propose an sparse sensor selection (SSS-EH) scheme. In this scheme, we propose to promote sparsity in the power allocation using a log-sum penalty term, this in turn resulting into sparse sensor selection policies. We provide a majorization-minimization algorithm to find a stationary solution of the problem, which

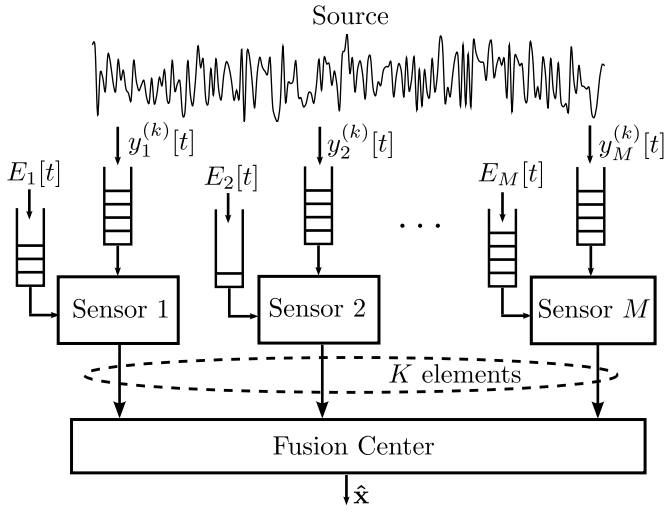

Figure 5.1: System model.

consists in the iterative minimization of a reweighted ℓ_1 penalty function. Finally, we also discuss the interplay between and conduct an extensive performance assessment of all the schemes by means of computer simulations.

The remainder of this chapter is organized as follows. In Section 5.2, we present the signal and system model. In Section 5.3, we formulate the sensor selection and power allocation problem in an energy-harvesting framework. Sections 5.4 and 5.5 are devoted to present the two proposed strategies to compute joint (JSS-EH) and separate (SS-EH) suboptimal solutions to the aforementioned optimization problem, respectively. Then, in Section 5.6 we propose an alternative scheme (SSS-EH) based on promoting sparsity in the power allocation vector. Next, in Section 5.7, we extensively assess the performance of the proposed strategies. Finally, we close the chapter by providing some concluding remarks in Section 5.8.

5.2 System Model

Consider the system model illustrated in Figure 5.1, comprising a wireless sensor network composed of M energy harvesting sensor nodes (with index set $\mathcal{M} \triangleq \{1, \ldots, M\}$) and one fusion center deployed to estimate an underlying source $\mathbf{x} \in \mathbb{R}^m$, with $\mathbf{x} \sim \mathcal{N}(0, \mathbf{\Sigma}_x)$. We consider a time-slotted system with T time slots indexed by the set $\mathcal{T} \triangleq \{1, \ldots, T\}$ of duration T_s. In time slot t, the stationary source $\mathbf{x}$ generates an independent and identically distributed (i.i.d.) large sequence of n samples $\{\mathbf{x}^{(k)}[t]\}_{k=1}^n = \{\mathbf{x}^{(1)}[t], \ldots, \mathbf{x}^{(n)}[t]\}$. As in [95], source samples and sensor measurements are related through the following linear model:

$$y_i^{(k)}[t] = \mathbf{a}_i^T \mathbf{x}^{(k)}[t] + w_i^{(k)}[t], \qquad \begin{array}{l} k = 1, \ldots, n \\ i \in \mathcal{Z}_t, \end{array} \tag{5.1}$$

where $\{w_i^{(k)}[t]\}_{k=1}^n$ stands for i.i.d., zero-mean Gaussian observation noise of variance σ_w^2; vector $\mathbf{a}_i$ gathers the *known* coefficients of the linear model at the i-th sensor; and $\mathcal{Z}_t \subseteq \mathcal{M}$ denotes the subset of active (selected) sensors in time slot t, with cardinality $|\mathcal{Z}_t|$. The ultimate goal is to reconstruct at the FC the sequence $\{\mathbf{x}^{(k)}[t]\}_{k=1}^n$ in each time slot. To that aim, a total of $K \leq M$ *orthogonal* channels are available for sensor-to-FC channel communications. Therefore, the number of sensors selected in each time slot must satisfy $|\mathcal{Z}_t| \leq K$.

In the sequel, we assume separability of source and channel coding. As far as *source* coding is concerned, we adopt a rate-distortion optimal encoder. Assuming a quadratic distortion measure at the FC, the encoded measurements at the sensor nodes can be modeled as a sequence of auxiliary random variables $\{u_i^{(k)}[t]\}_{k=1}^n$ [90]:

$$u_i^{(k)}[t] = \mathbf{a}_i^T \mathbf{x}^{(k)}[t] + w_i^{(k)}[t] + q_i^{(k)}[t], \qquad \begin{matrix} k = 1, \ldots, n \\ i \in \mathcal{Z}_t, \end{matrix} \tag{5.2}$$

with $q_i^{(k)}[t] \sim \mathcal{N}\left(0, \sigma_{q_i}^2[t]\right)$ modeling the i.i.d. encoding noise. The average encoding rate per sample $R_i[t]$ must satisfy the rate-distortion theorem [85], that is,

$$\begin{aligned} R_i[t] \geq I(y_i[t]; u_i[t]) &= h(u_i[t]) - h(u_i[t]|y_i[t]), \\ &= \frac{1}{2} \log\left(1 + \frac{\mathbf{a}_i^T \boldsymbol{\Sigma}_x \mathbf{a}_i + \sigma_w^2}{\sigma_{q_i}^2[t]}\right) \end{aligned} \tag{5.3}$$

for all $i \in \mathcal{Z}_t$. Further, we assume that each *active* sensor encodes its observations at the maximum *channel* rate which is given by the Shannon capacity formula[1]. Hence we have $R_i[t] = \frac{1}{2}\log(1 + h_i[t]p_i[t])$, where $p_i[t]$ and $h_i[t]$ stand for the average transmit power and channel gain, respectively. From this and (5.3), the variance of the encoding noise reads

$$\sigma_{q_i}^2[t] = \frac{\mathbf{a}_i^T \boldsymbol{\Sigma}_x \mathbf{a}_i + \sigma_w^2}{h_i[t]p_i[t]}, \quad i \in \mathcal{Z}_t. \tag{5.4}$$

Finally, by means of a Minimum Mean Square Error (MMSE) estimator [94] the FC[2] reconstructs $\{\mathbf{x}^{(k)}[t]\}_{k=1}^n$ from the received codewords $\{u_i^{(k)}[t]\}_{k=1}^n$ $i \in \mathcal{Z}_t$. The average (MSE) distortion in time slot $t \in \mathcal{T}$ is given by [94]

$$D[t] = \operatorname{tr}\left(\sum_{i=1}^{M} \frac{z_i[t]}{\sigma_w^2 + \sigma_{q_i}^2[t]} \mathbf{a}_i \mathbf{a}_i^T + \boldsymbol{\Sigma}_x^{-1}\right)^{-1}, \tag{5.5}$$

[1]For simplicity, we let the number of channel uses per sensor be equal to the number of samples in a time slot.

[2]The FC collects all measurements and computes the MMSE estimate of the underlying source. Given a general linear model of the form $\mathbf{y} = \mathbf{A}\mathbf{x} + \mathbf{w}$, with $\mathbf{x} \sim \mathcal{N}(0, \mathbf{C_x})$, and $\mathbf{w} \sim \mathcal{N}(0, \mathbf{C_w})$, the MMSE estimate turns out to be $\hat{\mathbf{x}} = \mathbf{C_{xy}}\mathbf{C_y}^{-1}\mathbf{y}$ with distortion given by $D_{\text{MMSE}} = \operatorname{tr}(\mathbf{C_{xy}}\mathbf{C_y}^{-1}\mathbf{C_{xy}}^T + \mathbf{C_x})^{-1}$, where $\mathbf{C_y} = \mathbb{E}[\mathbf{y}\mathbf{y}^T]$ and $\mathbf{C_{xy}} = \mathbb{E}[\mathbf{x}\mathbf{y}^T]$.

where $\mathrm{tr}(\cdot)$ denotes the trace operator[3], and $\mathbf{z}[t] = [z_1[t], \ldots, z_M[t]]^T$ stands for the sensor selection vector, with $z_i[t] = 1$ if $i \in \mathcal{Z}_t$ and $z_i[t] = 0$ otherwise. By substituting expression (5.4) in (5.5) and defining $\xi_i[t] \triangleq \left(\frac{\mathbf{a}_i^T \boldsymbol{\Sigma}_x \mathbf{a}_i / \sigma_w^2 + 1}{h_i[t]}\right)$, the distortion can be rewritten as

$$D[t] = \mathrm{tr}\left(\frac{1}{\sigma_w^2}\sum_{i=1}^{M}\frac{p_i[t]z_i[t]}{p_i[t]+\xi_i[t]}\mathbf{a}_i\mathbf{a}_i^T + \boldsymbol{\Sigma}_x^{-1}\right)^{-1}. \tag{5.6}$$

5.3 Problem Statement: Sensor Selection and Power Allocation in an Energy Harvesting Framework

Since sensor nodes are capable of harvesting energy from the environment, the average transmit power, $p_i[t]$ in (5.6), is necessarily constrained by the amount of scavenged energy. Hence, in time slot $t \in \mathcal{T}$ we have

$$T_s\sum_{l=1}^{t} p_i[l] \leq \sum_{l=1}^{t} E_i[l], \quad t \in \mathcal{T}, i \in \mathcal{M}. \tag{5.7}$$

where $E_i[t]$ denotes the energy harvested by the i-th sensor node in time slot t. In this context, our goal is to *jointly* determine the optimal sensor selection and power allocation strategy that (i) satisfies the above constraints imposed by the energy harvesting process; (ii) selects K sensors in each time slot; and, by doing so, (iii) minimizes the sum distortion (5.6) over the T time slots. Accordingly, the optimization problem reads

$$\underset{\mathbf{z}[t],\mathbf{p}[t]}{\text{minimize}} \quad \sum_{t=1}^{T}\mathrm{tr}\left(\frac{1}{\sigma_w^2}\sum_{i=1}^{M}\frac{p_i[t]z_i[t]}{p_i[t]+\xi_i[t]}\mathbf{a}_i\mathbf{a}_i^T + \boldsymbol{\Sigma}_x^{-1}\right)^{-1} \tag{5.8a}$$

$$\text{subject to} \quad T_s\sum_{l=1}^{t} p_i[l] \leq \sum_{l=1}^{t} E_i[l], \forall t \in \mathcal{T}, \forall i \in \mathcal{M} \tag{5.8b}$$

$$\mathbf{1}^T\mathbf{z}[t] = K, \quad \forall t \in \mathcal{T} \tag{5.8c}$$

$$\mathbf{z}[t] \in \{0,1\}^M, \quad \forall t \in \mathcal{T} \tag{5.8d}$$

$$\mathbf{p}[t] \geq \mathbf{0}, \quad \forall t \in \mathcal{T} \tag{5.8e}$$

where $\mathbf{p}[t] = [p_1[t], \ldots, p_M[t]]^T$ stands for the power allocation vector in a given time slot; $\mathbf{1}$ and $\mathbf{0}$ denote the all-ones and all-zeros vectors of appropriate dimension, respectively; and vector inequality (5.8e) is defined element-wise. By introducing the auxiliary vector

[3]Throughout this chapter we adopt the widely accepted notational convention by which the inverse operator precedes the trace operator. That is, $\mathrm{tr}(\mathbf{X})^{-1}$ is understood as $\mathrm{tr}((\mathbf{X})^{-1})$.

$\mathbf{s}[t] = [s_1[t], \ldots, s_M[t]]^T$, the optimization problem can be conveniently rewritten as:

$$\underset{\mathbf{z}[t],\mathbf{s}[t],\mathbf{p}[t]}{\text{minimize}} \quad \sum_{t=1}^{T} \operatorname{tr}\left(\sum_{i=1}^{M} \frac{s_i[t]}{\sigma_w^2}\mathbf{a}_i\mathbf{a}_i^T + \mathbf{\Sigma}_x^{-1}\right)^{-1} \tag{5.9a}$$

$$\text{subject to} \quad s_i[t] \leq \frac{p_i[t]z_i[t]}{p_i[t] + \xi_i[t]}, \forall t \in \mathcal{T}, \forall i \in \mathcal{M} \tag{5.9b}$$

$$T_s \sum_{l=1}^{t} p_i[l] \leq \sum_{l=1}^{t} E_i[l], \forall t \in \mathcal{T}, \forall i \in \mathcal{M} \tag{5.9c}$$

$$\mathbf{1}^T\mathbf{z}[t] = K, \quad \forall t \in \mathcal{T} \tag{5.9d}$$

$$\mathbf{z}[t] \in \{0,1\}^M, \quad \forall t \in \mathcal{T} \tag{5.9e}$$

$$\mathbf{p}[t] \geq \mathbf{0}, \quad \forall t \in \mathcal{T} \tag{5.9f}$$

$$\mathbf{s}[t] \geq \mathbf{0}, \quad \forall t \in \mathcal{T}. \tag{5.9g}$$

Clearly, the optimization problems (5.8) and (5.9) are equivalent. To see that, note that the objective function is strictly decreasing in $s_i[t]$. Therefore, the optimal solution to problem (5.9), namely $\{(z_i^\star[t], s_i^\star[t], p_i^\star[t])\}_{i\in\mathcal{M},t\in\mathcal{T}}$, must satisfy constraint (5.9b) with equality (since, otherwise, there would be some $s_i[t] > s_i^\star[t]$ for which distortion would be lower, which is a contradiction). That is, we necessarily have $s_i[t] = s_i^\star[t] = p_i^\star[t]z_i^\star[t]/(p_i^\star[t] + \xi_i[t]), \forall t \in \mathcal{T}, \forall i \in \mathcal{M}$ which renders the two optimization problems equivalent.

Unfortunately, problem (5.9) is non-convex due to the Boolean variable $\mathbf{z}[t] \in \{0,1\}^M$ and the product of variables $p_i[t]$ and $z_i[t]$ in constraint (5.9b). The use of Boolean variables in constraint (5.9e), renders the sensor selection problem combinatorial in nature and, in general, NP-hard. To circumvent that, we relax the boolean constraint by letting variable $z_i[t]$ take values in the real-valued interval $[0, 1]$ [95]. The optimization problem now reads

$$\underset{\mathbf{z}[t],\mathbf{s}[t],\mathbf{p}[t]}{\text{minimize}} \quad \sum_{t=1}^{T} \operatorname{tr}\left(\sum_{i=1}^{M} \frac{s_i[t]}{\sigma_w^2}\mathbf{a}_i\mathbf{a}_i^T + \mathbf{\Sigma}_x^{-1}\right)^{-1} \tag{5.10a}$$

$$\text{subject to} \quad s_i[t] \leq \frac{p_i[t]z_i[t]}{p_i[t] + \xi_i[t]}, \forall t \in \mathcal{T}, \forall i \in \mathcal{M} \tag{5.10b}$$

$$T_s \sum_{l=1}^{t} p_i[l] \leq \sum_{l=1}^{t} E_i[l], \forall t \in \mathcal{T}, \forall i \in \mathcal{M} \tag{5.10c}$$

$$\mathbf{1}^T\mathbf{z}[t] = K, \quad \forall t \in \mathcal{T} \tag{5.10d}$$

$$\mathbf{z}[t] \in [0,1]^M, \quad \forall t \in \mathcal{T} \tag{5.10e}$$

$$\mathbf{p}[t] \geq \mathbf{0}, \quad \forall t \in \mathcal{T} \tag{5.10f}$$

$$\mathbf{s}[t] \geq \mathbf{0}, \quad \forall t \in \mathcal{T}. \tag{5.10g}$$

Still, constraint (5.10b) prevents the optimization problem from being convex. Consequently, one cannot find a global minimizer without resorting to an exhaustive search of

the optimization space. Global optimization techniques such as the so-called branch and bound [103] can yield an ϵ-optimal solution but typically exhibit low converge rates and poor scalability with problem dimension.

To alleviate this, we propose two *suboptimal* strategies: an iterative scheme capable of finding a stationary solution to the problem (5.10) of *jointly* determining the sensor selection and power allocation policies (Section 5.4); and a method to *separately* identify a sensible sensor selection and a power allocation policy (Section 5.5). Also, we highlight the interplay between these two strategies.

5.4 Joint Sensor Selection and Power Allocation with Energy Harvesting (JSS-EH)

Here, we focus on finding a stationary (i.e., at least locally optimal) solution to the problem. To that aim, we resort to a Majorization-Minimization procedure (MM) which is explained below. This technique allows us to iteratively identify a sequence of surrogate (and approximate) convex optimization problems that we attempt to solve.

We start by rearranging the terms of the non-convex constraint (5.10b) as follows:

$$s_i[t]p_i[t] - p_i[t]z_i[t] + s_i[t]\xi_i[t] \leq 0. \tag{5.11}$$

The terms $f(s_i[t], p_i[t]) \triangleq s_i[t]p_i[t]$ and $g(p_i[t], z_i[t]) \triangleq -p_i[t]z_i[t]$, which are bilinear in the optimization variables, can be alternatively expressed as a difference of convex functions:

$$f(s_i[t], p_i[t]) = \frac{1}{2}\left(s_i[t] + p_i[t]\right)^2 - \frac{1}{2}\left(s_i[t]^2 + p_i[t]^2\right), \tag{5.12}$$

$$g(p_i[t], z_i[t]) = \frac{1}{2}\left(z_i[t]^2 + p_i[t]^2\right) - \frac{1}{2}\left(z_i[t] + p_i[t]\right)^2. \tag{5.13}$$

In the k-th iteration, we obtain a *majorizer* of expression (5.11) by linearizing the concave (second) terms of (5.12) and (5.13) in the neighborhood of the solution found in the previous iteration $(z_i^{(k)}[t], s_i^{(k)}[t], p_i^{(k)}[t])$, namely

$$\begin{aligned}\bar{f}^{(k)}(s_i[t], p_i[t]) \triangleq\ & \frac{1}{2}\left(s_i[t] + p_i[t]\right)^2 - \frac{1}{2}\left(s_i^{(k)}[t]^2 + p_i^{(k)}[t]^2\right) \\ & - s_i^{(k)}[t]\left(s_i[t] - s_i^{(k)}[t]\right) \\ & - p_i^{(k)}[t]\left(p_i[t] - p_i^{(k)}[t]\right),\end{aligned} \tag{5.14}$$

$$\begin{aligned}\bar{g}^{(k)}(z_i[t], p_i[t]) \triangleq\ & \frac{1}{2}\left(z_i[t]^2 + p_i[t]^2\right) - \frac{1}{2}\left(z_i^{(k)}[t] + p_i^{(k)}[t]\right)^2 \\ & - \left(z_i^{(k)}[t] + p_i^{(k)}[t]\right)\left(z_i[t] - z_i^{(k)}[t]\right) \\ & - \left(z_i^{(k)}[t] + p_i^{(k)}[t]\right)\left(p_i[t] - p_i^{(k)}[t]\right).\end{aligned} \tag{5.15}$$

Algorithm 5.1 Joint sensor selection and power allocation.

1: **Initialize:** Set $k := 0$ and initialize $(\mathbf{z}^{(0)}[t], \mathbf{s}^{(0)}[t], \mathbf{p}^{(0)}[t])$ to a feasible point.
2: **Step 1:** Update $\bar{f}^{(k)}$ and $\bar{g}^{(k)}$ according (5.14) and (5.15), respectively.
3: **Step 2:** Compute $(\mathbf{z}^{(k+1)}[t], \mathbf{s}^{(k+1)}[t], \mathbf{p}^{(k+1)}[t])$ by solving the optimization problem (5.16).
4: **Step 3:** Let $k := k + 1$ and go to Step 1 until convergence.
5: **Step 4:** Set $\mathbf{z}^{\star}[t]$ to 1 for the K largest entries in each time slot and 0 otherwise.

All this results into the following surrogate convex optimization problem for the k-th iteration:

$$\underset{\mathbf{z}[t],\mathbf{s}[t],\mathbf{p}[t]}{\text{minimize}} \quad \sum_{t=1}^{T} \operatorname{tr}\left(\sum_{i=1}^{M} \frac{s_i[t]}{\sigma_w^2}\mathbf{a}_i\mathbf{a}_i^T + \mathbf{\Sigma}_x^{-1}\right)^{-1} \tag{5.16a}$$

$$\text{subject to} \quad \bar{f}^{(k)}(s_i[t], p_i[t]) + \bar{g}^{(k)}(p_i[t], z_i[t]) + s_i[t]\xi_i[t] \leq 0, \forall t \in \mathcal{T}, \forall i \in \mathcal{M} \tag{5.16b}$$

$$T_s \sum_{l=1}^{t} p_i[l] \leq \sum_{l=1}^{t} E_i[l], \forall t \in \mathcal{T}, \forall i \in \mathcal{M} \tag{5.16c}$$

$$\mathbf{1}^T\mathbf{z}[t] = K, \quad \forall t \in \mathcal{T} \tag{5.16d}$$

$$\mathbf{z}[t] \in [0,1]^M, \quad \forall t \in \mathcal{T} \tag{5.16e}$$

$$\mathbf{p}[t] \geq \mathbf{0}, \quad \forall t \in \mathcal{T} \tag{5.16f}$$

$$\mathbf{s}[t] \geq \mathbf{0}, \quad \forall t \in \mathcal{T}. \tag{5.16g}$$

Finally, a stationary point of the original (non-convex) optimization problem (5.10) can be iteratively found by using Algorithm 5.1.

Proposition 5.1. *Algorithm 5.1 converges to a stationary solution (a point satisfying the KKT conditions) of the optimization problem* (5.10).

Proof. For the ease of notation, let us first collect the vectors of primal variables $\mathbf{z} = [\mathbf{z}[1]^T, \ldots, \mathbf{z}[T]^T]^T$, $\mathbf{s} = [\mathbf{s}[1]^T, \ldots, \mathbf{s}[T]^T]^T$, $\mathbf{p} = [\mathbf{p}[1]^T, \ldots, \mathbf{p}[T]^T]^T$. Let $(\mathbf{z}^{(0)}, \mathbf{s}^{(0)}, \mathbf{p}^{(0)})$ be a feasible point of the original optimization problem (5.10). Since the linearized constraint (5.16b) is an upper bound on the original constraint (5.10b), it follows that the feasible set of the surrogate problem (5.16) at iteration k, is contained in the feasible set of the original problem (5.10). Hence, all iterates are feasible.

Now, solving the optimization problem (5.16) at iteration k leads to a solution $(\mathbf{z}^{(k+1)}, \mathbf{s}^{(k+1)}, \mathbf{p}^{(k+1)})$ satisfying $\sum_{t=1}^{T} \operatorname{tr}(\sum_{i=1}^{M}(s_i^{(k+1)}[t]/\sigma_w^2)\mathbf{a}_i\mathbf{a}_i^T + \mathbf{\Sigma}_x^{-1})^{-1} \leq \sum_{t=1}^{T} \operatorname{tr}(\sum_{i=1}^{M}(s_i^{(k)}[t]/\sigma_w^2)\mathbf{a}_i\mathbf{a}_i^T + \mathbf{\Sigma}_x^{-1})^{-1}$. This follows from the fact that, by definition, the linearization is tight at the point $(\mathbf{z}^{(k)}, \mathbf{s}^{(k)}, \mathbf{p}^{(k)})$, and that by convexity of problem (5.16) we have $(\mathbf{z}^{(k+1)}, \mathbf{s}^{(k+1)}, \mathbf{p}^{(k+1)}) = (\mathbf{z}^{(k)}, \mathbf{s}^{(k)}, \mathbf{p}^{(k)})$ if $(\mathbf{z}^{(k)}, \mathbf{s}^{(k)}, \mathbf{p}^{(k)})$ is a minimizer of the $k+1$ iteration. Thus, the sequence of objective functions generated by Algorithm 5.1 is nonincreasing and bounded, therefore it converges. Denote the primal variables at this

point by $(\mathbf{z}^\star, \mathbf{s}^\star, \mathbf{p}^\star)$, and the corresponding dual variables by $\boldsymbol{\lambda}^\star$. Since problem (5.16) satisfies Slater's condition, its Lagrangian has a saddle point in $\big((\mathbf{z}^\star, \mathbf{s}^\star, \mathbf{p}^\star), \boldsymbol{\lambda}^\star\big)$.

However, since the linearization is tight at the point $(\mathbf{z}^\star, \mathbf{s}^\star, \mathbf{p}^\star)$, the gradients in the KKT conditions of problems (5.10) and (5.16) match. To see this, let $s_i[t] = s_i^\star[t] = s_i^{(k)}[t]$ and $p_i[t] = p_i^\star[t] = p_i^{(k)}[t]$ in expressions (5.14) and (5.15) (they become equivalent to (5.12) and (5.13), respectively). Therefore, Algorithm 5.1 converges to a KKT point of the optimization problem (5.10). ■

5.4.1 Remarks

A few considerations are in line. First, in order to select a subset of sensors after convergence, the (relaxed) solution $\mathbf{z}^\star[t] \in [0,1]^M$ must be forced to take Boolean values again, namely $\mathbf{z}^\star[t] \in \{0,1\}^M$. To that aim, the $\mathbf{z}^\star[t]$ vectors are cropped to their K largest entries. After that, however, we do not recompute the associated power allocation. This, however, has a negligible impact on performance since, as discussed in the numerical results section, typically just K entries in vector $\mathbf{z}^\star[t]$ are numerically close to 1, whereas the rest are approximately 0.

The second consideration is that, being the problem non-convex and Algorithm 5.1 iterative, the stationary solution at which it converges depends on the initialization (and so does performance). Hence, providing it with a suitable initialization is crucial. This will be further discussed in the next section.

Finally, note that one full convex optimization problem has to be solved in each iteration, the computational burden of which might not be negligible (in particular if the number of constraints is large). Therefore, special attention should be paid to the number of iterations needed and the increased computational burden that this entails (for some initializations, convergence can be particulary slow, see numerical results).

5.5 Separate Sensor Selection and Power Allocation with Energy Harvesting (SS-EH)

Here, we depart from the *iterative* scheme presented in the previous section. Instead, we propose a lower complexity *one shot* approach. Specifically, we propose to determine the subset of active sensors first, and then compute the optimal power allocation policy for such selection. Interestingly, the latter turns out to be a convex (and, thus, easily solvable) problem.

5.5.1 Optimal Power Allocation for a Given Sensor Selection

For a given subset $\{\mathcal{Z}_t\}_{t\in\mathcal{T}}$ of active sensors in *each* time slot, the resulting optimization problem (5.9) reads

$$\underset{\mathbf{s}[t],\mathbf{p}[t]}{\text{minimize}} \quad \sum_{t=1}^{T} \operatorname{tr}\left(\sum_{i\in\mathcal{Z}_t} \frac{s_i[t]}{\sigma_w^2}\mathbf{a}_i\mathbf{a}_i^T + \mathbf{\Sigma}_x^{-1}\right)^{-1} \tag{5.17a}$$

$$\text{subject to} \quad s_i[t] \leq \frac{p_i[t]}{p_i[t]+\xi_i[t]}, \forall t \in \mathcal{T}, \forall i \in \mathcal{M} \tag{5.17b}$$

$$T_s \sum_{l=1}^{t} p_i[l] \leq \sum_{l=1}^{t} E_i[l], \forall t \in \mathcal{T}, \forall i \in \mathcal{Z}_t \tag{5.17c}$$

$$\mathbf{p}[t] \geq \mathbf{0}, \quad \forall t \in \mathcal{T} \tag{5.17d}$$

$$\mathbf{s}[t] \geq \mathbf{0}, \quad \forall t \in \mathcal{T} \tag{5.17e}$$

where, clearly, the sensor selection vector $\mathbf{z}[t]$ has been removed from the problem formulation. Since the objective function (5.17a) is convex and the constraints (5.17b)-(5.17e) define a convex feasible set, the resulting optimization problem (5.17) is convex and therefore has a global minimizer [67]. By satisfying the Karush-Kuhn-Tucker (KKT) conditions, we can identify the necessary and sufficient conditions for optimality. Specifically, the Lagrangian of (5.17) is given by

$$\begin{aligned}\mathcal{L} = &\sum_{t=1}^{T} \operatorname{tr}\left(\sum_{i\in\mathcal{Z}_t} \frac{s_i[t]}{\sigma_w^2}\mathbf{a}_i\mathbf{a}_i^T + \mathbf{\Sigma}_x^{-1}\right)^{-1} \\ &+ \sum_{t=1}^{T}\sum_{i\in\mathcal{Z}_t} \lambda_i[t]\left(s_i[t] - \frac{p_i[t]}{p_i[t]+\xi_i[t]}\right) \\ &+ \sum_{t=1}^{T}\sum_{i\in\mathcal{Z}_t} \beta_i[t]\left(T_s\sum_{l=1}^{t} p_i[l] - \sum_{l=1}^{t} E_i[l]\right) \\ &- \sum_{t=1}^{T}\sum_{i\in\mathcal{Z}_t} \eta_i[t]p_i[t] - \sum_{t=1}^{T}\sum_{i\in\mathcal{Z}_t} \theta_i[t]s_i[t],\end{aligned} \tag{5.18}$$

where $\lambda_i[t] \geq 0$, $\beta_i[t] \geq 0$, $\eta_i[t] \geq 0$ and $\theta_i[t] \geq 0$ are the corresponding dual variables. By taking the derivative of the Lagrangian with respect to $p_i[t]$, we get

$$\frac{\partial\mathcal{L}}{\partial p_i[t]} = \frac{-\lambda_i[t]\left(p_i[t]+\xi_i[t]\right) + \lambda_i[t]p_i[t]}{\left(p_i[t]+\xi_i[t]\right)^2} + T_s\sum_{l=t}^{T}\beta_i[l] - \eta_i[t]$$

By letting $\frac{\partial\mathcal{L}}{\partial p_i[t]} = 0$ and applying the complementary slackness condition $\eta_i[t]p_i^\star[t] = 0$, the optimal power allocation $p_i^\star[t]$ follows:

$$p_i^\star[t] = \sqrt{\frac{\xi_i[t]\lambda_i[t]}{T_s}}\left[\frac{1}{\sqrt{\sum_{l=t}^{T}\beta_i[l]}} - \sqrt{\frac{\xi_i[t]T_s}{\lambda_i[t]}}\right]^+. \tag{5.19}$$

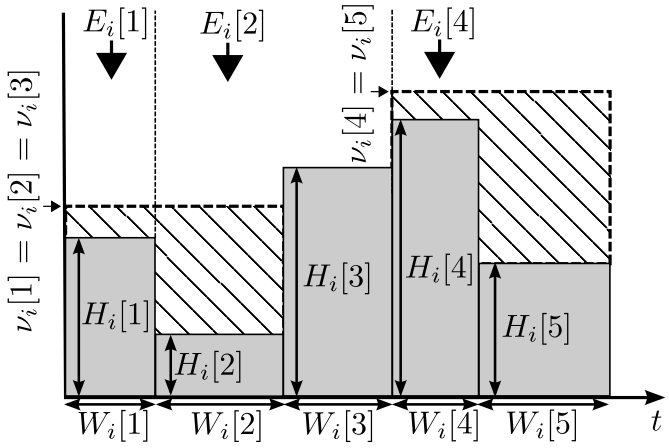

Figure 5.2: Two-dimensional directional waterfilling for a sensor $i \in \mathcal{M}$ in a scenario with $T = 5$ time slots and energy arrivals in time slots 1,2 and 4.

This solution can be interpreted as the two-dimensional directional waterfilling shown in Figure 5.2. For an arbitrary sensor i, each time slot is associated to a rectangle of solid material of width $W_i[t] \triangleq \sqrt{\xi_i[t]\lambda_i[t]/T_s}$ and height $H_i[t] \triangleq \sqrt{\xi_i[t]T_s/\lambda_i[t]}$. Right-permeable walls are placed at each time slot with an energy arrival ($t = 1, 2, 4$), this accounting for the causality of energy consumption. Water is then poured up to a waterlevel given by $\nu_i[t] \triangleq 1/\sqrt{\sum_{l=t}^{T} \beta_i[l]}$. Finally, the corresponding power allocation is given by the area of water above the solid rectangle.

Next, the derivative of the Lagrangian w.r.t. $s_i[t]$ yields

$$\frac{\partial \mathcal{L}}{\partial s_i[t]} = -\operatorname{tr}\left(\left(\sum_{j\in\mathcal{Z}_t} \frac{s_j[t]}{\sigma_w^2}\mathbf{a}_j\mathbf{a}_j^T + \mathbf{\Sigma}_x^{-1}\right)^{-2}\left(\mathbf{a}_i\mathbf{a}_i^T\right)\right) + \lambda_i[t] - \theta_i[t]. \tag{5.20}$$

Unfortunately, from (5.20) no closed-form expression can be found for $s_i^\star[t]$. Hence, $s_i[t]$ will be iteratively updated by means of the projected gradient method [68].

Algorithm 5.2 summarizes the proposed procedure for the computation of the optimal power allocation. Specifically, we use an Uzawa update step [104] to find the optimal primal-dual saddle point of the optimization problem (5.17). In this way, at each iteration we do an exact minimization of the power allocation $\{p_i[t]\}$ while we iteratively update both the auxiliary $\{s_i[t]\}$ and the dual $\{\lambda_i[t]\}$ variables. Convergence of Algorithm 2 is trivially satisfied by the Arrow-Hurwicz-Uzawa method, as it is shown next.

Proposition 5.2. *Algorithm 5.2 converges to the global minimum of the optimization problem* (5.17).

Proof. For the ease of notation, let us first collect the vectors of primal variables $\mathbf{s} = [\mathbf{s}[1]^T, \ldots, \mathbf{s}[T]^T]^T$, $\mathbf{p} = [\mathbf{p}[1]^T, \ldots, \mathbf{p}[T]^T]^T$, and let $\boldsymbol{\lambda}$ be the vector of all dual variables. Since problem (5.17) satisfies Slater's condition, the Lagrangian (5.18) of this

Algorithm 5.2 Optimal power allocation for a given sensor selection.

1: **Initialize:** $\{\lambda_i[t]\} := 0$, $\{s_i[t]\} := 0$, select ϵ.
2: **Step 1:** For all $t \in \mathcal{T}$ and $i \in \mathcal{Z}_t$, update primal variables.
3: $s_i^{(k+1)}[t] := \left[s_i^{(k)}[t] - \epsilon \left(\lambda_i^{(k)}[t] - \operatorname{tr}\left(\left(\sum_{j \in \mathcal{Z}_t} \frac{s_j^{(k)}}{\sigma_w^2}[t] \mathbf{a}_j \mathbf{a}_j^T + \boldsymbol{\Sigma}_x^{-1} \right)^{-2} \left(\mathbf{a}_i \mathbf{a}_i^T \right) \right) \right) \right]^+$
4: $p_i^{(k+1)}[t] := \sqrt{\frac{\xi_i[t]\lambda_i^{(k)}[t]}{T_s}} \left[\frac{1}{\sqrt{\sum_{l=t}^{T} \beta_i[l]}} - \sqrt{\frac{\xi_i[t] T_s}{\lambda_i^{(k)}[t]}} \right]^+$
5: **Step 2:** For all $t \in \mathcal{T}$ and $i \in \mathcal{Z}_t$, update dual variable.
6: $\lambda_i^{(k+1)}[t] := \left[\lambda_i^{(k)}[t] + \epsilon \left(s_i^{(k+1)}[t] - \frac{p_i^{(k+1)}[t]}{p_i^{(k+1)}[t] + \xi_i[t]} \right) \right]^+$
7: **Step 3:** Go to Step 1 until termination condition is met.

optimization problem satisfies the saddle-point property, namely

$$\min_{\mathbf{s},\mathbf{p}} \max_{\boldsymbol{\lambda}} \mathcal{L}(\mathbf{s}, \mathbf{p}, \boldsymbol{\lambda}) = \max_{\boldsymbol{\lambda}} \min_{\mathbf{s},\mathbf{p}} \mathcal{L}(\mathbf{s}, \mathbf{p}, \boldsymbol{\lambda}). \tag{5.21}$$

Let us define $\mathbf{p}^\star(\boldsymbol{\lambda}) \triangleq \arg\min_{\mathbf{p}} \mathcal{L}(\mathbf{s}, \mathbf{p}, \boldsymbol{\lambda})$, then for Algorithm 5.2 to converge by the Uzawa method [104], the saddle-point property must also be satisfied given $\mathbf{p}^\star(\boldsymbol{\lambda})$ for all $\mathbf{s}$, that is

$$\min_{\mathbf{s}} \max_{\boldsymbol{\lambda}} \mathcal{L}(\mathbf{s}, \mathbf{p}^\star(\boldsymbol{\lambda}), \boldsymbol{\lambda}) = \max_{\boldsymbol{\lambda}} \min_{\mathbf{s}} \mathcal{L}(\mathbf{s}, \mathbf{p}^\star(\boldsymbol{\lambda}), \boldsymbol{\lambda}). \tag{5.22}$$

This is equivalent to

$$\min_{\mathbf{s}} \min_{\mathbf{p}} \max_{\boldsymbol{\lambda}} \mathcal{L}(\mathbf{s}, \mathbf{p}, \boldsymbol{\lambda}) = \min_{\mathbf{s}} \max_{\boldsymbol{\lambda}} \min_{\mathbf{p}} \mathcal{L}(\mathbf{s}, \mathbf{p}, \boldsymbol{\lambda}), \tag{5.23}$$

which is to say that the Lagrangian (5.18) must have a saddle point in $(\mathbf{p}, \boldsymbol{\lambda})$ for all $\mathbf{s}$, namely

$$\min_{\mathbf{p}} \max_{\boldsymbol{\lambda}} \mathcal{L}(\mathbf{s}, \mathbf{p}, \boldsymbol{\lambda}) = \max_{\boldsymbol{\lambda}} \min_{\mathbf{p}} \mathcal{L}(\mathbf{s}, \mathbf{p}, \boldsymbol{\lambda}). \tag{5.24}$$

This corresponds to solving optimization problem (5.17) with a fixed value of $\mathbf{s}$. Since this problem also satisfies Slater's condition, the saddle-point property (5.24) is satisfied. Therefore, convergence of the Algorithm 5.2 follows by convergence of the inexact Uzawa algorithm [105, Theorem 3.1]. ■

5.5.2 EH-aware Sensor Selection

For a system *without* energy harvesting sensors, Joshi and Boyd [95] propose to compute the sensor selection policy by solving the convex program

$$\begin{aligned} \underset{\mathbf{z}}{\text{minimize}} \quad & \operatorname{tr}\left(\sigma_w^{-2} \sum_{i=1}^{M} z_i \mathbf{a}_i \mathbf{a}_i^T + \boldsymbol{\Sigma}_x^{-1} \right)^{-1} \\ \text{subject to} \quad & \mathbf{1}^T \mathbf{z} = K, \;\; \mathbf{z} \in [0,1]^M. \end{aligned} \tag{5.25}$$

and constructing the selection sets $\{\mathcal{Z}_t\}_{t\in\mathcal{T}}$ from the K largest elements in the *sensor selection* vector $\mathbf{z}^\star[t]$ (in our case, the *same* subset of sensors for *all* time slots). This indexed family of sets $\{\mathcal{Z}_t\}_{t\in\mathcal{T}}$ can then be used to solve the optimization problem (5.17) in the preceding subsection and, by doing so, compute the (associated) optimal power allocation.

This EH-agnostic policy[4] might select sensors which do not have any harvested energy yet. To circumvent that, we propose a (heuristic) EH-aware sensor selection policy. First, we let $\mathcal{Z}_t = \mathcal{M}$ and solve problem (5.17). Clearly, $s_i[t]$ in (5.17) plays the same role as z_i does in (5.25), namely, it weights the contribution of each sensor to the resulting distortion. Motivated by this, an intuitive selection rule consists in choosing for *each* time slot t the K largest elements in vector $\mathbf{s}^\star[t]$. With the indexes of these elements, we form the new selection sets $\{\mathcal{Z}_t\}_{t\in\mathcal{T}}$. And by solving problem (5.17) again with this new indexed family of sets, we obtain the corresponding optimal power allocation. The main difference is that, now, $\mathbf{s}^\star[t]$ takes into account not only the impact of $\mathbf{a}_i$ but also the actual energy arrivals via the energy causality constraint (5.17c).

5.5.3 Remarks

As discussed earlier, the computational complexity of the *separate* sensor selection and power allocation approach (SS-EH), which is one-shot, is lower than that of the *joint* one (JSS-EH) presented in the previous section, which is iterative. However, no guarantee on the optimality of either solution can be given. Still, if the former is initialized with the solution to the latter, it will be capable of *refining* it. To recall, we proved that JSS-EH always converges to a stationary solution of the original problem. Therefore, the resulting distortion after convergence will necessary be lower (i.e., a *refined* solution). In general, the solution to the separate optimization problem turns out to be a suitable initialization for the JSS-EH scheme.

5.5.4 Online SS-EH Strategy

The proposed SS-EH scheme requires *non-causal* knowledge on energy arrivals. Here, instead, we introduce a more realistic *online* version just requiring *causal* knowledge[5].

Inspired by [52], a *myopic* online policy can be computed as follows. Assume for a moment that, after harvesting some energy in the initial time slot, no additional energy is harvested by the sensors. Hence, we let $E_i[1] > 0$ and $E_i[2] = \cdots = E_i[T] = 0$ for all i, and solve the sensor selection and power allocation problem (5.17) for $t = 1, \ldots, T$.

[4]Note that it only takes into account the impact of $\mathbf{a}_i$, i.e., the set of coefficients in the linear observation model of each node.

[5]Likewise, an online version can be derived for the JSS-EH scheme. However, we focus on SS-EH, for brevity. Nonetheless, numerical results are provided in Section 5.7 for both schemes.

In the absence of knowledge on future energy arrivals, this is also a sensible approach. After all, the reconstruction distortion is minimized if no additional energy is harvested. Let $t_o \leq T$ denote the next time slot in which some energy is harvested by an arbitrary sensor i_o i.e., $E_{i_o}[t_o] > 0$). For the preceding time slots (i.e., $t = 1, \ldots, t_o - 1$), we impose that the subsets of active sensors and the power allocation just computed remain unchanged. Hence, the remaining (unspent) energy at the beginning of time slot t_o reads $E_i^u[t_o] = \sum_{t=1}^{t_o-1} E_i[t] - T_s \sum_{t=1}^{t_o-1} p_i[t]$ for *all* i. Further, we let

$$E_i[t_o] := \begin{cases} E_i^u[t_o] + E_i[t_o] & \text{if } i = i_o, \\ E_i^u[t_o] & \text{if } i \neq i_o, \end{cases} \tag{5.26}$$

$E_i[t_o + 1], \ldots, E_i[T] := 0$ for all i and, then, we compute the sensor selection and power allocation for $t = t_o, \ldots, T$, that is, for all subsequent time slots. This procedure is iterated until all energy arrivals have been accounted for. The interesting property of such scheme is its ability to adjust (recompute) the remaining subsets of active sensors and power allocations whenever some additional energy is harvested. By doing so, the additional (and causal) knowledge on energy arrivals is effectively exploited. This myopic policy, however, has side effect: it tends to generate *conservative* power allocation patterns. That is, it tends to shift power allocation towards the *end* of the observation period (i.e., time slot T). To recall, when the power allocation is recomputed after harvesting some energy, the working assumption is that no additional energy will be harvested anymore. Consequently, the algorithm tends to spend energy very slowly, to make sure that for each sensor some energy is left for data transmission for the whole observation window (since, it can be shown that transmitting over longer time periods results into lower distortion).

5.6 Sparse Sensor Selection and Power Allocation with Energy Harvesting (SSS-EH)

As thoroughly discussed in the previous sections, the introduction of the selection variable $z_i[t]$ in optimization problem (5.9) leads to the non-convex bilinear form $p_i[t]z_i[t]$. In this section, we propose an alternative approach to circumvent this problem. Instead of restricting the selection to a *predefined* number of sensors, we promote *sparsity* in the

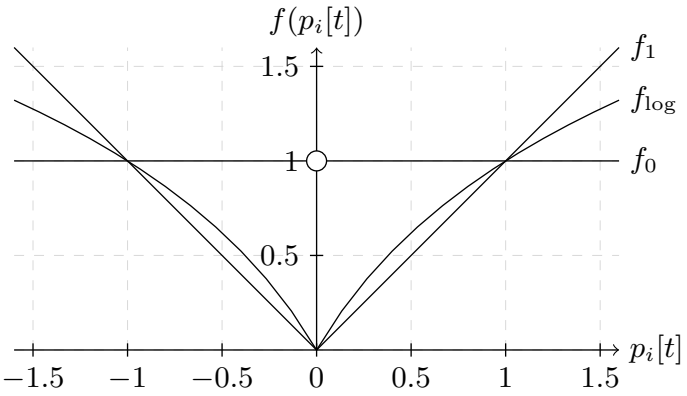

Figure 5.3: Sparsity-promoting penalty functions.

power allocation vector $\mathbf{p}[t]$ itself. The resulting optimization problem thus reads

$$\underset{\mathbf{s}[t],\mathbf{p}[t]}{\text{minimize}} \quad \sum_{t=1}^{T} \operatorname{tr}\left(\sum_{i=1}^{M} \frac{s_i[t]}{\sigma_w^2}\mathbf{a}_i\mathbf{a}_i^T + \mathbf{\Sigma}_x^{-1}\right)^{-1} + \lambda \sum_{t=1}^{T} f(\mathbf{p}[t]) \tag{5.27a}$$

$$\text{subject to} \quad s_i[t] \leq \frac{p_i[t]}{p_i[t]+\xi_i[t]}, \forall t \in \mathcal{T}, \forall i \in \mathcal{M} \tag{5.27b}$$

$$T_s \sum_{l=1}^{t} p_i[l] \leq \sum_{l=1}^{t} E_i[l], \forall t \in \mathcal{T}, \forall i \in \mathcal{M} \tag{5.27c}$$

$$\mathbf{p}[t] \geq \mathbf{0}, \quad \forall t \in \mathcal{T} \tag{5.27d}$$

$$\mathbf{s}[t] \geq \mathbf{0}, \quad \forall t \in \mathcal{T}, \tag{5.27e}$$

where $f : \mathbb{R}^M \to \mathbb{R}$ is a sparsity-inducing penalty function and λ is the corresponding sparsity parameter. For the ease of notation, in the sequel we will denote the constraints (5.27b)-(5.27e) by the convex set $\mathcal{C}$. Three common penalty functions are illustrated in Figure 5.3 for the scalar case. Namely, the ℓ_0 norm, the ℓ_1 norm and the log-sum function. Function $f_0 = \|\mathbf{p}[t]\|_0$ merely counts the non-zero elements of the input vector $\mathbf{p}[t]$, which leads to an optimization problem which is combinatorial in nature (and thus intractable). The most common convex (and thus tractable) approximation of f_0 is given by the ℓ_1 norm $f_1(\mathbf{p}[t]) = \|\mathbf{p}[t]\|_1$, which has been shown to provide good performance [106]. In our scenario, however, this results in an *homogeneous* penalization of the allocated power. That is, an increase in power allocation in an already selected sensor will be penalized the same way as an increase in power allocation in a non-selected sensor. This leads to scenarios where only a small subset of the most informative sensors are repeatedly selected without using their total available energy. To circumvent that, we need a better approximation of f_0. In particular, we adopt the well known log-sum penalty function $f_{\log}(\mathbf{p}[t]) = \sum_{i=1}^{M} \log(|p_i[t]| + \epsilon)$, which promotes sparsity more efficiently than the ℓ_1 norm (see e.g., [107, 108]).

However, the log-sum penalty function $f_{\log}$ is concave (see Fig. 5.3), thus turning

Algorithm 5.3 Reweighted ℓ_1 minimization algorithm.

1: **Initialize:** $\{w_i[t]\} := 1$, set λ and ϵ.
2: **Step 1:** Solve reweighted ℓ_1 problem:
3: $(\mathbf{s}^{(k)}[t], \mathbf{p}^{(k)}[t]) := \underset{\mathbf{s}[t],\mathbf{p}[t]\in\mathcal{C}}{\arg\min} \left\{ \sum_{t=1}^{T} \left(\mathrm{tr}\left(\sum_{i=1}^{M} \frac{s_i[t]}{\sigma_w^2} \mathbf{a}_i \mathbf{a}_i^T + \mathbf{\Sigma}_x^{-1} \right)^{-1} + \lambda \|\mathbf{W}^{(k)}[t]\mathbf{p}[t]\|_1 \right) \right\}$
4: **Step 2:** Update weights:
5: $w_i^{(k+1)}[t] := \frac{1}{|p_i^{(k)}[t]|+\epsilon}$
6: **Step 3:** Go to Step 1 until convergence.

the objective function of the optimization problem (5.27) into a difference of convex functions. Though a global minimizer of this problem cannot be expected to be found without resorting to an exhaustive search, we can find a local minimum of the problem by resorting to a Majorization-Minimization algorithm [107]. In doing so, we can converge to a stationary solution of the problem (5.27) by iteratively minimizing a surrogate optimization problem in which, at iteration k, we approximate $f(\mathbf{p}[t])$ in (5.27a) by its linearization around $\mathbf{p}^{(k-1)}[t]$, that is,

$$\hat{f}_{\log}^{(k)}(\mathbf{p}[t]) = f_{\log}(\mathbf{p}^{(k-1)}[t]) + \nabla f_{\log}(\mathbf{p}^{(k-1)}[t])^T \left(\mathbf{p}[t] - \mathbf{p}^{(k-1)}[t] \right) \tag{5.28}$$

with $f_{\log}(\mathbf{p}[t]) = \sum_{i=1}^{M} \log(|p_i[t]| + \epsilon)$ and removing the constant terms

$$\hat{f}_{\log}^{(k)}(\mathbf{p}[t]) = \sum_{i=1}^{M} \frac{|p_i[t]|}{|p_i^{(k-1)}[t]| + \epsilon}. \tag{5.29}$$

By defining the set of weights as

$$w_i^{(k)}[t] = \frac{1}{|p_i^{(k-1)}[t]| + \epsilon}, \tag{5.30}$$

which can be more conveniently expressed by the diagonal matrix $\mathbf{W}^{(k)}[t] = \mathrm{diag}(w_1^{(k)}[t], \ldots, w_M^{(k)}[t])$, we can then interpret this as the following reweighted ℓ_1 penalty function

$$\hat{f}_{\log}^{(k)}(\mathbf{p}[t]) = \|\mathbf{W}^{(k)}[t]\mathbf{p}[t]\|_1, \tag{5.31}$$

where at each iteration, we solve the optimization problem (5.27), with the penalty function given by (5.31), and the weights are updated after each iteration according to (5.30). This procedure is summarized in Algorithm 5.3.

5.7 Numerical Results

In this section, we assess the performance of the proposed energy harvesting-aware sensor selection and power allocation strategies. Unless otherwise stated, the algorithm to solve the JSS-EH problem is initialized with the solution of the SS-EH problem. As a

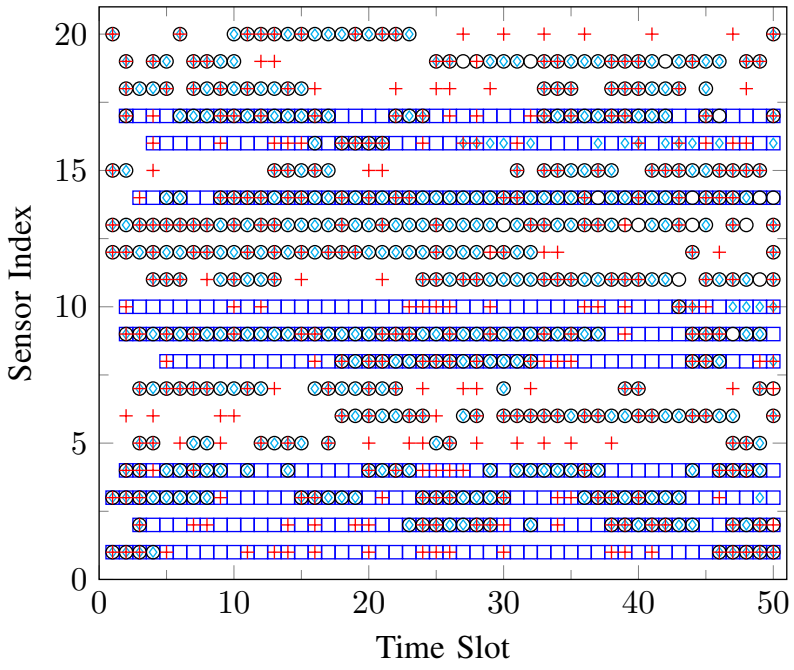

Figure 5.4: Sensor selection policies. Energy arrivals are denoted by $+$. The sensors selected by the SS, SS-EH and JSS-EH policies are denoted by $\square$, $\circ$ and $\diamond$, respectively ($M = 20$, $T = 50$, $K = 10$, $\mu = 0.5$, $\sigma_w^2 = 0.1$).

benchmark, we use the EH-agnostic policy (SS) proposed in [95] and succinctly described in Section 5.5.2. For simulation purposes, we consider linear combination coefficients (which, to recall, are held fixed for all time slots) given by $\mathbf{a}_i \sim \mathcal{N}(0, \mathbf{I}/\sqrt{m})$, with $m = 5$ for the underlying source. Energy arrivals $E_i[t]$ are modeled as Poisson processes of intensity rate μ and $|E_i[t]| = E$. Further, we assume static (i.e., non-fading) sensor-to-FC channels[6].

5.7.1 Subsets of Active Sensors

In Figure 5.4, we depict an individual realization of *subsets* of active sensors associated to the JSS-EH, SS-EH and SS strategies. Specifically, a marker is shown whenever a particular sensor belongs to the subset of selected sensors *and* some transmit power is allocated to it (i.e., $p_i[t] > 0$)[7]. The number of selected sensors in each time slot is set to $K = 10$ (out of $M = 20$).

As discussed earlier, the SS strategy selects the *same* subset of sensors for all time slots, that is, irrespectively of energy arrivals. Specifically, it tends to select the sensors with the most informative observations according to the generated $\mathbf{a}_i$ vectors. On the

[6]This is a reasonable assumption for static wireless sensor networks.

[7]Notice that the former does not necessary imply the latter for the SS strategy until some energy is harvested by each sensor.

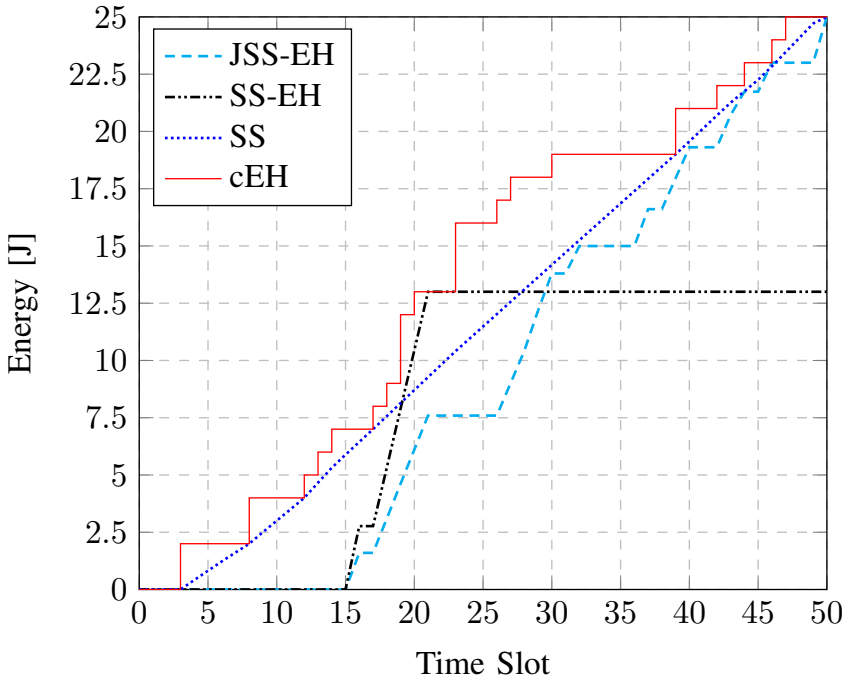

Figure 5.5: Power allocation policies corresponding to sensor 16 in Fig. 5.4 for the Joint (JSS-EH) and Separate (SS-EH) EH-aware Sensor Selection and Power Allocation strategies, and the EH-agnostic Sensor Selection (SS) one. The cumulative energy harvesting (cEH) curve is shown as a reference.

contrary, the active sensors resulting from the proposed SS-EH and JSS-EH strategies vary from time slot to time slot (since they *do* take into account energy arrivals). This results into a more efficient use of the available energy.

Interestingly enough, the subsets of active sensors for the SS-EH and JSS-EH strategies are very similar. The most notable difference is sensor 16, which remains inactive after time slot 21 for SS-EH, whereas it is included in the scheduling pattern of JSS-EH until the very last time slot. As discussed earlier, JSS-EH manages to *refine* the solution of the SS-EH problem and, hence, no radical changes can, in principle, be expected. However, selectively introducing some adjustments may have a considerable impact on the resulting distortion (see Section 5.7.3 ahead). To illustrate this, Figure 5.5 shows the power allocation for sensor 16 associated to the three strategies. Since the SS-EH strategy does not select this sensor after time slot 21, part of the harvested energy is wasted (i.e., not used for transmission). This stems from the fact that the actual selection rule (based on the $\mathbf{s}[t]$ values) yet more sophisticated than a EH-agnostic one is, in fact, heuristic. The JSS-EH strategy fixes this inefficiency by properly adjusting the power allocation policy. This allows to schedule sensor 16 after time slot 21 too and, by doing so, consume the energy that is harvested after that time slot.

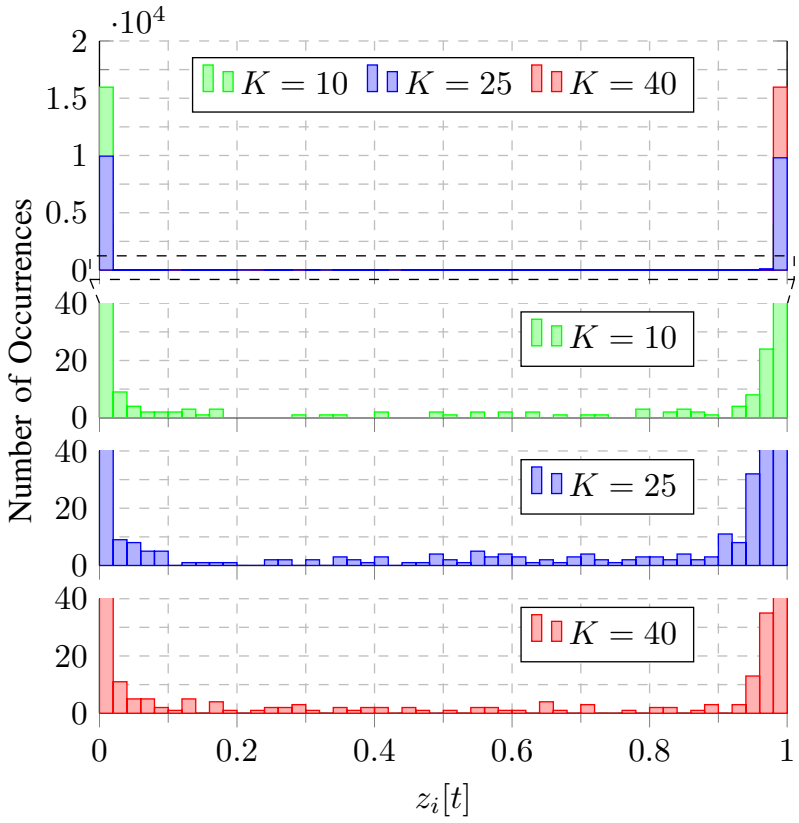

Figure 5.6: Histogram of the selection variable $z_i[t]$ after convergence of the JSS-EH scheme (top) and zoomed-in area with details (bottom). Results are shown for a total of 20 independent runs with random initializations ($M = 50$, $T = 20$, $\mu = 1$, $\sigma_w^2 = 0.1$).

5.7.2 Impact of Cropping the Selection Vector

To recall, in order to effectively select a subset of sensors the JSS-EH scheme forces (crops) $\mathbf{z}^\star[t]$ to 1 for the K largest entries in each time slot (and 0 otherwise). However, we argued, there is no need to recompute corresponding power allocation. Figure 5.6, which shows a histogram of the $z_i[t]$ variables after convergence (and right before cropping, for 20 independent runs with random initializations and repeated for a different number of selected sensors, K), evidences why: with high probability, those values already lie in a close neighborhood of 0 or 1. Also, as the figure reveals, for the intermediate values of $z_i[t]$ in the histogram (i.e., those in between 0 and 1) the actual K parameter setting has virtually no impact. Take for example the case $K = 25$, since the percentage of active sensors is $K/M = 25/50 = 50\%$ the bar in 1 is of (roughly) the same height as that in 0. The zoomed-in area reveals that only a small percentage of values lie in between 0 and 1: 1.72% (or 342 out of 20,000) in the interval $(0.01, 0.99)$; or 0.38% (or 76 out of 20,000) in the interval $(0.1, 0.9)$. The constraint $\mathbf{1}^T\mathbf{z}[t] = K$ thus implies that, for the largest K values in each time slot (and only those ones), we have $z_i[t] \approx 1$. Therefore, the

impact of not recomputing the power allocation for such a reduced subset of K sensors is negligible.

5.7.3 Distortion Performance

Now, we focus our attention on the reconstruction distortion (MSE) for the proposed JSS-EH and SS-EH strategies (see Fig. 5.7). For any strategy, a trivial Lower Bound (LB) of the optimal distortion can be found by letting $\mathcal{Z}_t = \mathcal{M}$ for all $t \in \mathcal{T}$ in problem (5.17). By doing so, we allow all sensors to be selected[8] and, hence, all the observations can be used to reconstruct the source at the FC.

As expected, distortion monotonically decreases with K in all cases. And, further, the resulting distortion is lower for the high-SNR scenario ($\sigma_w^2 = 0.01$). More importantly, the proposed JSS-EH and SS-EH strategies outperform the benchmark (SS), in particular for the high-SNR regime. Interestingly too, the gap between the JSS-EH curve and the lower bound is narrower than that of SS-EH for a low number of selected sensors, which turns out to be the region of interest. Also, for this scenario our proposed strategies attain the lower bound when the number of active sensors is set to 30% and 50%, for the high- and low-SNR regimes, respectively. This implies that, yet suboptimal, the proposed JSS-EH and SS-EH strategies effectively attain the performance of the *optimal* solution (which cannot be computed) when the number of active sensors is set to those values or higher. On the contrary, the benchmark SS strategy only attains the lower bound when all sensors are active. Next, in Fig. 5.8, we investigate the impact of the initialization on the performance (convergence rate, distortion after convergence) of the JSS-EH scheme. By far, the all-zeros initialization results into a slower convergence. Resorting to random initialization definitely helps speed up convergence. However, distortion can be further reduced by initializing the JSS-EH scheme with the solution to the SS-EH problem (including the resulting power allocation). This, in addition, results into faster convergence.

5.7.4 Comparison of the Online and Offline Strategies

Figure 5.9 illustrates the performance of the offline and online strategies vs. the intensity rate of energy arrivals. Clearly, the distortion of the offline versions is lower and both the JSS-EH and SS-EH *online* policies exhibit a similar behavior (yet distortion is lower for the former). To stress, distortion in all cases decreases for an increasing intensity rate of energy arrivals since, accordingly, the overall harvested energy increases too. Interestingly, in the SS-EH case, the gap between the online and offline curves is broader for a scenario with a low number of selected sensors ($K = 10$ out of $M = 50$, or 20%). However, this gap is particularly marginal for the JSS-EH scheme. For a conservative

[8]Note this is not feasible since there are only $K \leq M$ orthogonal channels.

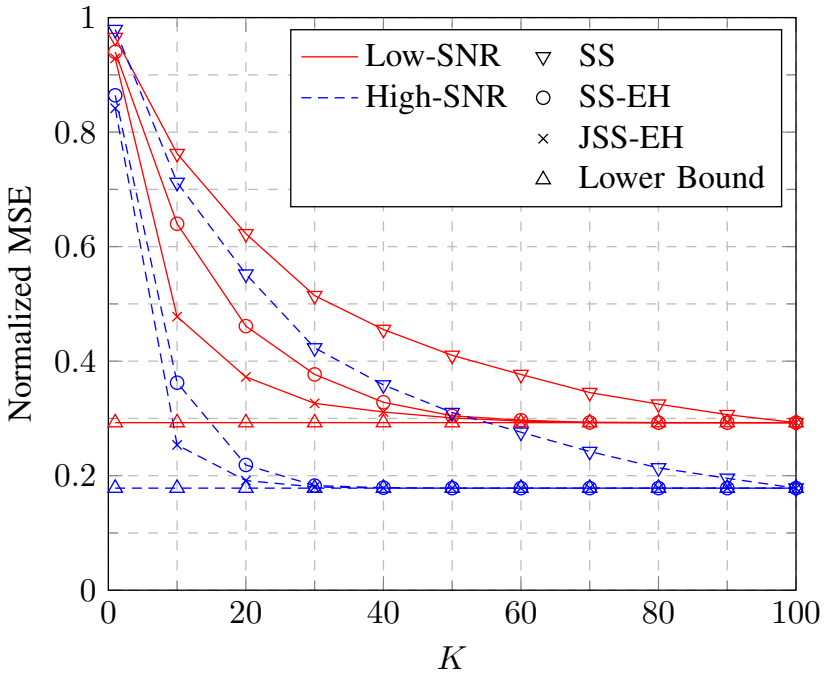

Figure 5.7: Reconstruction distortion vs. number of active sensors, for high ($\sigma_w^2 = 0.01$) and low-SNR scenarios ($\sigma_w^2 = 0.5$) and lower bound ($M = 100$, $T = 20$, $\mu = 0.25$).

power allocation policy, if a substantial number of sensors with unspent energy are not scheduled in the final time slots, the remaining energy is wasted. And, clearly, this is more likely to happen for a lower number of selected sensors (20% vs. 80%).

To alleviate this, one can think of mechanisms to stimulate a more *aggressive* (earlier) consumption of the harvested energy. For instance, rather than recomputing the solution for the remaining time slots, we can do so for a *sliding window* of duration T_w, namely, for $t = t_o, \ldots, t_o + T_w$. The implicit assumption here is that no additional energy will be harvested in the few coming T_w slots. By that time instant, the harvested energy should be consumed and, consequently, it favors an earlier consumption.

In Figure 5.10, we illustrate the impact of the window size (T_w) on the reconstruction distortion. Two different scenarios are considered: (i) low intensity rate, with high amounts of harvested energy in each arrival ($\mu = 0.1$ and $E = 25$); and (ii) high intensity rate, with low amounts of harvested energy ($\mu = 2.5$ and $E = 1$). In both scenarios, though, the average harvested energy is identical ($\mu \cdot E = 2.5$). There exists a trade-off in the duration of the sliding window T_w, as the curves for a low intensity rate of energy arrivals evidence. For very low T_w values, energy is consumed shortly after being harvested (e.g., in the same time slot, for $T_w = 1$). Consequently, transmission might need to be prematurely interrupted (i.e., K might be larger than the number of sensors with available energy) which results into higher distortion. On the contrary, for high T_w values (or when recomputing the solution for the whole remaining observation period),

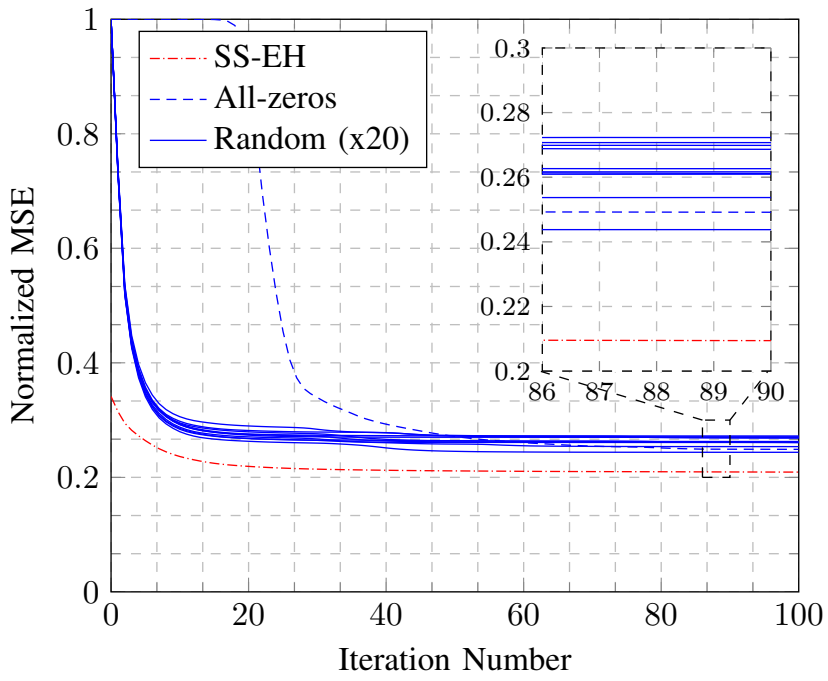

Figure 5.8: Reconstruction distortion vs. number of iterations for various initializations of the JSS-EH algorithm: SS-EH, all-zeros, and random for 20 different realizations ($M = 50$, $T = 20$, $K = 10$, $\mu = 1$, $\sigma_w^2 = 0.1$).

energy consumption is slower, which might result into some wasted energy in the final time slots (and, again, increased distortion). Therefore, there exists some intermediate (optimal) value yielding a minimum distortion (e.g., $T_w = 2$ for $K = 5$ in the SS-EH policy). Interestingly, the optimal duration of the sliding window becomes higher for an increasing number of selected sensors (namely, $T_w = 4$ for $K = 10$, $T_w = 6$ for $K = 20$ in the SS-EH policy). Intuitively, the risk of wasting energy when the percentage of scheduled sensors is higher turns out to be lower and, thus, sliding windows of a higher duration are advisable. For scenarios with high intensity rate ($\mu = 2.5$, and $E = 1$), curves are flatter. On the one hand, for low T_w the risk of running out of energy before the next energy arrival is lower now and so is the distortion penalty (interestingly enough, the optimal duration of the sliding window is one time slot, for $K = 5$ and $K = 10$). On the other hand, for high T_w chances are lower that sensors remain unscheduled for a long time since energy arrives more frequently and the sensor selection and power allocation policies are more frequently recomputed too (lower distortion penalty again). Again, Figure 5.10 reveals a very similar behavior of the JSS-EH and SS-EH approaches for a varying window size (yet, unsurprisingly, distortion for the former is lower). We also observe that the optimal window size tends to be smaller for the online JSS-EH policy.

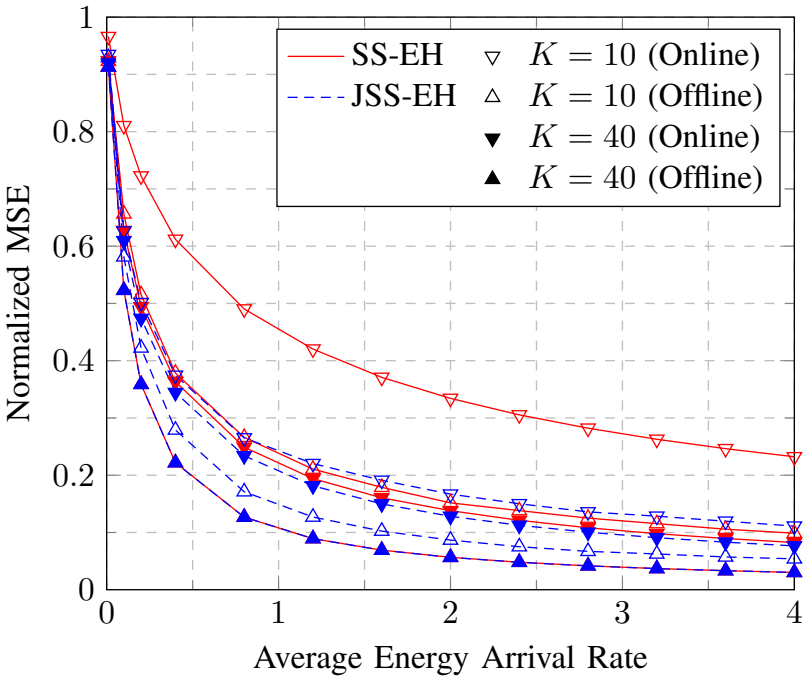

Figure 5.9: Distortion associated to the online and offline SS-EH and JSS-EH strategies, for scenarios with a low ($K = 10$) and high ($K = 40$) number of selected sensors ($M = 50$, $T = 20$, $\sigma_w^2 = 0.01$).

5.7.5 Sparse Sensor Selection

Now, we study the performance of the alternative sparse sensor selection scheme. For this purpose, we consider a wireless sensor network composed of $M = 100$ sensors over $T = 20$ time slots. Further, the variance of the measurement noise is given by $\sigma_w^2 = 0.01$ and the energy arrival intensity rate is $\mu = 1$.

In Figure 5.11, we compare the resulting distortion of our proposed scheme when using the ℓ_1 norm as a penalty function (f_1) and the reweighted ℓ_1 penalty function ($f_{\log}$). Two different scenarios are compared, consisting of energy arrivals of low and high harvested energy E. As the sparsity parameter λ is not comparable between the two algorithms, we solve the optimization problem (5.27) for different values of λ and map the resulting distortion to the average number of selected sensors. As expected, the distortion monotonically decreases as the average number of selected sensors increases. More importantly, the reweighted ℓ_1 penalty function clearly outperforms the non-reweighted ℓ_1 norm. Also, note that the gap between the solutions of the two penalty functions becomes broader for scenarios with larger amounts of harvested energy. This is due to the linear nature of the ℓ_1 norm and its impact on the resource allocation, as discussed in the next paragraph.

In Figure 5.12, we depict the power allocation of an individual sensor. This sensor

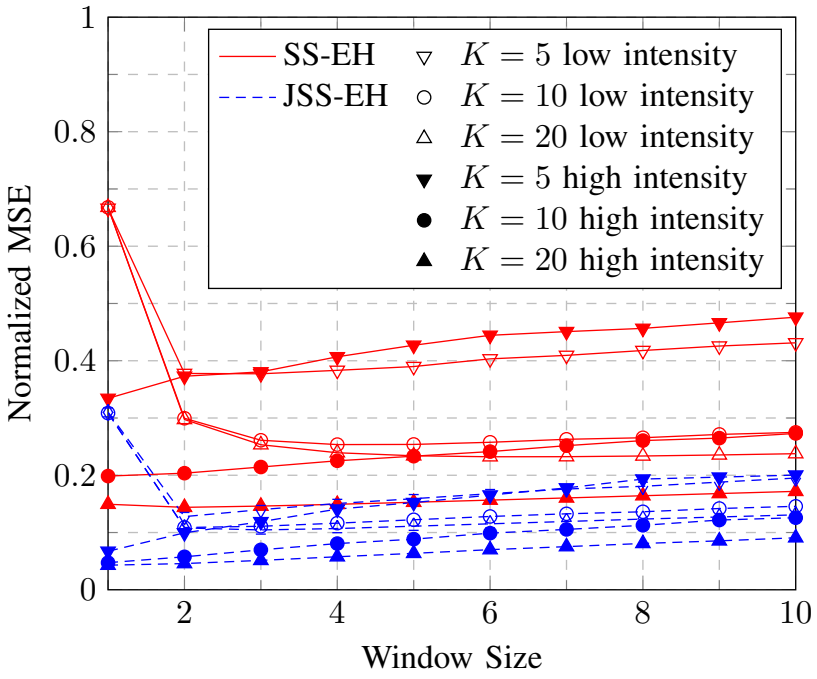

Figure 5.10: Reconstruction distortion for the online SS-EH and JSS-EH strategies, in scenarios with low ($\mu = 0.1$, $E = 25$) and high ($\mu = 2.5$, $E = 1$) intensity rates ($M = 50$, $T = 20$, $\sigma_w^2 = 0.01$).

is taken from the selection of approximately 30 sensors and $E = 0.1$. We observe that, in the solution obtained when using the ℓ_1 penalty function, the sensor node still has a considerable amount of unused energy at the end of the observation period ($t = 20$). A solution leading to lower distortion and the same sensor selection schedule can be found by simply increasing the transmit power during time slots 5 to 20 so as to consume all the available energy by the deadline. On that account, we confirm that the ℓ_1 norm does not lead to good solutions. Also, note how the sensor is selected during most of the time, with the exception of time slots 3 and 4, which is not a very sparse schedule. In contrast, when using the reweighted ℓ_1 penalty function, the sensor allocates all of its available energy by the last time slot and exhibits a more sparse sensor selection schedule, being selected only 6 out of the 20 total time slots.

5.8 Conclusions

In this chapter, we have proposed two suboptimal strategies to solve the non-convex problem of *jointly* selecting a predefined number of energy-harvesting sensors and computing the optimal power allocation policy. Further, we have also provided an alternative sparsity-based policy. The joint sensor selection and power allocation (JSS-EH) scheme is capable of finding a stationary solution (a proof is provided) on the basis of a

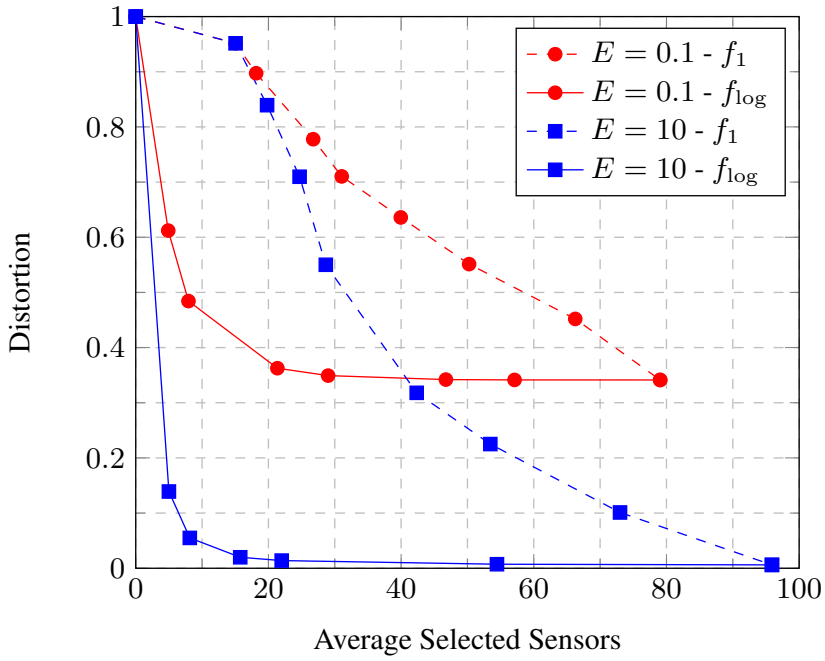

Figure 5.11: Distortion vs. Average number of selected sensors for high and low energy scenarios in the SSS-EH policy.

majorization-minimization procedure. This allows us to identify a sequence of surrogate convex optimization problems that we iteratively solve. As an alternative, we propose a method to *separately* identify a sensible sensor selection and power allocation policies (SS-EH scheme) which does takes into account the actual energy arrivals. The resulting power allocation strategy can be interpreted as a two-dimensional waterfilling solution. We have also learned that the SS-EH solution turns out to be a suitable initialization to compute a *decent* stationary solution to the JSS-EH problem in a relatively low number of iterations. The latter solution can be regarded as a *refined* version with lower reconstruction distortion. Computer simulations revealed that the subsets of active sensors for the JSS-EH and SS-EH strategies are very similar. However, the corresponding power allocation policies differ. For the analyzed scenario, the proposed strategies attain the lower bound when the number of active sensors is set to 30% (50%) in the high- (low-) SNR regime. We have also found that cropping the relaxed sensor selection vector of the JSS-EH scheme to the largest K values without re-computing the power allocation policy has a negligible impact on distortion. Also, we have proposed an *online* version of the strategies. The associated distortion, however, is higher. This is in part motivated by the fact that it tends to generate *conservative* power allocation patterns with slow energy consumption. Should a substantial fraction of those sensors not be scheduled by the end of the observation period, the harvested energy is wasted and, thus, distortion increases. By resorting to a sliding window, one can generate more *aggressive* power allocation

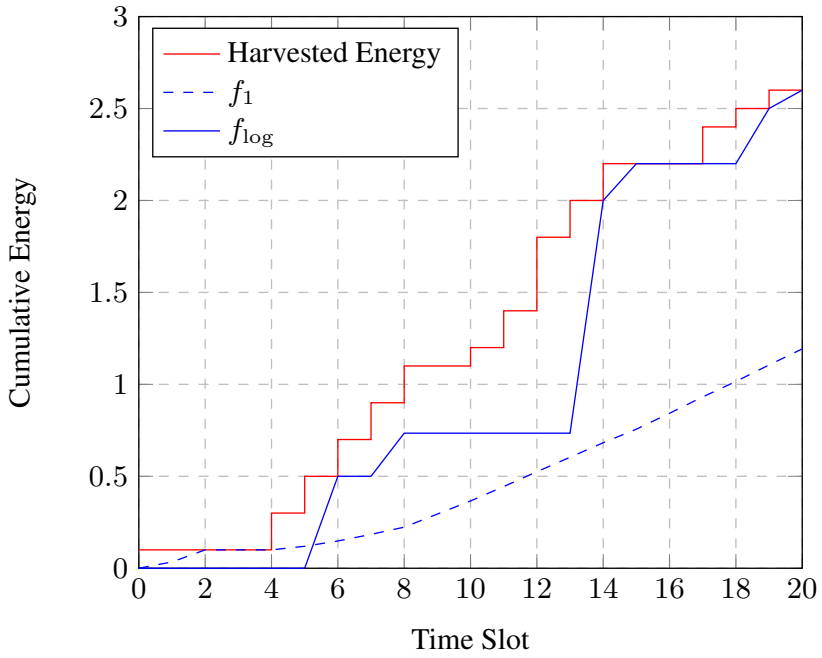

Figure 5.12: Power allocation for a single sensor in the SSS-EH policy.

patterns (i.e., faster energy consumption). We have empirically shown that, for a given setting, an optimal duration of such sliding window exists (which might be in some cases, a single time slot). Finally, due to the non-convexity of the classical formulation, we have also proposed an alternative sparsity-promoting approach to solving the problem. This has been accomplished by introducing a regularization term that promotes sparsity in the power allocation, which in turn leads to sparse sensor selection schedules. Further, we have found that strictly concave penalty functions are desirable in order to ensure the proper consumption of the harvested energy. Specifically, we have proposed the use of a log-sum penalty function, which can be interpreted as a reweighted ℓ_1 norm. Numerical results show that the proposed solution rapidly approaches the asymptotic distortion, by just selecting 20% of the available sensors in average.

Chapter 6

Stochastic Routing and Scheduling Policies

In this chapter, we study the joint routing-scheduling problem in energy harvesting communication networks. Our policies, which are based on stochastic subgradient methods on the dual domain, act as an energy harvesting variant of the stochastic family of backpresure algorithms. Specifically, we propose two policies: (i) the Stochastic Backpressure with Energy Harvesting (SBP-EH), in which a node's routing-scheduling decisions are determined by the difference between the Lagrange multipliers associated to their queue stability constraints and their neighbors'; and (ii) the Stochastic Soft Backpressure with Energy Harvesting (SSBP-EH), an improved algorithm where the routing-scheduling decision is of a probabilistic nature. For both policies, we show that given sustainable data and energy arrival rates, the stability of the data queues over all network nodes is guaranteed. Numerical results corroborate the stability guarantees and illustrate the minimal gap in performance that our policies offer with respect to classical ones which work with an unlimited energy supply.

6.1 Introduction

The appearance of multiple interconnected devices powered by energy harvesting results in communication networks formed by self-sustainable and perpetually communicating nodes. In such scenarios, there is the necessity of designing efficient routing and scheduling algorithms that explicitly take into account the energy harvesting process. In this sense, there have been some previous efforts in developing communication policies for these types of multi-hop networks. In general, the full characterization of the optimal transmission policies is a difficult problem, as optimal transmission policies are heavily coupled throughout the network. Under full non-causal knowledge of the energy harvesting process, the optimal transmission policies of a simpler two-hop network have been

studied in [62]. A more realistic approach is the consideration of non-causal knowledge of the energy harvesting process. Under this assumption, the authors in [109] jointly optimize data compression and transmission tasks to obtain a close-to-optimal policy. In [110], the authors propose an EH-aware routing scheme that is asymptotically optimal with respect to the network size. The authors in [111], address the EH scheduling problem for both single-hop and multi-hop networks, and provide a joint admission control and routing policy. Also, in the same line, the authors in [112] propose a policy which improves on the multi-hop performance bounds of [111]. Overall, non-causal policies are typically designed under the assumption of independent and identically distributed (i.i.d.) or Markov energy harvesting and data arrival processes, and Lyapunov optimization techniques are used to derive their queue stability results.

In this chapter, we study the problem of jointly routing and scheduling data packets in an energy harvesting communication network. Each node independently generates traffic for delivery to a specific destination and collaborates with the other nodes in the network to ensure the delivery of all data packets. In this way, each node decides the next suitable hop for each packet in its queue (routing), and when to transmit it (scheduling). The solution to this problem—when the nodes are not EH-powered—is given by the backpressure (BP) algorithm [113]. The previous works [111] and [112] considered a similar problem which consists in finding admission control and resource allocation policies that satisfy network stability and energy causality while attaining close-to-optimal performance. In this work, instead, our goal is to find stabilizing policies given the data rates. Also, while previous works [111,112] require data and energy arrival processes to be i.i.d. or Markov, we only require them to be ergodic, which is a weaker requirement. Furthermore, our approach to the problem is also markedly different. While the works [111] and [112] relied on queueing theory and Lyapunov drift arguments to find stabilizing policies, we instead interpret the scheduling and routing problem as a stochastic optimization problem. This allows us to resort to a dual stochastic subgradient descent algorithm [70] to solve the joint routing-scheduling problem. However, the introduction of energy harvesting constraints results in an energy causality problem in the problem. In order to solve this, we introduce a modified problem formulation and derive the conditions that ensure causality in the energy consumption. Under this framework, we propose two different policies. The first, which we denote Stochastic Backpressure with Energy Harvesting (SBP-EH), is a policy of rather simple nature. The network nodes track the pressure of the data flows by computing the difference between the Lagrange multipliers associated to their queue stability constraints and the ones of their neighbors (instead of their data queues as in the classical backpressure algorithm). Then, the Lagrange multipliers associated with the battery state reduce the pressure when the stored energy in the node decreases. The resulting routing-scheduling decision is to transmit the flow with highest pressure. The second policy, which we name Stochastic Soft Backpressure with Energy Harvesting

(SSBP-EH), is a probabilistic policy. In this policy, the nodes perform the same tracking of pressure as the SBP-EH policy. However, instead of transmitting the flow with the highest pressure, the flows are equalized in an inverse waterfilling manner. This results in a routing-scheduling probability mass function, where the transmit decision is taken as a sample of this distribution. This second policy, while not as simple as the previous one, provides several improvements in the stabilization speed of the network, as well as a reduction in the packets in queue and packet delivery delay once the network is stabilized. For both policies, we provide the necessary battery capacity which ensures the proper behavior of the algorithms. Furthermore, we also provide theoretical guarantees certifying that given sustainable data and energy arrival rates, the stability of the data queues over all network nodes is guaranteed. Finally, we study the policies numerically and verify that they show a minimal gap in performance with respect to classical policies operating with an unlimited energy supply.

The rest of the chapter is organized as follows. In Section 6.2 we introduce the system model and provide details on the data and energy queue dynamics. Section 6.3 develops the framework of the proposed joint routing and scheduling algorithms, with the SBP-EH and SSBP-EH policies introduced in Sections 6.3.1 and 6.3.2, respectively. Theoretical guarantees, namely, queue stability and energy causality are discussed in Section 6.4. After this, we devote Section 6.5 to simulations assessing the performance of our proposed policies. Finally, we provide some concluding remarks in Section 6.6.

6.2 System Model

Consider a communication network given by the graph $\mathcal{G} = (\mathcal{N}, \mathcal{E})$, where $\mathcal{N}$ is the set of N nodes in the network and $\mathcal{E} \subseteq \mathcal{N} \times \mathcal{N}$ is the set of communication links, such that if node i is capable of communicating with node j, we have $(i, j) \in \mathcal{E}$. Moreover, we define the neighborhood of node i as the set $\mathcal{N}_i = \{j | (i, j) \in \mathcal{E}\}$. The network supports K information flows (which we index by the set $\mathcal{K}$), where for a flow $k \in \mathcal{K}$, the destination node is denoted by $N^k_{(dest)}$. At a time slot t, each $k \in \mathcal{K}$ flow at the i-th node generates $a^k_i[t]$ packets to be delivered to the node $N^k_{(dest)}$. This packet arrival process is assumed to be stationary with mean $\mathbb{E}\big[a^k_i[t]\big] = a^k_i$. At the same time, the i-th node routes $r^k_{ij}[t]$ packets to its neighbors $j \in \mathcal{N}_i$, while simultaneously being routed $r^k_{ji}[t]$ packets. For simplicity, at each time slot, we restrict each node to route one single packet to its neighbors. Therefore, the nodes have the following routing constraint

$$\sum_{k \in \mathcal{K}} \sum_{j \in \mathcal{N}_i} r^k_{ij}[t] \leq 1, \quad i \in \mathcal{N}. \tag{6.1}$$

Furthermore, each node in the network keeps track of the number of packets awaiting to be transmitted for each flow. Denoting by $q^k_i[t]$ the k-th flow data queue at the i-th

node and time slot t, the evolution of the queue is given by

$$q_i^k[t+1] = q_i^k[t] + a_i^k[t] + \sum_{j\in\mathcal{N}_i} r_{ji}^k[t] - \sum_{j\in\mathcal{N}_i} r_{ij}^k[t], \tag{6.2}$$

for all $i \in \mathcal{N}$ and $k \in \mathcal{K}$. The objective is to determine routing policies $r_{ij}^k[t]$ such that the queues in (6.2) remain stable while satisfying the routing constraints given by (6.1). By grouping the all the queues in a vector $\mathbf{q}[t] = \{q_i[t]\}$, we say that the routing policies $r_{ij}^k[t]$ guarantee stability if there exists a constant Q such that for some arbitrary time T we have

$$\Pr\left\{\max_{t\geq T} \|\mathbf{q}[t]\| \leq Q|\mathbf{q}[T]\right\} = 1. \tag{6.3}$$

This is to say that, almost surely, no queue becomes arbitrarily large. In turn, we can guarantee this if the average rate at which packets enter the queues is smaller than the rate at which they exit them. In order to formally state this, let us denote the ergodic limits of processes $a_i^k[t]$ and $r_{ij}^k[t]$ by

$$a_i^k = \mathbb{E}\big[a_i^k[t]\big] = \lim_{t\to\infty} \frac{1}{t}\sum_{l=1}^{t} a_i^k[l], \tag{6.4}$$

$$r_{ij}^k = \mathbb{E}\big[r_{ij}^k[t]\big] = \lim_{t\to\infty} \frac{1}{t}\sum_{l=1}^{t} r_{ij}^k[l]. \tag{6.5}$$

Then, in order to have stable data queues in the network, it suffices to satisfy the condition

$$a_i^k \leq \sum_{j\in\mathcal{N}_i} r_{ij}^k - \sum_{j\in\mathcal{N}_i} r_{ji}^k. \tag{6.6}$$

for all $i \in \mathcal{N}$ and $k \in \mathcal{K}$. If there exist routing variables r_{ij}^k satisfying this inequality, then the queue evolution in (6.2) follows a supermartingale expression, and the stability condition given by (6.3) is then guaranteed by the martingale convergence theorem [114, Theorem 5.2.9]. Alternatively, by introducing arbitrary concave functions $f_{ij}^k : \mathbb{R} \to \mathbb{R}$, we can formulate this as the following optimization problem

$$\underset{\sum_{k,j} r_{ij}^k \leq 1}{\text{maximize}} \quad \sum_{i\in\mathcal{N}}\sum_{k\in\mathcal{K}}\sum_{j\in\mathcal{N}_i} f_{ij}^k\left(r_{ij}^k\right) \tag{6.7a}$$

$$\text{subject to} \quad a_i^k \leq \sum_{j\in\mathcal{N}_i} r_{ij}^k - \sum_{j\in\mathcal{N}_i} r_{ji}^k, \quad k\in\mathcal{K}, i\in\mathcal{N}, \tag{6.7b}$$

where we have left the routing constraints given by (6.1) implicit, and the optimization is over the nonnegative routing variables $r_{ij}^k \geq 0$. Furthermore, we have substituted the per time slot constraints in (6.1) for average ones. Then, assuming data arrival rates satisfying inequality (6.7b) exist, the objective is to design an algorithm such that the

instantaneous routing variables $r_{ij}^k[t]$ satisfy $\mathbb{E}\big[r_{ij}^k[t]\big] = r_{ij}^k$ and the routing constraints in (6.1) are satisfied for all time slots. This is the optimization problem that the backpressure family of algorithms solve. By resorting to a stochastic subgradient method on the dual domain, a direct comparison can be established between data queues and Lagrange multipliers [115]. Then, the choice of objective function in the optimization problem (6.7) determines the resulting variant of the backpressure algorithm. For example, on one hand, the stochastic backpressure (SBP) algorithm [113] can be recovered by the use of a linear objective function. On the other hand, the choice of a strongly concave objective function leads to the soft stochastic backpressure (SSBP) algorithm [116].

6.2.1 Routing and Scheduling with Energy Harvesting

Different from classical approaches [113, 116], we consider that the network nodes are powered by energy harvesting. At time slot t, the i-th node harvests $e_i[t]$ units of energy, where the energy harvesting process is assumed to be stationary with mean $\mathbb{E}\big[e_i[t]\big] = e_i$. We consider a normalized energy harvesting process, where the routing of one packet consumes one unit of energy. Furthermore, we consider packet transmission to be the only energy-consuming action taken by the nodes. Under these conditions and denoting by $b_i[t]$ the energy stored in the i-th node's battery at time t, the following energy causality constraint must be satisfied for all time slots

$$\sum_{k\in\mathcal{K}}\sum_{j\in\mathcal{N}_i} r_{ij}^k[t] \leq b_i[t], \quad i \in \mathcal{N}. \tag{6.8}$$

Additionally, we consider that nodes have a finite battery of capacity $b_i^{\max}$. Then, we can write the battery dynamics as

$$b_i[t+1] = \left[b_i[t] - \sum_{k\in\mathcal{K}}\sum_{j\in\mathcal{N}_i} r_{ij}^k[t] + e_i[t]\right]_0^{b_i^{\max}} \tag{6.9}$$

for $i \in \mathcal{N}$. In order to introduce these constraints into the optimization problem (6.7), we denote the ergodic limit of the energy harvesting process $e_i[t]$ by

$$e_i = \mathbb{E}\big[e_i[t]\big] = \lim_{t\to\infty} \frac{1}{t}\sum_{l=1}^{t} e_i[l]. \tag{6.10}$$

Then, substituting the battery dynamics given by (6.9) in the energy causality constraint(6.8) and then taking the ergodic limits on both sides of the inequality, we obtain the following average constraint in the routing variables

$$\sum_{k\in\mathcal{K}}\sum_{j\in\mathcal{N}_i} r_{ij}^k \leq e_i, \quad i \in \mathcal{N}. \tag{6.11}$$

This states that the average amount of energy spent must be less than the average energy harvested. Then, we introduce this constraint in problem (6.7), resulting in the following

optimization problem

$$\underset{\sum_{k,j} r_{ij}^k \leq 1}{\text{maximize}} \quad \sum_{i\in\mathcal{N}} \sum_{k\in\mathcal{K}} \sum_{j\in\mathcal{N}_i} f_{ij}^k \left(r_{ij}^k\right) \tag{6.12a}$$

$$\text{subject to} \quad a_i^k \leq \sum_{j\in\mathcal{N}_i} r_{ij}^k - \sum_{j\in\mathcal{N}_i} r_{ji}^k, \quad k \in \mathcal{K}, i \in \mathcal{N} \tag{6.12b}$$

$$\sum_{k\in\mathcal{K}} \sum_{j\in\mathcal{N}_i} r_{ij}^k \leq e_i, \quad i \in \mathcal{N}. \tag{6.12c}$$

Assuming data and energy arrival rates satisfying (6.12b) and (6.12c) exist, the goal is to design an algorithm such that the instantaneous routing variables $r_{ij}^k[t]$ satisfy $\mathbb{E}\big[r_{ij}^k[t]\big] = r_{ij}^k$ and the constraints (6.1) and (6.8) are satisfied for all time slots. However, the use of the average energy constraint (6.12c) presents a causality problem, as a solution satisfying (6.12c) does not guarantee that the energy causality constraint in (6.8) is satisfied for all time slots. In order to circumvent this, we propose the introduction of the following modified optimization problem

$$\underset{\substack{\sum_{k,j} r_{ij}^k \leq 1,\\ x_i^k \in [0,\bar{x}_i^k]}}{\text{maximize}} \quad \sum_{i\in\mathcal{N}} \sum_{k\in\mathcal{K}} \sum_{j\in\mathcal{N}_i} f_{ij}^k \left(r_{ij}^k\right) - \sum_{i\in\mathcal{N}} \sum_{k\in\mathcal{K}} \bar{\gamma}_i^k x_i^k \tag{6.13a}$$

$$\text{subject to} \quad a_i^k \leq \sum_{j\in\mathcal{N}_i} \left(r_{ij}^k - r_{ji}^k\right) + x_i^k, k \in \mathcal{K}, i \in \mathcal{N} \tag{6.13b}$$

$$\sum_{k\in\mathcal{K}} \sum_{j\in\mathcal{N}_i} r_{ij}^k \leq e_i, \quad i \in \mathcal{N}. \tag{6.13c}$$

This optimization problem differs from (6.12) in the introduction of an auxiliary variable x_i^k. This variable is restricted to lie in the interval $[0, \bar{x}_i^k]$, with $\bar{x}_i^k$ being a constant whose value is determined by the system parameters. This auxiliary variable appears in the queue stability constraint (6.13b), where it helps to satisfy the constraint if necessary. Furthermore, we have added the term $-\sum_{i\in\mathcal{N}} \sum_{k\in\mathcal{K}} \bar{\gamma}_i^k x_i^k$ in the objective function, where $\bar{\gamma}_i^k$ is a constant parameter. The value of this parameter $\bar{\gamma}_i^k$ is chosen such that the optimal value of the Lagrange multipliers of the queue constraint (6.13b) lies in the interval $[0, \bar{\gamma}_i^k]$.

The reasoning behind using the modified optimization problem (6.13) becomes more clear when attempting to solve the problem. We take an approach consisting of a primal-dual method and a stochastic approximation. Hence, we use the instantaneous values of the variables instead of their ergodic limits. In the modified problem, the instantaneous values of the dual variables can be shown to be bounded above. This is not the case in the original problem (6.12). In turn, this allows us to establish conditions on $\bar{x}_i^k$ that ensure that the energy causality constraints (6.8) are satisfied for all time slots. At the same time, if $\bar{\gamma}_i^k$ is chosen correctly such that the optimal queue multipliers lie in the interval $[0, \bar{\gamma}_i^k]$, then the ergodic limits of the auxiliary variables go to zero, i.e.,

$\lim_{t\to\infty} \frac{1}{t}\sum_{l=1}^{t} x_i^k[l] = x_i^k = 0$. As a consequence, both the optimal solutions of problems (6.12) and (6.13) are equivalent and therefore the solution of (6.13) also satisfies the original stability constrains constraint (6.12b).

6.3 Joint Routing and Scheduling Algorithm

As we mentioned previously, in order to solve optimization problem posed in (6.13) we resort to a primal-dual method. To start, let us define the vector $\mathbf{r} = \{r_{ij}^k, x_i^k\}$ collecting the routing variables r_{ij}^k and auxiliary variables x_i^k and the vector $\boldsymbol{\lambda} = \{\gamma_i^k, \beta_i\}$ collecting the queue multipliers γ_i^k associated with constraint (6.13b) and battery multipliers β_i corresponding to constraint (6.13c). Furthermore, we collect the implicit optimization constraints in the set $\mathcal{R} = \left\{\sum_{k,j} r_{ij}^k \leq 1, x_i^k \in [0, \bar{x}_i^k]\right\}$. Then, we write the Lagrangian of the optimization problem (6.13) as follows

$$\begin{aligned}\mathcal{L}(\mathbf{r}, \boldsymbol{\lambda}) = &\sum_{i\in\mathcal{N}}\sum_{k\in\mathcal{K}}\sum_{j\in\mathcal{N}_i} f_{ij}^k\left(r_{ij}^k\right) - \sum_{i\in\mathcal{N}}\sum_{k\in\mathcal{K}} \bar{\gamma}_i^k x_i^k \\ &+ \sum_{k\in\mathcal{K}}\sum_{i\in\mathcal{N}} \gamma_i^k\left(\sum_{j\in\mathcal{N}_i} r_{ij}^k - \sum_{j\in\mathcal{N}_i} r_{ji}^k + x_i^k - a_i^k\right) \\ &+ \sum_{i\in\mathcal{N}} \beta_i\left(e_i - \sum_{k\in\mathcal{K}}\sum_{j\in\mathcal{N}_i} r_{ij}^k\right).\end{aligned} \tag{6.14}$$

The Lagrange dual function is then given by

$$g(\boldsymbol{\lambda}) = \max_{\mathbf{r}\in\mathcal{R}} \mathcal{L}(\mathbf{r}, \boldsymbol{\lambda}). \tag{6.15}$$

An immediate issue that arises when trying to solve this problem is that network nodes have no knowledge of the data arrival rates a_i^k nor the energy harvesting rates e_i. Nonetheless, the nodes observe the instantaneous rates $a_i^k[t]$ and $e_i[t]$, hence we resort to using these instantaneous variables. Furthermore, we can reorder the Lagrangian (6.14) to allow for a separate maximization over network nodes, where each node only needs the queue multipliers of its neighboring nodes. The routing variables can then be obtained as follows

$$r_{ij}^k[t] := \underset{\sum_{k,j} r_{ij}^k \leq 1}{\arg\max} \sum_{k\in\mathcal{K}}\sum_{j\in\mathcal{N}_i} \left(f_{ij}^k\left(r_{ij}^k\right) + r_{ij}^k\left(\gamma_i^k[t] - \gamma_j^k[t] - \beta_i[t]\right)\right), \tag{6.16}$$

for $i \in \mathcal{N}$. In a similar way, the auxiliary variables at each node are given by

$$x_i^k[t] := \underset{x_i^k\in[0,\bar{x}_i^k]}{\arg\max}\, x_i^k\left(\gamma_i^k[t] - \bar{\gamma}_i^k\right). \tag{6.17}$$

This is simply a threshold operation, where $x_i^k[t] = 0$ if $\gamma_i^k[t] \leq \bar{\gamma}_i^k$ and $x_i^k[t] = \bar{x}_i^k$ if $\gamma_i^k[t] > \bar{\gamma}_i^k$. Now, since the dual function in (6.15) is convex, we can minimize it by

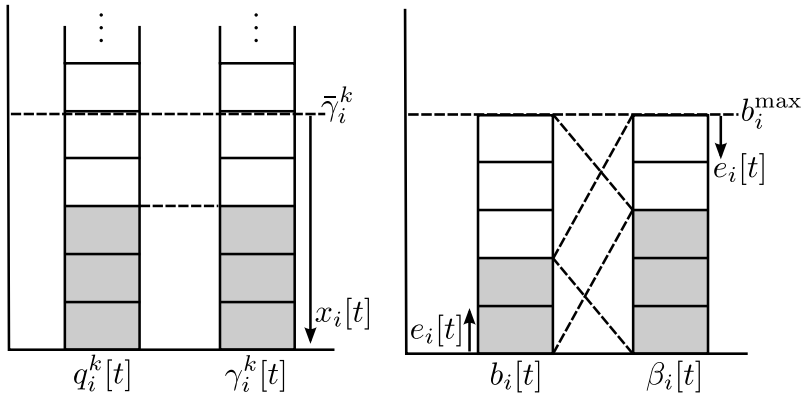

(a) Data queues. (b) Batteries.

Figure 6.1: Relationship between data queues, batteries and their Lagrange multipliers. Example with $\bar{\gamma}_i^k = 5$ and $b_i^{\max} = 5$.

performing a stochastic subgradient descent. Then, the dual updates are given by the following expressions

$$\gamma_i^k[t+1] := \left[\gamma_i^k[t] + a_i^k[t] - x_i^k[t] + \sum_{j\in\mathcal{N}_i}\left(r_{ji}^k[t] - r_{ij}^k[t]\right)\right]^+ \tag{6.18}$$

$$\beta_i[t+1] := \left[\beta_i[t] - e_i[t] + \sum_{k\in\mathcal{K}}\sum_{j\in\mathcal{N}_i} r_{ij}^k[t]\right]^+ \tag{6.19}$$

where $[\cdot]^+$ is the projection on the nonnegative orthant. For compactness, we also express the dual updates in vector form as $\boldsymbol{\lambda}[t+1] := [\boldsymbol{\lambda}[t] - \mathbf{s}[t]]^+$, where $\mathbf{s}[t]$ corresponds to the vector collecting the stochastic subgradients. Since the algorithm that we propose is designed to be run in an online fashion, we have considered a fixed step size in the dual updates. Specifically, we have used a unit step size. This allows a clear comparison between dual variables and data queues and battery dynamics as outlined in Figure 6.1. For the case of the data queues, the difference between their dynamics (6.2) and those of their Lagrange multiplier counterparts (6.18) is given by the auxiliary variable in the dual update. Assume a packet is either routed or not, i.e., $r_{ij}^k[t] \in \{0, 1\}$. Then the dual variables $q_i^k[t]$ follow the data queues $\gamma_i^k[t]$ until $\gamma_i^k[t] > \bar{\gamma}_i^k$, at which point, the dual variables are pushed back by the auxiliary variable $x_i^k[t] = \bar{x}_i^k$. From this point forward, the queue and multiplier dynamics lose their symmetry, coupling again when the queue empties. In a similar way, a comparison can also be drawn between the battery dynamics (6.9) and the battery dual update (6.19). In this case, the symmetry exists in a mirrored way, as the relationship between the battery state $b_i[t]$ and its multipliers $\beta_i[t]$ is given by $b_i[t] = b_i^{\max} - \beta_i[t]$. Different from the case of data queues, the coupling between the battery state and its multipliers is never lost.

Algorithm 6.1 Stochastic Backpressure with Energy Harvesting.

1: **Initialize:** Set $\gamma_i^k[0] := 0$ and $\beta_i[0] := b_i^{\max} - b_i[0]$.
2: **Step 1(a):** Routing-scheduling decision (SBP-EH).
3: $r_{ij}^k[t] := \underset{\sum_{k,j} r_{ij}^k \leq 1}{\arg\max} \sum_{k\in\mathcal{K}} \sum_{j\in\mathcal{N}_i} r_{ij}^k \big(w_{ij}^k + \gamma_i^k[t] - \gamma_j^k[t] - \beta_i[t]\big)$
4: **Step 1(b):** Routing-scheduling decision (SSBP-EH).
5: $r_{ij}^k[t] := \frac{1}{2}\Big[w_{ij}^k + \gamma_i^k[t] - \gamma_j^k[t] - \beta_i[t] - \nu_i[t]\Big]^+$
6: **Step 2:** Compute auxiliary variable.
7: $x_i^k[t] := \underset{x_i^k\in[0,\bar{x}_i^k]}{\arg\max}\, x_i^k \left(\gamma_i^k[t] - \bar{\gamma}_i^k\right)$
8: **Step 3:** Update dual variables.
9: $\gamma_i^k[t+1] := \Big[\gamma_i^k[t] + a_i^k[t] - x_i^k[t] + \sum_{j\in\mathcal{N}_i} \big(r_{ji}^k[t] - r_{ij}^k[t]\big)\Big]^+$
10: $\beta_i[t+1] := \Big[\beta_i[t] - e_i[t] + \sum_{k\in\mathcal{K}} \sum_{j\in\mathcal{N}_i} r_{ij}^k[t]\Big]^+$
11: **Step 4:** For all neighbors $j \in \mathcal{N}_i$, send dual variables $\gamma_i^k[t+1]$ and receive dual variables $\gamma_j^k[t+1]$.
12: **Step 5:** Set $t := t + 1$ and go to Step 1.

Next, we consider some choices of the objective function $f_{ij}^k\big(r_{ij}^k\big)$ in the optimization problem (6.13) which lead to familiar formulations of the backpressure algorithm adapted to the energy harvesting process. The steps of the two resulting policies are summarized in Algorithm 6.1.

6.3.1 Stochastic Backpressure with Energy Harvesting (SBP-EH)

Consider functions $f_{ij}^k\big(r_{ij}^k\big)$ which are linear with respect to the routing variables, i.e., taking the form $f_{ij}^k\big(r_{ij}^k\big) = w_{ij}^k r_{ij}^k$, where w_{ij}^k is an arbitrary weight. In this case, we recover a version of the stochastic backpressure algorithm adapted to the energy harvesting process. For a linear objective function, the maximization in (6.16) leads to the routing variables

$$r_{ij}^k[t] := \underset{\sum_{k,j} r_{ij}^k \leq 1}{\arg\max} \sum_{k\in\mathcal{K}} \sum_{j\in\mathcal{N}_i} r_{ij}^k \left(w_{ij}^k + \gamma_i^k[t] - \gamma_j^k[t] - \beta_i[t]\right). \tag{6.20}$$

To solve the maximization in (6.20) it suffices to find the flow over the neighboring nodes with the largest differential $w_{ij}^k + \gamma_i^k[t] - \gamma_j^k[t] - \beta_i[t]$ and if it is positive, set its corresponding routing variable $r_{ij}^k[t]$ to one while the other variables are kept to zero. This algorithm, when $w_{ij}^k = 0$, is analogous to the stochastic form of backpressure. In the classical backpressure algorithm, the flow with the largest queue differential $q_i^k[t] - q_j^k[t]$ is chosen. Interpreted in its stochastic form, the flow with the largest Lagrange multiplier difference $\gamma_i^k[t] - \gamma_j^k[t]$ is chosen. In the SBP-EH policy, the stochastic form

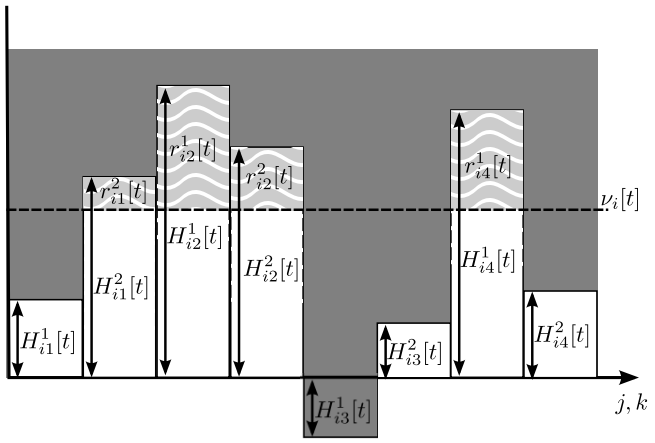

Figure 6.2: Example of a SSBP-EH routing decision for a node node serving two flows and four neighbors.

of backpressure adds the battery multiplier $\beta_i[t]$. As the battery depletes, the value of $\beta_i[t]$ increases and the pressure to transmit of this node decreases.

6.3.2 Stochastic Soft Backpressure with Energy Harvesting (SSBP-EH)

Now, we consider a quadratic plus linear term function given by $f^k_{ij}\big(r^k_{ij}\big) = -\big(r^k_{ij}\big)^2 + w^k_{ij} r^k_{ij}$. This leads to a stochastic soft backpressure algorithm [116], where the routing variables obtained by the maximization in (6.16) are given by

$$r^k_{ij}[t] := \frac{1}{2}\Big[w^k_{ij} + \gamma^k_i[t] - \gamma^k_j[t] - \beta_i[t] - \nu_i[t]\Big]^+, \tag{6.21}$$

where $\nu_i[t]$ are the Lagrange multipliers ensuring $\sum_{k\in\mathcal{K}}\sum_{j\in\mathcal{N}_i} r^k_{ij} \leq 1$ for all $i \in \mathcal{N}$. This expression can be understood a form of inverse waterfilling. An example of this solution is shown in Figure 6.2. Let us construct rectangles of height $H^k_{ij}[t] = w^k_{ij} + \gamma^k_i[t] - \gamma^k_j[t] - \beta_i[t]$ and scale them by the widths $W^k_{ij}[t] = 1/2$. For each node, every possible flow and neighbor routing destination is represented by one of these rectangles. Then, water is poured from the bottom, in an inverse manner until the $\nu_i[t]$ waterlevel is reached. The resulting area of water filled inside the rectangles represents the probability mass function of the routing variables. Then, the node takes its routing decision by drawing a sample from this distribution.

While not as simple as the SBP-EH algorithm, the SSBP-EH algorithm presents an important improvement over the former. The introduction of an strongly concave objective function allows the dual function in (6.15) to be differentiable. This, in turn, makes the algorithm take the form of an stochastic gradient rather than a stochastic subgradient (which is the case of SBP-EH), therefore improving the expected rate of stabilization of the algorithm from $O(1/\sqrt{t})$ to $O(1/t)$ [117, Chapter 3.2].

6.4 Causality and Stability Analysis

In this section, we provide theoretical guarantees on the behavior of the proposed policies. On one hand, we establish the conditions under which the routing policies generated by Algorithm 6.1 satisfy the energy causality constraints (6.8). And, on the other hand, we provide stability guarantees on the network queues.

6.4.1 Energy Causality

As we mentioned previously in Section 6.2, the presence of the energy harvesting constraints in the stochastic optimization problem (6.12) introduces the question of causality. In order to have a tractable problem, we have introduced the energy harvesting constraints in an average sense to the routing-scheduling problem. This includes an additional issue, as not all possible solutions satisfy the original causality constraints (6.8) for all time slots. In order to deal with this, we have modified the problem formulation with the introduction of an auxiliary variable. By appropriately choosing the domain of this auxiliary variable and the nodes' battery capacity, we can ensure that the causality constraints are satisfied.

Proposition 6.1 (Energy Causality)**.** *Let the data arrivals of a node $i \in \mathcal{N}$ satisfy $a_i^k[t] \leq \bar{a}_i^k$ for all $k \in \mathcal{K}$ flows and all time slots t. Further, let $\bar{x}_i^k \geq \bar{\gamma}_i^k + \bar{a}_i^k + |\mathcal{N}_i|$ and let the battery capacity satisfy $b_i^{\max} \geq w_{ij}^k + \bar{\gamma}_i^k + \bar{a}_i^k + |\mathcal{N}_i|$. Then both the SBP-EH and SSBP-EH policies shown in Algorithm 6.1 satisfy the energy consumption causality constraint $\sum_{k\in\mathcal{K}} \sum_{j\in\mathcal{N}_i} r_{ij}^k[t] \leq b_i[t]$ of this node for all time slots.*

Proof. To satisfy the energy causality constraints it suffices to show that no transmission occurs when there is no available energy in the battery. This is to say that $r_{ij}^k[t] = 0$ for all j, k if $b_i[t] = 0$. In expressions (6.20) and (6.21), corresponding to the SBP-EH and SSBP-EH algorithms, it suffices to ensure that $w_{ij}^k + \gamma_i^k[t] - \gamma_j^k[t] - \beta_i[t] < 0$ when the battery is empty. In this case, when $b_i[t] = 0$, the battery dual update takes the value $\beta_i[t] = b_i^{\max}$. By the dual update (6.18) and the minimum value of $\bar{x}_i^k$, the data arrival bound $\bar{a}_i^k$ and the number of neighbors $|\mathcal{N}_i|$, we can upper bound the multiplier difference by $\gamma_i^k[t] - \gamma_j^k[t] \leq \bar{\gamma}_i^k + \bar{a}_i^k + |\mathcal{N}_i|$ over all time slots t. We can write then $w_{ij}^k + \bar{\gamma}_i^k + \bar{a}_i^k + |\mathcal{N}_i| - b_i^{\max} \leq 0$, and since $b_i^{\max} \geq w_{ij}^k + \bar{\gamma}_i^k + \bar{a}_i^k + |\mathcal{N}_i|$, this ensures that $r_{ij}^k[t] = 0$. Hence, satisfying the energy causality constraint $\sum_{k\in\mathcal{K}} \sum_{j\in\mathcal{N}_i} r_{ij}^k[t] \leq b_i[t]$ for all time slots. ■

In order to ensure that the energy causality constraints are satisfied, the stochastic subgradients are required to be bounded. This, in turn, forces the probability distribution of the data arrival process to be bounded above by a constant $\bar{a}_i^k$. In practice, for the case in which the probability distribution is not bounded, when a time slot with over

$\bar{a}_i^k$ packets occurs, only $\bar{a}_i^k$ data packets can be kept in the queue and the rest must be discarded to satisfy the energy causality constraints.

6.4.2 Queue Stability

Now, we provide guarantees on the queue stability of the proposed policies. Different from other works (such as [111, 112]), which analyze queue stability with Lyapunov drift notions, we resort to duality theory arguments. We do this by leveraging on the fact that the proposed algorithm is a type of stochastic subgradient algorithm. The approach we take to showing that our algorithm makes the queues stable in the sense of (6.3) is to show that the solution provided by Algorithm 6.1 satisfies the queue stability constraints (6.13b) almost surely. Then, we show that if the optimal queue multipliers γ_i^k are upper bounded by $\bar{\gamma}_i^k$, the solution provided by Algorithm 6.1 also satisfies the stability constraint without auxiliary variable (6.12b). Hence, the data queues satisfy the stability condition (6.3).

First, we start by recalling a common property of the stochastic subgradient.

Proposition 6.2. *Given the dual variables $\boldsymbol{\lambda}[t]$, the conditional expected value $\mathbb{E}\left[\mathbf{s}[t]|\boldsymbol{\lambda}[t]\right]$ of the stochastic subgradient $\mathbf{s}[t]$ is a subgradient of the dual function. Namely, for any $\boldsymbol{\lambda}$,*

$$\mathbb{E}\left[\mathbf{s}^T[t]|\boldsymbol{\lambda}[t]\right](\boldsymbol{\lambda}[t]-\boldsymbol{\lambda}) \geq g(\boldsymbol{\lambda}[t]) - g(\boldsymbol{\lambda}). \tag{6.22}$$

Proof. Take the Lagrangian (6.14) and substitute the ergodic definitions $\mathbb{E}\big[a_i^k[t]\big] = a_i^k$ and $\mathbb{E}\big[e_i[t]\big] = e_i$. Then, the resulting Lagrangian is given by

$$\begin{aligned}\mathcal{L}(\mathbf{r},\boldsymbol{\lambda}) = &\sum_{i\in\mathcal{N}}\sum_{k\in\mathcal{K}}\sum_{j\in\mathcal{N}_i} f_{ij}^k\left(r_{ij}^k\right) - \sum_{i\in\mathcal{N}}\sum_{k\in\mathcal{K}}\bar{\gamma}_i^k x_i^k \\ &+ \sum_{k\in\mathcal{K}}\sum_{i\in\mathcal{N}}\gamma_i^k\left(\sum_{j\in\mathcal{N}_i}\left(r_{ij}^k - r_{ji}^k\right) + x_i^k - \mathbb{E}\big[a_i^k[t]\big]\right) \\ &+ \sum_{i\in\mathcal{N}}\beta_i\left(\mathbb{E}\big[e_i[t]\big] - \sum_{k\in\mathcal{K}}\sum_{j\in\mathcal{N}_i} r_{ij}^k\right).\end{aligned} \tag{6.23}$$

Now, recall that the dual function is then given by $g(\boldsymbol{\lambda}) = \max_{\mathbf{r}\in\mathcal{R}}\mathcal{L}(\mathbf{r},\boldsymbol{\lambda})$, and consider the dual function at time t, given by $g(\boldsymbol{\lambda}[t])$. The primal maximization of this dual function is given by the variables $r_{ij}^k[t]$ and $x_i^k[t]$ in (6.16) and (6.17), respectively. Hence, we can write the dual function as

$$\begin{aligned}g(\boldsymbol{\lambda}[t]) = &\sum_{i\in\mathcal{N}}\sum_{k\in\mathcal{K}}\sum_{j\in\mathcal{N}_i} f_{ij}^k\left(r_{ij}^k[t]\right) - \sum_{i\in\mathcal{N}}\sum_{k\in\mathcal{K}}\bar{\gamma}_i^k x_i^k[t] \\ &+ \sum_{k\in\mathcal{K}}\sum_{i\in\mathcal{N}}\gamma_i^k[t]\,\mathbb{E}\left[\sum_{j\in\mathcal{N}_i}\left(r_{ij}^k[t] - r_{ji}^k[t]\right) + x_i^k[t] - a_i^k[t]\right] \\ &+ \sum_{i\in\mathcal{N}}\beta_i[t]\,\mathbb{E}\left[e_i[t] - \sum_{k\in\mathcal{K}}\sum_{j\in\mathcal{N}_i} r_{ij}^k[t]\right],\end{aligned} \tag{6.24}$$

where we have moved the expectation operator $\mathbb{E}[\cdot]$ out of the subgradients due to its linearity. Then we can use the compact notation for the multiplier vector $\boldsymbol{\lambda}[t]$ and the subgradient $\mathbf{s}[t]$, and substitute the conditional expected value of the subgradients $\mathbb{E}\left[\mathbf{s}[t]|\boldsymbol{\lambda}[t]\right]$ to obtain

$$g(\boldsymbol{\lambda}[t]) = \sum_{i\in\mathcal{N}}\sum_{k\in\mathcal{K}}\sum_{j\in\mathcal{N}_i} f_{ij}^k\left(r_{ij}^k[t]\right) - \sum_{i\in\mathcal{N}}\sum_{k\in\mathcal{K}} \bar{\gamma}_i^k x_i^k[t] + \mathbb{E}\left[\mathbf{s}^T[t]|\boldsymbol{\lambda}[t]\right]\boldsymbol{\lambda}[t]. \tag{6.25}$$

For any arbitrary $\boldsymbol{\lambda}$ we simply have

$$g(\boldsymbol{\lambda}) \geq \sum_{i\in\mathcal{N}}\sum_{k\in\mathcal{K}}\sum_{j\in\mathcal{N}_i} f_{ij}^k\left(r_{ij}^k[t]\right) - \sum_{i\in\mathcal{N}}\sum_{k\in\mathcal{K}} \bar{\gamma}_i^k x_i^k[t] + \mathbb{E}\left[\mathbf{s}^T[t]|\boldsymbol{\lambda}[t]\right]\boldsymbol{\lambda}. \tag{6.26}$$

Then it simply suffices to subtract expression (6.26) from (6.25) to obtain inequality (6.22). ■

Proposition 6.2 shows that the stochastic subgradient is an average descent direction of the dual function $g(\boldsymbol{\lambda}[t])$. Now, we proceed to quantify the average descent distance of the dual update.

Lemma 6.3. *Consider the dual updates of Algorithm 6.1 given by* (6.18) *and* (6.19)*, and let* $\mathbb{E}\left[\|\mathbf{s}[t]\|^2|\boldsymbol{\lambda}[t]\right] \leq S^2$ *be a bound on the second moment of the norm of the stochastic subgradients* $\mathbf{s}[t]$*. Then, the dual updates satisfy the inequality*

$$\mathbb{E}\left[\|\boldsymbol{\lambda}[t+1]-\boldsymbol{\lambda}^\star\|^2|\boldsymbol{\lambda}[t]\right] \leq \|\boldsymbol{\lambda}[t]-\boldsymbol{\lambda}^\star\|^2 + S^2 - 2\left(g(\boldsymbol{\lambda}[t]) - g(\boldsymbol{\lambda}^\star)\right) \tag{6.27}$$

Proof. Start by considering the squared distance between the dual variables at time $t+1$ and their optimal value. This distance is given by $\|\boldsymbol{\lambda}[t+1]-\boldsymbol{\lambda}^\star\|^2$. Then, we substitute the dual variable $\boldsymbol{\lambda}[t+1]$ by its update $\boldsymbol{\lambda}[t+1] = [\boldsymbol{\lambda}[t] - \mathbf{s}[t]]^+$. Then, since the projection is nonexpansive we can upper bound the aforementioned distance by

$$\|\boldsymbol{\lambda}[t+1]-\boldsymbol{\lambda}^\star\|^2 \leq \|\boldsymbol{\lambda}[t]-\mathbf{s}[t]-\boldsymbol{\lambda}^\star\|^2. \tag{6.28}$$

Then, we simply expand the square norm to obtain the expression

$$\|\boldsymbol{\lambda}[t+1]-\boldsymbol{\lambda}^\star\|^2 \leq \|\boldsymbol{\lambda}[t]-\boldsymbol{\lambda}^\star\|^2 + \|\mathbf{s}[t]\|^2 - 2\mathbf{s}^T[t]\left(\boldsymbol{\lambda}[t]-\boldsymbol{\lambda}^\star\right). \tag{6.29}$$

Now, by taking the expectation conditioned by $\boldsymbol{\lambda}[t]$ on both sides we obtain

$$\mathbb{E}\left[\|\boldsymbol{\lambda}[t+1]-\boldsymbol{\lambda}^\star\|^2|\boldsymbol{\lambda}[t]\right] \leq \|\boldsymbol{\lambda}[t]-\boldsymbol{\lambda}^\star\|^2 + \mathbb{E}\left[\|\mathbf{s}[t]\|^2|\boldsymbol{\lambda}[t]\right] - 2\,\mathbb{E}\left[\mathbf{s}^T[t]|\boldsymbol{\lambda}[t]\right]\left(\boldsymbol{\lambda}[t]-\boldsymbol{\lambda}^\star\right) \tag{6.30}$$

And then by substituting the second term on the right hand side of the previous expression by the bound $\mathbb{E}\left[\|\mathbf{s}[t]\|^2|\boldsymbol{\lambda}[t]\right] \leq S^2$ and the third term by the application of Proposition 6.2 with $\boldsymbol{\lambda} = \boldsymbol{\lambda}^\star$, we have expression (6.27). ■

Then, we leverage on this lemma to show that Algorithm 6.1 converges to a neighborhood of the optimal solution of the dual function.

Lemma 6.4. *Consider the dual updates of Algorithm 6.1 given by* (6.18) *and* (6.19)*, and let* $\mathbb{E}\left[\|\mathbf{s}[t]\|^2|\boldsymbol{\lambda}[t]\right] \leq S^2$ *be a bound on the second moment of the norm of the stochastic subgradients* $\mathbf{s}[t]$*. Assume that the dual variable* $\boldsymbol{\lambda}[T]$ *is given for an arbitrary time* T *and define as* $\boldsymbol{\lambda}_{\text{best}}[t] := \arg\min_{\boldsymbol{\lambda}[l]} g(\boldsymbol{\lambda}[l])$ *the dual variable leading to the best value of the of the dual function for the interval* $l \in [T, t]$*. Then, we have*

$$\lim_{t\to\infty} g(\boldsymbol{\lambda}_{\text{best}}[t]|\boldsymbol{\lambda}[T]) \leq g(\boldsymbol{\lambda}^\star) + \frac{S^2}{2} \quad a.s. \tag{6.31}$$

Proof. For ease of exposition, let $T = 0$. Then, define the stopped process $\alpha[t]$, tracking the distance between the dual variables at time t and their optimal value, i.e., $\|\boldsymbol{\lambda}[t]-\boldsymbol{\lambda}^\star\|^2$, until the optimality gap $g(\boldsymbol{\lambda}[t]) - g(\boldsymbol{\lambda}^\star)$ falls below $S^2/2$. This expression is given by

$$\alpha[t] := \|\boldsymbol{\lambda}[t] - \boldsymbol{\lambda}^\star\|^2 \mathbb{I}\left\{g(\boldsymbol{\lambda}_{\text{best}}[t]) - g(\boldsymbol{\lambda}^\star) > S^2/2\right\}. \tag{6.32}$$

where $\mathbb{I}\{\cdot\}$ denotes the indicator function. In a similar way, define the sequence $\beta[t]$ which follows $2\left(g(\boldsymbol{\lambda}[t]) - g(\boldsymbol{\lambda}^\star)\right) - S^2$ until the optimality gap $g(\boldsymbol{\lambda}[t]) - g(\boldsymbol{\lambda}^\star)$ becomes smaller than $S^2/2$,

$$\beta[t] := \big(2\big(g(\boldsymbol{\lambda}[t])-g(\boldsymbol{\lambda}^\star)\big) - S^2\big)\mathbb{I}\left\{g(\boldsymbol{\lambda}_{\text{best}}[t]) - g(\boldsymbol{\lambda}^\star) > S^2/2\right\}. \tag{6.33}$$

Now, let $\mathcal{F}[t]$ be the filtration measuring $\alpha[t]$ and $\beta[t]$. Since $\alpha[t]$ and $\beta[t]$ are completely determined by $\boldsymbol{\lambda}[t]$, and $\boldsymbol{\lambda}[t]$ is a Markov process, conditioning on $\mathcal{F}[t]$ is equivalent to conditioning on $\boldsymbol{\lambda}[t]$. Hence, by application of Lemma 6.3, we can write $\mathbb{E}\left[\alpha[t+1]|\mathcal{F}[t]\right] \leq \alpha[t] - \beta[t]$. Since by definitions (6.32) and (6.33), the processes $\alpha[t]$ and $\beta[t]$ are non-negative, the sequence $\alpha[t]$ follows a supermartingale expression. Then, by the supermartingale convergence theorem [114, Theorem 5.2.9], the sequence $\alpha[t]$ converges almost surely, and the sum $\sum_{t=1}^{\infty} \beta[t] < \infty$ is almost surely finite. The latter implies that $\liminf_{t\to\infty} \beta[t] = 0$ almost surely. Given the definition of $\beta[t]$, this is implied by either of two events. (i) If the indicator function goes to zero, i.e., $g(\boldsymbol{\lambda}_{\text{best}}[t]) - g(\boldsymbol{\lambda}^\star) \leq S^2/2$ for a large t; or (ii) $\liminf_{t\to\infty} 2\big(g(\boldsymbol{\lambda}[t]) - g(\boldsymbol{\lambda}^\star)\big) - S^2 = 0$. From any of those events, expression (6.31) follows. ■

The convergence of the dual function as asserted in the previous lemma allows us to prove that the sequences of routing decision $\{r_{ij}^k[t]\}_{t=1}^{\infty}$ and auxiliary variables $\{x_i^k[t]\}_{t=1}^{\infty}$ generated by Algorithm 6.1 are almost surely feasible.

Proposition 6.5 (Auxiliary Feasibility)**.** *Assume there exist strictly feasible primal variables* r_{ij}^k *and* x_i^k *such that* $\sum_{j\in\mathcal{N}_i} r_{ij}^k - \sum_{j\in\mathcal{N}_i} r_{ji}^k - a_i^k + x_i^k > \xi$ *and* $e_i - \sum_{k\in\mathcal{K}} \sum_{j\in\mathcal{N}_i} r_{ij}^k > \xi$*, for some* $\xi > 0$*. Then, the constraints* (6.13b) *and* (6.13c) *are almost surely satisfied by Algorithm 6.1.*

Proof. First, let us collect the feasible routing variables r_{ij}^k and auxiliary variables x_i^k in the vector $\hat{\mathbf{r}} = \{r_{ij}^k, x_i^k\}$. Then, if there exist strictly feasible variables $\hat{\mathbf{r}}$, we can bound the value of the dual function $g(\boldsymbol{\lambda})$ as follows. The dual function is defined as the maximum over primal variables $g(\boldsymbol{\lambda}) = \max_{\mathbf{r}} \mathcal{L}(\mathbf{r}, \boldsymbol{\lambda})$, hence $g(\boldsymbol{\lambda}) \geq \mathcal{L}(\hat{\mathbf{r}}, \boldsymbol{\lambda})$. From this, by using the $\sum_{j\in\mathcal{N}_i} r_{ij}^k - \sum_{j\in\mathcal{N}_i} r_{ji}^k - a_i^k + x_i^k > \xi$ and $e_i - \sum_{k\in\mathcal{K}} \sum_{j\in\mathcal{N}_i} r_{ij}^k > \xi$ terms we establish the following bound

$$g(\boldsymbol{\lambda}) \geq \sum_{i\in\mathcal{N}} \sum_{k\in\mathcal{K}} \sum_{j\in\mathcal{N}_i} f_{ij}^k \left(r_{ij}^k\right) - \sum_{i\in\mathcal{N}} \sum_{k\in\mathcal{K}} \bar{\gamma}_i^k x_i^k + \xi \boldsymbol{\lambda}^T \mathbf{1}. \tag{6.34}$$

Then, by simply reordering terms we obtain the following upper bound on the dual variables

$$\boldsymbol{\lambda} \leq \frac{1}{\xi}\left(g(\boldsymbol{\lambda}) - \sum_{i\in\mathcal{N}} \sum_{k\in\mathcal{K}} \Big(\sum_{j\in\mathcal{N}_i} f_{ij}^k \left(r_{ij}^k\right) + \bar{\gamma}_i^k x_i^k\Big)\right). \tag{6.35}$$

Lemma 6.4 certifies the existence of a time $t \geq T_0$ for which $g(\boldsymbol{\lambda}[t]) \leq g(\boldsymbol{\lambda}^\star) + S^2/2$. Hence,

$$\boldsymbol{\lambda}[t] \leq \frac{1}{\xi}\left(g(\boldsymbol{\lambda}^\star) + \frac{S^2}{2} - \sum_{i\in\mathcal{N}} \sum_{k\in\mathcal{K}} \Big(\sum_{j\in\mathcal{N}_i} f_{ij}^k \left(r_{ij}^k\right) + \bar{\gamma}_i^k x_i^k\Big)\right) \tag{6.36}$$

for $t \geq T_0$. Now, recall that the feasibility conditions (6.13b) and (6.13c) are given by the limits

$$\lim_{t\to\infty} \frac{1}{t} \sum_{l=1}^{t} \left(\sum_{j\in\mathcal{N}_i} \left(r_{ij}^k[l] - r_{ji}^k[l]\right) - a_i^k[l] + x_i^k[t]\right) \geq 0 \tag{6.37}$$

$$\lim_{t\to\infty} \frac{1}{t} \sum_{l=1}^{t} \left(e_i[l] - \sum_{k\in\mathcal{K}} \sum_{j\in\mathcal{N}_i} r_{ij}^k[l]\right) \geq 0 \tag{6.38}$$

which, by recalling that the constraints are simply the stochastic subgradients $\mathbf{s}[t]$ of the problem, they can also be written in compact form as $\lim_{t\to\infty} \frac{1}{t} \sum_{l=1}^{t} \mathbf{s}[l] \geq 0$. Now, consider the dual updates (6.18) and (6.19) given by $\boldsymbol{\lambda}[t+1] = [\boldsymbol{\lambda}[t] - \mathbf{s}[t]]^+$. Since the $[\cdot]^+$ operator corresponds to a nonnegative projection, the dual variables can be lower bounded by removing the projection and recursively substituting the updates

$$\boldsymbol{\lambda}[t+1] \geq \boldsymbol{\lambda}[t] - \mathbf{s}[t] \geq \boldsymbol{\lambda}[1] - \sum_{l=1}^{t} \mathbf{s}[l] \geq -\sum_{l=1}^{t} \mathbf{s}[l]. \tag{6.39}$$

To prove almost sure feasibility, we will follow by contradiction. First, assume that conditions (6.37) and (6.38) are infeasible. In compact form, this means the existence of a time $t \geq T_1$, for which there is a constant $\delta > 0$ such that $\frac{1}{t} \sum_{l=1}^{t} \mathbf{s}[l] \leq -\delta$. By substituting in (6.39), we have that the dual variables are lower bounded by $\boldsymbol{\lambda}[t+1] \geq \delta t$. Now, we can freely choose a time $t \geq T_2$ such that

$$\boldsymbol{\lambda}[t] > \frac{1}{\xi}\left(g(\boldsymbol{\lambda}^\star) + \frac{S^2}{2} - \sum_{i\in\mathcal{N}} \sum_{k\in\mathcal{K}} \Big(\sum_{j\in\mathcal{N}_i} f_{ij}^k \left(r_{ij}^k\right) + \bar{\gamma}_i^k x_i^k\Big)\right) \tag{6.40}$$

for all $t \geq T_2$. However, this contradicts the upper bound established in (6.36). This means that there do not exist sequences generated by Algorithm 6.1 such that (6.37) and (6.38) are not satisfied. Therefore, the constraints (6.13b) and (6.13c) are satisfied almost surely. ■

Finally, it suffices to show that if the optimal dual variables are upper bounded by the constants $\bar{\gamma}_i^k$, the system satisfies the original problem without the auxiliary variable. Thus, satisfying the original constraint (6.12b) and hence the queue stability condition (6.3).

Proposition 6.6 (Feasibility)**.** *Assume that there exist strictly feasible routing variables* r_{ij}^k *such that* $\sum_{j\in\mathcal{N}_i} r_{ij}^k - \sum_{j\in\mathcal{N}_i} r_{ji}^k - a_i^k > \xi$ *and* $e_i - \sum_{k\in\mathcal{K}}\sum_{j\in\mathcal{N}_i} r_{ij}^k > \xi$*, for some* $\xi > 0$*. Furthermore, assume the optimal Lagrange multipliers of the queue stability constraints satisfy* $\gamma_i^{k,\star} \leq \bar{\gamma}_i^k$*. Then, the constraints* (6.12b) *and* (6.12c) *are almost surely satisfied by Algorithm 6.1.*

Proof. Take the difference between the Lagrangian (6.14) of the optimization problem with the auxiliary variable (6.13) and the original problem (6.12). The difference between them is given by

$$\mathcal{L}(\mathbf{r},\boldsymbol{\lambda}) - \hat{\mathcal{L}}(\mathbf{r},\boldsymbol{\lambda}) = \sum_{i\in\mathcal{N}}\sum_{k\in\mathcal{K}}\big(-\bar{\gamma}_i^k + \gamma_i^k + \theta_i^k - \nu_i^k\big)x_i^k + \sum_{i\in\mathcal{N}}\sum_{k\in\mathcal{K}} \nu_i^k \bar{x}_i^k \tag{6.41}$$

where $\theta_i^k \geq 0$ and $\nu_i^k \geq 0$ are the Lagrange multipliers of the $x_i^k \geq 0$ and $x_i^k \leq \bar{x}_i^k$ constraints, respectively. In order for both problems to be equivalent, the minimization of (6.41), which is the solution of the dual problem, must be zero. This implies the existence of Lagrange multipliers satisfying the constraints $\bar{\gamma}_i^k - \gamma_i^k - \theta_i^k + \nu_i^k = 0$, for all $i \in \mathcal{N}$ and $k \in \mathcal{K}$. Since $\gamma_i^{k,\star} \leq \bar{\gamma}_i^k$, the constraints can be satisfied by letting $\nu_i^{k,\star} = 0$, and $\theta_i^{k,\star}$ acting as a slack variable. Then, $\mathcal{L}(\mathbf{r},\boldsymbol{\lambda}) - \hat{\mathcal{L}}(\mathbf{r},\boldsymbol{\lambda}) = 0$, which implies that the optimal solution of both problems is the same. Hence, $\lim_{t\to\infty} \frac{1}{t}\sum_{l=1}^{t} x_i^k[l] = x_i^k = 0$, and by Proposition 6.5 the routing variables r_{ij}^k of Algorithm 6.1 satisfy the constraint $\sum_{j\in\mathcal{N}_i} r_{ij}^k - \sum_{j\in\mathcal{N}_i} r_{ji}^k - a_i^k \geq 0$. ■

Corollary 6.7 (Queue Stability)**.** *Consider the conditions of Proposition 6.6. Then, there exists a constant* Q *such that for some arbitrary time* T *the queues of the system under Algorithm 6.1 satisfy* $\Pr\{\max_{t\geq T} \|\mathbf{q}[t]\| \leq Q|\mathbf{q}[T]\} = 1$.

Proof. Denote by $\mathcal{F}_i^k[t]$ the filtration measuring $q_i^k[l]$. Then, since the routing variables r_{ij}^k generated by Algorithm 6.1 satisfy $\sum_{j\in\mathcal{N}_i} r_{ij}^k - \sum_{j\in\mathcal{N}_i} r_{ji}^k - a_i^k \geq 0$, the queue evolution (6.2) obeys the supermartingale expression $\mathbb{E}\left[q_i^k[t+1]|\mathcal{F}_i^k[t]\right] \leq q_i^k[t]$. By the supermartingale convergence theorem [114, Theorem 5.2.9], the sequence $q_i^k[t]$ converges almost surely, therefore satisfying the stability condition $\Pr\{\max_{t\geq T} \|\mathbf{q}[t]\| \leq Q|\mathbf{q}[T]\} = 1$. ■

Given an appropriate choice of $\bar{\gamma}_i^k$ and feasible data and energy arrivals, Proposition 6.6 guarantees that the nodes route in average as many packets as they receive from neighbors and the arrival process (i.e., the constraint (6.12b) is satisfied). Then, Corollary 6.7 shows that this implies that the queues themselves are almost surely stable.

6.4.3 Remarks and Practical Considerations

As we have thoroughly examined, the introduction of energy harvesting constraints in the routing-scheduling problem also introduces a causality problem. In order to handle this problem, we have resorted to the auxiliary formulation introduced in (6.13). Under this new formulation, we have shown the ability of Algorithm 6.1 to stabilize the data queues while guaranteeing the energy causality constrains. This modified formulation serves to bound the values of the dual variables. Hence, one might think that a simpler approach would be to simply project the dual variables to a restricted domain and remove the auxiliary variables x_i^k altogether from the optimization problem. We studied the consequences of this formulation in our previous work [8]. The main drawback of using a dual projection is that in order to ensure the almost sure feasibility of such scheme (as in Proposition 6.5), the maximum value of the projection $\boldsymbol{\lambda}^{\max}$ must be lower bounded by

$$\boldsymbol{\lambda}^{\max} > \frac{1}{\xi}\left(g(\boldsymbol{\lambda}^\star) + \frac{S^2}{2} - \sum_{i\in\mathcal{N}}\sum_{k\in\mathcal{K}}\sum_{j\in\mathcal{N}_i} f_{ij}^k\left(r_{ij}^k\right)\right). \tag{6.42}$$

This is a very loose requirement, which does not provide the clear theoretical guaranties that our proposed formulation offers. Nonetheless, the numerical results provided in [8] seem to indicate that simply having the optimal dual variables in the range $[0, \boldsymbol{\lambda}^{\max}]$ can be sufficient. Thus, the simpler use a projection of the dual variables can also be used as a less theoretically robust but practical option.

6.5 Numerical Results

In this section, we conduct numerical experiments aimed at evaluating the performance of the proposed SBP-EH and SSBP-EH policies. As a means of comparison, when indicated, we also provide the non-energy harvesting counterparts of our proposed policies. Namely, the Stochastic Backpressure (SBP) [113] and Stochastic Soft Backpressure (SSBP) [116] policies. These policies correspond to solving (6.7), the original optimization problem without the energy harvesting constraints, with the objective functions shown in Sections 6.3.1 and 6.3.2, respectively. Hence, these policies assume the availability of an unlimited energy supply. We consider the communication network shown in Figure 6.3, where we let nodes 1 and 14 act as sink nodes and the rest of the nodes support a single flow with packet arrival rates of $a_i^k = 0.35$ packets per time slot. Moreover, we consider the nodes

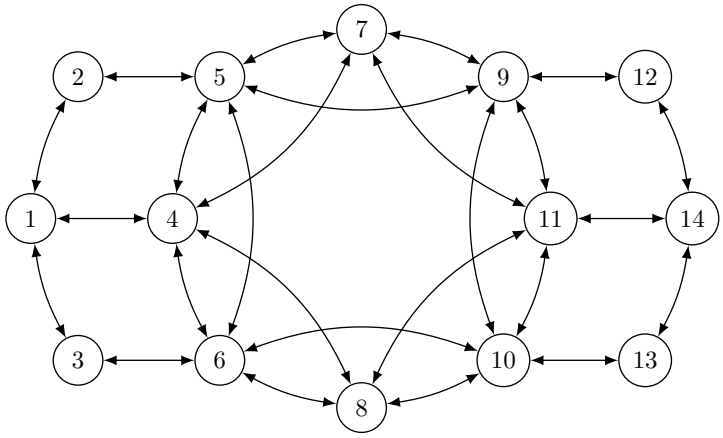

Figure 6.3: Connectivity graph of the simulated network.

to be harvesting energy at a rate of $e_i = 1$ units of energy per time slot and storing it in a battery of capacity $b_i^{\max} = 15$. Furthermore, we set the routing weights to $w_{ij}^k = 0$, and let $\bar{\gamma}_i^k = 10$.

6.5.1 Network Queues

First, we plot in Figure 6.4 a sample path of the total number of queued packets in the network as a function of the elapsed time. As expected, all the policies are capable of stabilizing the queues in the network. Due to the random nature of the processes, it is difficult to say exactly at which point stabilization occurs. Nonetheless, for the SBP and SBP-EH policies, the data queues seem to stop growing after around $t = 200$ time slots. In the case of the SSBP and SSBP-EH policies, stabilization occurs much more rapidly rapidly, with less than $t = 100$ time slots necessary to obtain stability. Also, both soft policies (SSBP and SSBP-EH) stabilize the queues with a lower number of average queued packets than their counterpart non-soft policies (SBP and SBP-EH). Namely, at $t = 1000$, the average queued packets are 19.08 for SBP and 26.22 for SBP-EH. In the case of the soft policies, these numbers are much smaller, with 11.55 and 11.97 packets for SSBP and SSBP-EH, respectively. This also shows that the gap between the SSBP and SSBP-EH policies seems to vanish asymptotically (3.63% at $t = 1000$), while this is not the case for the non-soft policies (a gap of 37.42% at $t = 1000$). This occurs due to the fact that the SBP and SBP-EH policies choose their routing policy by maximizing the difference between queue multipliers. Hence, making the decision indifferent to the actual value of the multipliers as long as their differences stay the same. For the SSBP and SSBP-EH policies, this situation does not occur due to their randomized nature. Hence, pushing for lower average queued packets. Furthermore, since the data arrivals can be sustained by the energy harvesting process, the SSBP-EH policy tries to get as close a the non-EH one, leading to the small of the gap. Also, note that the SBP-EH

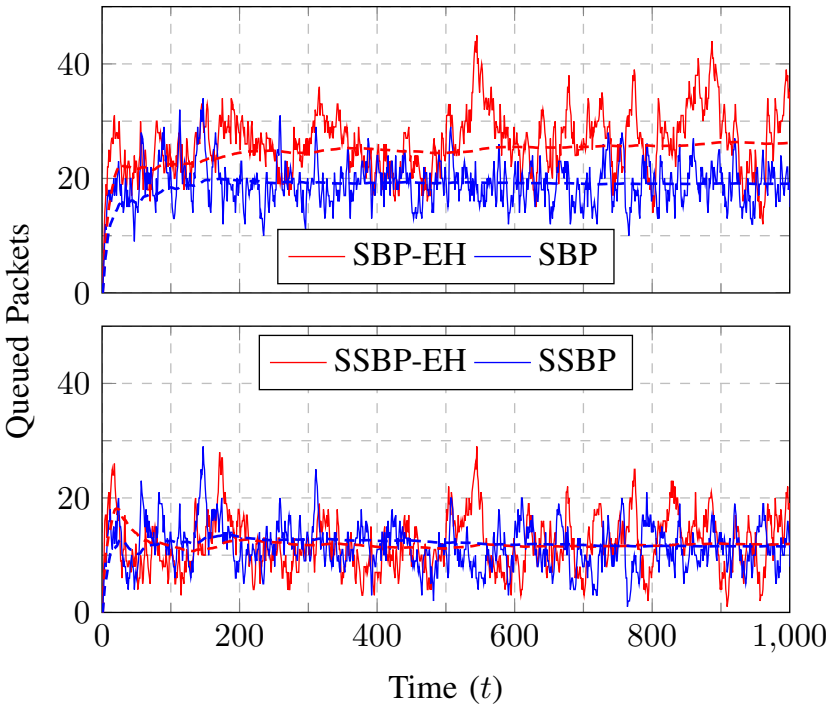

Figure 6.4: Total amount of packets queued in the network at each time slot. Average values are shown in dashed lines.

and SSBP-EH policies are more volatile than their non-EH counterparts. For example, around $t = 550$, the number of queued packets spikes for the energy harvesting policies, which is not the case in the non-EH ones. These types of spikes arise due to a certain lack of energy around those time instants.

In Figure 6.5 we have plotted the average queued packets at each node for the SBP-EH and SSBP-EH policies. In general, SSBP-EH shows a lower number of average queued packets over all the nodes and the improvements are more significant the lower the pressure the node supports. This tends to translate to better improvements for nodes far away from a sink that tend to be routed less traffic. For example, the nodes 7 and 8 (See Fig. 6.3), which are the furthest away from any sink, show a reduction of 1.92 and 1.81 average packets, respectively, when using SSBP-EH. The rest of the nodes also show significant improvements when using SSBP-EH. Nodes 5, 6, 9 and 10, all lying at two hops of distance of a sink are more critical for accessing a sink, as having them congested blocks the access to the sink of the previous nodes 7 and 8. In this case, the improvements range from 1.57 to 1.79 average data packets. Finally, there are the nodes that lie at one hop distance from any sink (nodes 2, 3, 4, 11, 12 and 13) . These nodes sustain a significant amount of traffic and show improvements ranging from 0.51 to 1.78. With the nodes with the highest traffic, nodes 4 and 11, improving by 0.73 and 1.28 data packets, respectively.

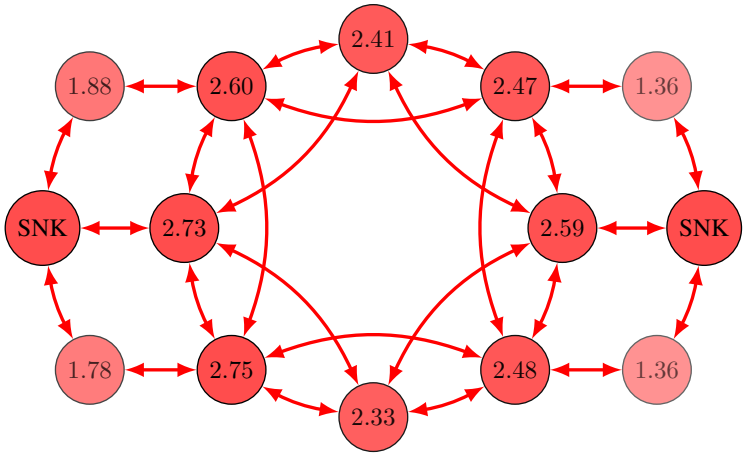

(a) SBP-EH.

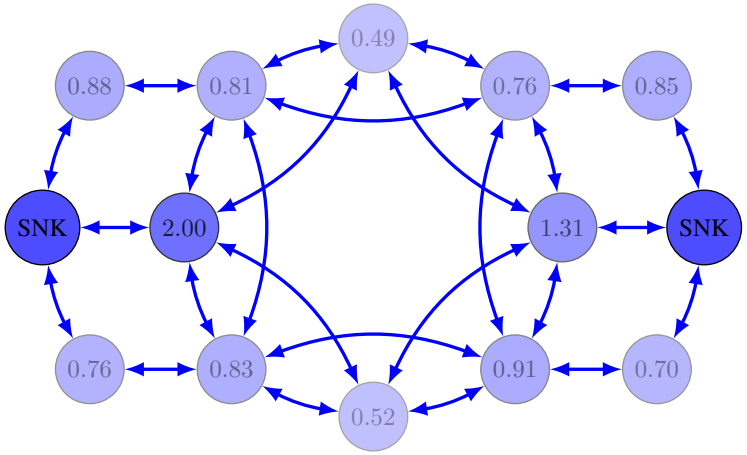

(b) SSBP-EH.

Figure 6.5: Average data queues at each node in the network.

The differences between SBP-EH and SSBP-EH are also evidenced in terms of their energy use. In Figure 6.6 we plot the total energy in the network at a given time slot for both the SBP-EH and the SSBP-EH policies. On one hand, this figure illustrates the high variability in the energy supply due to the energy harvesting process. On the other hand, the SSBP-EH policy is shown to be more aggressive in its energy use. Also, note that drops in total network energy are not necessarily correlated with increases in queued packets in the network. For example, the previously noticed peak of queued data packets at $t = 550$ in Fig. 6.4 does not have an equivalent large drop in network energy. This is due to the fact that it is better for energy in the network to overall be lower than to have a specific high-pressure node have an energy shortage. In general, spikes in queued data packets tend to occur when a specific route becomes blocked by the temporary lack of energy.

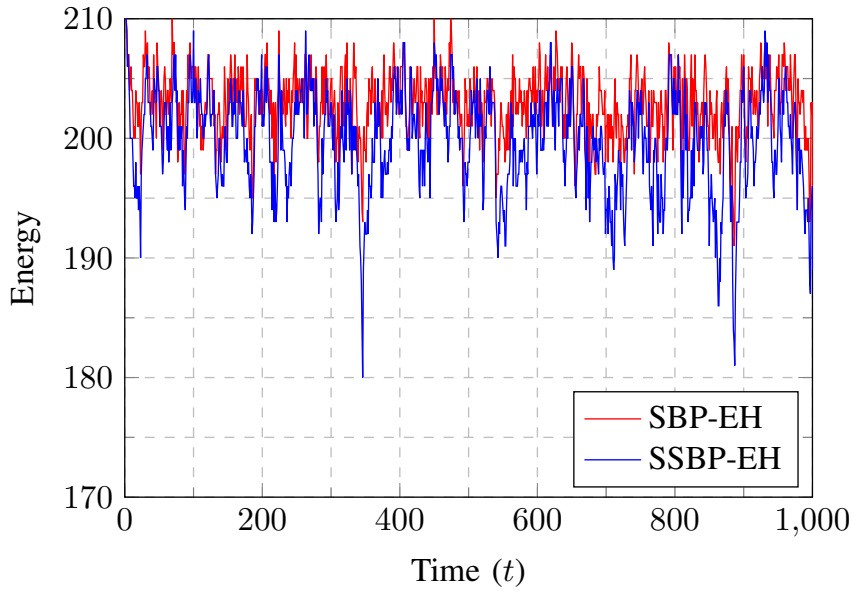

Figure 6.6: Total energy stored in the network at a given time slot.

6.5.2 Network Balance

As discussed in Section 6.4, the choice of the parameters $\bar{\gamma}_i^k$, which control the maximum values taken by the queue multipliers γ_i^k, is important to ensure the stability of the data queues. Namely, the optimal multipliers must be smaller than this $\bar{\gamma}_i^k$ parameter. In Figure 6.7, we plot the γ_i^k multipliers for one of the nodes which supports the most traffic in the network (node 5). The time-average of these dual variables converges to the optimal value. In the chosen scenario, the parameter used, $\bar{\gamma}_i^k = 10$, is well above the optimal value. Hence, the system satisfies Proposition 6.7, and can be ensured to stabilize the queues. Some additional insight into the importance of the queue multipliers can be gained by a pricing interpretation of the dual problem. Under this interpretation, the dual variables $\gamma_i^k[t]$ represent the unit price associated to the routing constraint $a_i^k[t] \leq \sum_{j \in \mathcal{N}_i} \left(r_{ij}^k[t] - r_{ji}^k[t]\right) + x_i^k[t]$. When the node does not satisfy this constraint, it pays $\gamma_i^k[t]$ per unit of constraint violation. Likewise, if it strictly satisfies this constraint, it receives $\gamma_i^k[t]$ per unit of constraint satisfaction. In this sense, the $\bar{\gamma}_i^k$ parameter represents both the maximum payment that a node can receive and the maximum price it can pay. Hence, the optimal value of γ_i^k must necessarily fall below $\bar{\gamma}_i^k$ in order to obtain a stable system. We can use this pricing interpretation to compare the different policies. In general, the energy harvesting policies have higher $\gamma_i^k[t]$ values than their non-EH counterparts. This is due to the fact that, due to the energy harvesting constraints, the unit violation of the routing constraint is harder to recoup in the EH-aware policies, hence the higher price paid. In a similar note, due to their more aggressive routing decisions, the soft policies also show higher $\gamma_i^k[t]$ values than their non-soft counterparts.

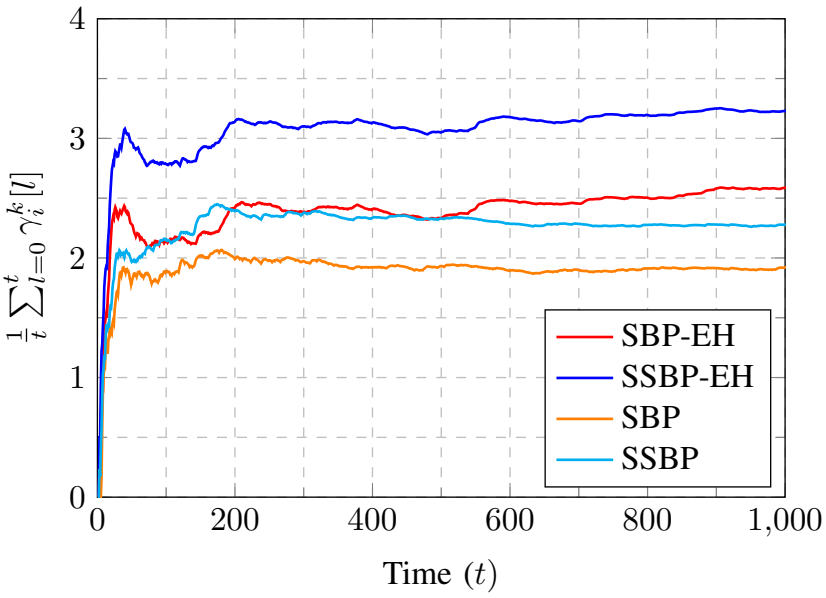

Figure 6.7: Average value of the queue multipliers γ_i^k for node 5 ($i = 5$, $k = 1$).

Also of interest is the study of the balance characteristics of the network. As discussed previously, the stability guarantees of the network are subject to the existence of a feasible routing solution given the data and energy arrival rates. This motivates another way of showing stability, different from the data queues shown in Fig. 6.4. We can consider that a successful routing strategy is expected to route to the sink nodes as many packets as generated by the network. This is given by the network balance expression $\sum_{i\in\mathcal{N}}\sum_{k\in\mathcal{K}}\left(a_i^k[t] - r_{ij}^k[t]\right)$, where $j = N_{(dest)}^k$. The time average of this measure is shown in Figure 6.8. As expected, the time average data network balance goes to zero for all policies. This illustrates that all policies are capable of routing to the sink nodes as many packets as they arrive to the network, hence ensuring queue stability. We previously observed in Fig. 6.8 that stability occurs around $t = 200$ time slots for the SBP and SBP-EH policies and less than $t = 100$ time slots for the SSBP and SSBP-EH ones. Those observations can be compared with the network balance of Fig. 6.8, where those values correspond to the time around when the slope of the data balance curve starts to go flat. Remarkably, the proposed energy harvesting policies do not lose convergence speed when compared to the non-EH ones. Also, convergence of the SSBP and SSBP-EH policies occurs at a faster rate, a point that we previously raised in Section 6.3.2.

Another measure of network balance of interest is related to the energy balance in the network. This can be expressed by $\sum_{i\in\mathcal{N}}\sum_{k\in\mathcal{K}}\left(e_i[t] - \sum_{j\in\mathcal{N}_i} r_{ij}^k[t]\right)$. This measure serves to quantify how much of the energy harvested in the network is actually being used. The time average of the energy balance is shown in Figure 6.9. As expected, given

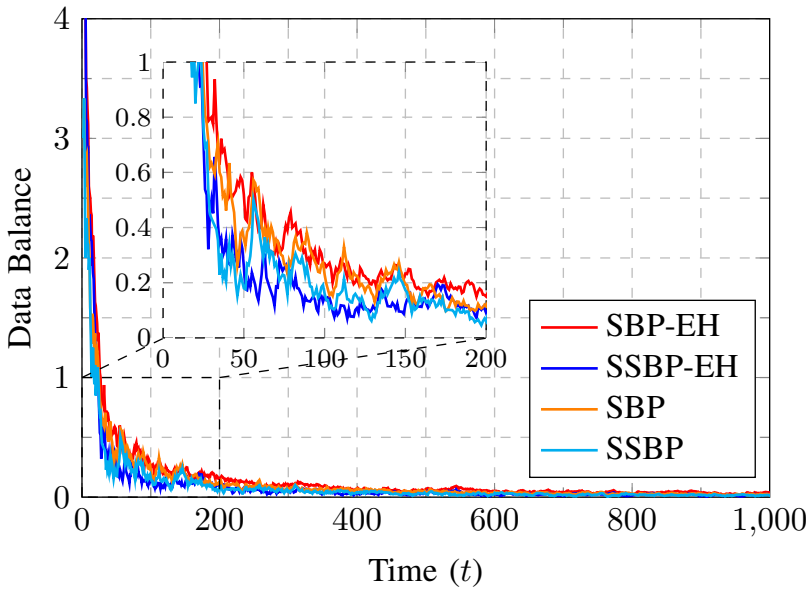

Figure 6.8: Average data balance in the network, given by the expression $\frac{1}{t}\sum_{l=0}^{t}\sum_{i\in\mathcal{N}}\sum_{k\in\mathcal{K}}\left(a_i^k[l]-r_{ij}^k[l]\right)$, where $j=N_{(dest)}^k$.

that the network harvests enough energy to support the routing-scheduling decisions, both policies converge to a non-zero value. Once stabilized, the SBP-EH policy has, in average, energy left for around 12 packet transmission in all of the network, while the SSBP-EH only has energy left for an average of 2 packet transmissions. We previously identified in Fig. 6.6 the SSBP-EH to be more aggressive in its energy use. At the same time, we can also say that the SSBP-EH policy uses its energy supply in a more efficient manner. Since the nodes are powered by energy harvesting instead of a limited energy supply, not using available energy can be considered wasteful, as batteries will tend to overflow. In this sense, to use more energy (as in SSBP-EH) rather than to use energy more conservatively (as in SBP-EH), can be seen as a better option. In this sense, SSBP-EH makes a more efficient use of the available energy, resulting in an overall better performance.

6.5.3 Network Delay

An additional important characteristic of routing-scheduling policies is their resulting delay in the packet delivery. While the average delay is proportional to the average number of queued packets in the network, we also study this measure explicitly. In order to do this, and under the assumption of first-in first-out queues, we compute the number of time slots it takes for a packet to be delivered to a sink node. We plot in Figure 6.10 the resulting histogram. In average, the number of time slots it takes to deliver a packet to a sink node is 4.04 for the SSBP-EH policy, while it is 5.36 for the SBP-EH policy.

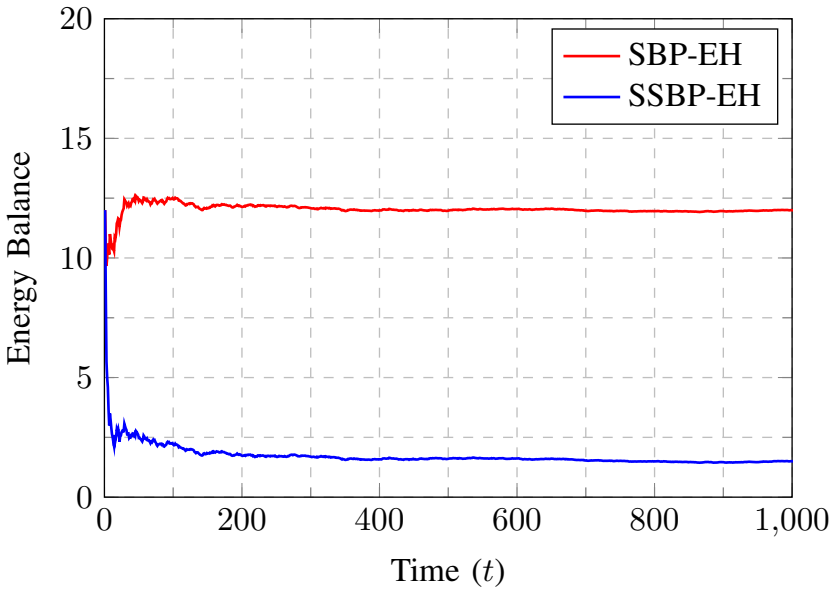

Figure 6.9: Average energy balance in the network, given by the expression $\frac{1}{t}\sum_{l=0}^{t} \sum_{i\in\mathcal{N}}\sum_{k\in\mathcal{K}}\left(e_i[l]-\sum_{j\in\mathcal{N}_i} r_{ij}^k[l]\right)$.

This is about a 1 time slot of difference between the policies. Taking a more detailed look at the histogram, we can see that the distribution for the SSBP-EH is very similar to the one of the SBP-EH, but with a 1 time slot shift to the left. As already seen in Fig. 6.5, the more aggressive behavior of the SSBP-EH policy leads to an overall reduction in the network queues. These smaller queues result in a reduction of the waiting time of packets at each hop, which results in a smaller delivery delay.

6.6 Conclusions

In this chapter, we have generalized the stochastic family of backpressure policies to energy harvesting networks. Different from other works, which are based on Lyapunov drift notions, we have resorted to duality theory. This has allowed us to study the problem under a framework based on the correspondence between queues and Lagrange multipliers. Under this framework, we have proposed two policies, (i) SBP-EH, an easy to implement policy where nodes track the difference between their queue multipliers and the ones of their neighbors. The pressure is further reduced by the battery multipliers as the stored energy decreases. Then, the transmit decision is to transmit the flow with the highest pressure. And (ii) SSBP-EH, a probabilistic policy with improved performance and convergence guarantees, where nodes track the pressure in the same way as SBP-EH but perform an equalization in the form of an inverse waterfilling. This results in a probability mass function for the routing-scheduling decision, where a sample of this

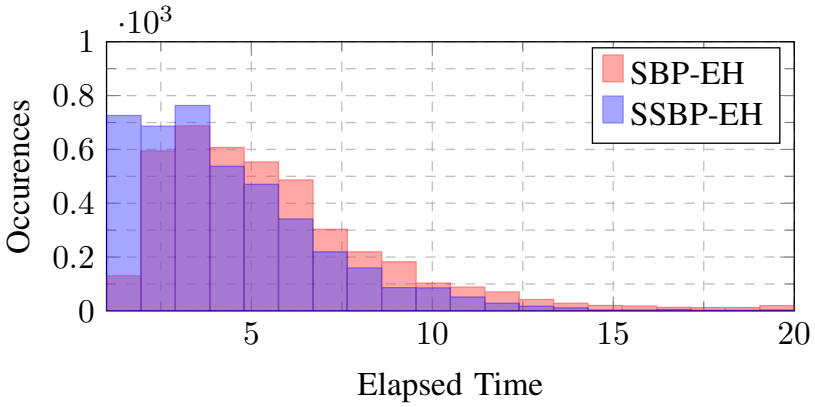

Figure 6.10: Histogram of packet elapsed time before reaching a sink node.

distribution is then taken to decide the transmission. For both policies, we have studied the conditions under which energy causality and queue stability are guaranteed, which we have also verified by means of simulations. The numerical results show that given feasible data and energy arrivals, both policies are capable of stabilizing the network. Overall, the SSBP-EH policy shows improvements in queued packets, stabilization speed and delay with respect to the SBP-EH policy. Furthermore, when compared to non-EH policies, the SSBP-EH policy shows to have an asymptotically vanishing gap.

Chapter 7

Random Access Policies for Wireless Networked Control Systems

In this chapter, we study wireless networked control systems with energy harvesting sensors. Multiple sensors share a wireless medium over which they transmit measurements to their respective controllers, and due to the shared medium, packet collisions occur if sensors transmit simultaneously. To alleviate this problem, we propose random access policies that satisfy a required control performance on each control loop, while also satisfying the energy constraints imposed by the energy harvesting process. The optimal scheduling policy is shown to follow a simple thresholding operation. Moreover, we provide a stochastic dual method for their computation, which is shown to be decoupled across sensors. Finally, we verify numerically the properties of the proposed policy.

7.1 Introduction

Wireless networked control systems are rapidly becoming prevalent in the modern world. They are present in smart homes, robotic automation, smart transportation, industrial plants and more. A critical component of these wireless control systems are the sensing devices. These sensor nodes measure the state of the system and transmit their observations over a wireless channel. However, due to the uncertain nature of the wireless channel, the choice of communication policy critically affects the closed loop performance of the control system. The sensors share the wireless communication medium and therefore one should aim for an efficient use of this resource in a way that meets the control performance requirements.

When dealing with classically powered sensors, the scheduling problem in wireless networked control systems has been previously studied in the literature. The most com-

mon approach to this problem is the design of centralized scheduling policies. In this setup, there exists an overseeing entity specifying which sensor is allowed to transmit at a given time slot, in order to avoid collisions between packets. These type of policies might be static [118,119] or of a more dynamic nature, where centralized decisions can be taken based on plant state information [120] or wireless channel conditions [121], among others.

7.1.1 Contribution

In this work, we study the design of random access policies for sensor nodes powered by energy harvesting. Different from previous works [119–121], we design decentralized scheduling policies. This is more in line with the random access policy presented in [122]. However, these policies are designed for traditionally powered systems and are not necessarily stable when the sensor nodes are powered by energy harvesting. In contrast, our goal is to design channel access policies such that all control loops satisfy their control performance requirements and the power consumption satisfies the energy causality constraints imposed by the energy harvesting process. To this end, we use a control performance abstraction which allows us to translate the control performance requirements to successful transmission probabilities of the random access scheme. Under ergodic assumptions on the channel states and energy harvesting process, we propose a simple dynamic threshold scheduling policy which accounts for the channel as well as the battery state of the sensor. Furthermore, the optimal scheduling policies are computed by means of a stochastic dual method. Finally, we numerically verify the behavior of the proposed policies.

7.2 System Model and Problem Formulation

Consider the wireless control system consisting of M different plants shown in Figure 7.1. The state of each of these plants is measured by a sensor powered by energy harvesting, and each of these sensors transmits the measurements to the plant controller through a shared wireless medium. Due to the nature of the shared medium, collisions will arise if more than one sensor decides to transmit at the same time. Under these conditions, our goal is to design medium access policies such that a specific control performance is guaranteed for all plants.

7.2.1 Control Model

Let us denote by $\gamma_i[t] \in \{0, 1\}$ whether the transmission by the i-th sensor at time slot t was successful or not. Then, under the assumption of a linear time-invariant system,

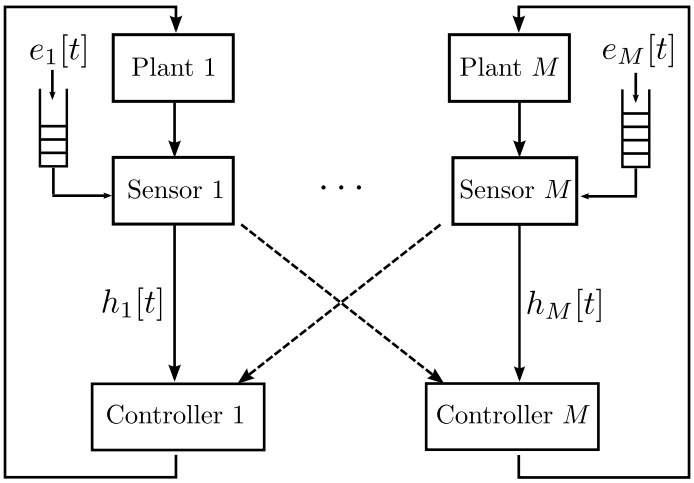

Figure 7.1: System model.

we can model the plant dynamics by the following discrete-time switched system

$$\mathbf{x}_i[t+1] = \begin{cases} \mathbf{A}_{c,i}\mathbf{x}_i[t] + \mathbf{w}_i[t], & \text{if } \gamma_i[t] = 1, \\ \mathbf{A}_{o,i}\mathbf{x}_i[t] + \mathbf{w}_i[t], & \text{if } \gamma_i[t] = 0, \end{cases} \tag{7.1}$$

where $\mathbf{x}_i[t] \in \mathbb{R}^{n_i}$ denotes the i-th plant state at time slot t, and the $\mathbf{w}_i[t]$ variables correspond to independent and identically distributed (i.i.d.) zero-mean Gaussian noise with covariance $\mathbf{C}_i$. Moreover, $\mathbf{A}_{c,i} \in \mathbb{R}^{n_i \times n_i}$ is the closed-loop dynamics matrix and $\mathbf{A}_{o,i} \in \mathbb{R}^{n_i \times n_i}$ is the open-loop dynamics matrix. The closed-loop matrix $\mathbf{A}_{c,i}$ corresponds to the system evolution when the plant successfully receives the measurement transmitted by the sensor node and is thus assumed to be asymptotically stable. On the other hand, the matrix $\mathbf{A}_{o,i}$ corresponds to the plant evolution when not receiving the sensor measurement (due to a lack of transmission by the sensor node or collision) and may be unstable.

7.2.2 Communication Model

Consider now the communication model. We have defined the variables $\gamma_i[t]$ to indicate the successful transmission of the sensor nodes measurements. Hence, they correspond to random variables whose distribution depends on the chosen communication policy. We consider a time slotted communication model in which at each time slot, the sensor either transmits a packet (containing the measurement at that time slot) over the shared wireless medium or not. We denote this decision to transmit by the scheduling variable $z_i[t] \in \{0, 1\}$. Then, if two sensors transmit at the same time slot, a collision will occur and neither packet will be received. Furthermore, the packet will be decoded with a certain probability depending on the channel state. Then, the probability of successful

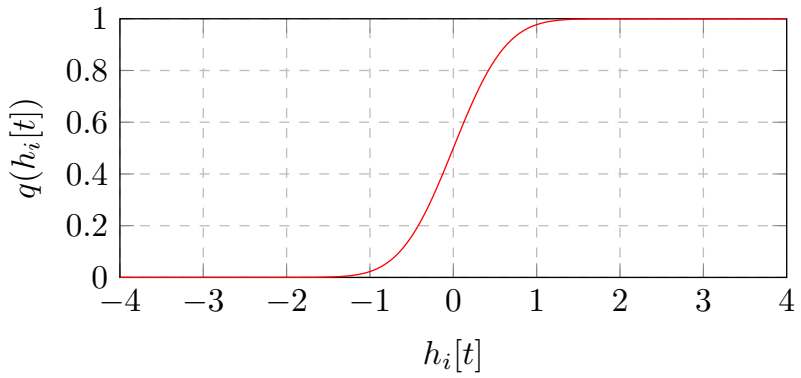

Figure 7.2: Probability of decoding as a function of the channel state.

transmission at a given time slot t is given by

$$\Pr\left(\gamma_i[t]=1\right) = q(h_i[t])z_i[t]\prod_{j\neq i}\left(1-z_j[t]\right) \tag{7.2}$$

where $q:\mathbb{R}\to[0,1]$ is a continuous strictly increasing decoding function, which depends on the channel state $h_i[t]$ (A typical decoding function is shown in Figure 7.2). Furthermore, the channel state variables $h_i[t]$ are assumed to have continuous probability density function[1]. Also, for notational compactness we define $q_i[t] \triangleq q(h_i[t])$.

7.2.3 Energy Harvesting

We consider the sensor nodes to be powered by energy harvesting. At time slot t, the i-th sensor harvests $e_i[t]$ units of energy, where the energy harvesting process is assumed to be stationary. This energy is then stored in a battery of capacity $b_i^{\max}$. Furthermore, we assume a normalized power consumption model, where accessing the medium consumes one unit of energy. By considering this transmission cost as the only energy-consuming action taken by the sensor nodes, we can model the battery dynamics as

$$b_i[t+1] = \left[b_i[t] - z_i[t] + e_i[t]\right]_0^{b_i^{\max}}. \tag{7.3}$$

Also, in order to ensure that the sensors do not consume more energy than they have available, the following energy causality constraint must be satisfied for all time slots

$$z_i[t] \leq b_i[t]. \tag{7.4}$$

7.2.4 Control Performance

We are interested in the design of communication policies that satisfy a required control performance criteria. Due to the nature of the communication system, we can establish

[1]This assumption holds true for many practical channel models such as Rician, Nakagami or Rayleigh fading [123].

a relationship between the sensor transmission probabilities and the control performance as stated by the following proposition.

Proposition 7.1 (Control performance abstraction [122])**.** *Consider the switched system described by* (7.1) *with* $\gamma_i[t]$ *given by a sequence of i.i.d. Bernoulli random variables, and the quadratic Lyapunov function* $V_i(\mathbf{x}_i) = \mathbf{x}_i^T \mathbf{P}_i \mathbf{x}_i$*, with* $\mathbf{P}_i$ *positive definite. Then the function* $V_i(\mathbf{x}_i)$ *decreases at an average rate* $\rho_i < 1$*, denoted by*

$$\mathbb{E}[V_i(\mathbf{x}_i[t+1])|\mathbf{x}_i[t]] \leq \rho_i V(\mathbf{x}_i[t]) + \mathrm{tr}(\mathbf{P}_i \mathbf{C}_i) \tag{7.5}$$

if and only if $\Pr(\gamma_i[t] = 1) \geq p_i$*, where* p_i *is given by*

$$p_i = \min\left\{\theta \geq 0 : \theta \mathbf{A}_{c,i}^T \mathbf{P}_i \mathbf{A}_{c,i} + (1-\theta)\mathbf{A}_{o,i}^T \mathbf{P}_i \mathbf{A}_{o,i} \leq \rho_i \mathbf{P}_i\right\} \tag{7.6}$$

Proof. By particularizing the function $V_i(\mathbf{x}_i) = \mathbf{x}_i^T \mathbf{P}_i \mathbf{x}_i$ with the system dynamics (7.1), we can write the equation

$$\begin{aligned}\mathbb{E}[V_i(\mathbf{x}_i[t+1])|\mathbf{x}_i[t]] = \mathbf{x}_i^T[t]\mathbf{A}_{c,i}^T \mathbf{P}_i \mathbf{A}_{c,i}\mathbf{x}_i[t]\Pr(\gamma_i[t]=1) \\ + \mathbf{x}_i^T[t]\mathbf{A}_{o,i}^T \mathbf{P}_i \mathbf{A}_{o,i}\mathbf{x}_i[t]\Pr(\gamma_i[t]=0) + \mathrm{tr}(\mathbf{P}_i\mathbf{C}_i).\end{aligned} \tag{7.7}$$

Then, by substituting this expression in the left hand side of the average decrease inequality (7.5) we have the following inequality

$$\begin{aligned}\mathbf{x}_i^T[t]\mathbf{A}_{c,i}^T \mathbf{P}_i \mathbf{A}_{c,i}\mathbf{x}_i[t]\Pr(\gamma_i[t]=1) \\ + \mathbf{x}_i^T[t]\mathbf{A}_{o,i}^T \mathbf{P}_i \mathbf{A}_{o,i}\mathbf{x}_i[t]\Pr(\gamma_i[t]=0) \leq \rho_i \mathbf{x}_i^T[t]\mathbf{P}_i\mathbf{x}_i[t].\end{aligned} \tag{7.8}$$

Since this condition needs to hold for all $x_i[t]$, we can equivalently rewrite this condition as the following linear matrix inequality

$$\mathbf{A}_{c,i}^T \mathbf{P}_i \mathbf{A}_{c,i}\Pr(\gamma_i[t]=1) + \mathbf{A}_{o,i}^T \mathbf{P}_i \mathbf{A}_{o,i}(1 - \Pr(\gamma_i[t]=1)) \leq \rho_i \mathbf{P}_i, \tag{7.9}$$

where we have also used the fact that $\Pr(\gamma_i[t] = 0) = (1 - \Pr(\gamma_i[t] = 1))$. Then, the $\Pr(\gamma_i[t] = 1)$ values satisfying this inequality define a convex set of which there is a minimum value p_i such that the condition is equivalent to $\Pr(\gamma_i[t] = 1) \geq p_i$. ■

7.2.5 Problem Formulation

The previous proposition allows us to relate the required control performance to the required packet success rates in the communication scheme. Our goal is then to design communication policies such that this control performance is attained, while also satisfying the energy causality constraints (7.4). Assuming an ergodic mode of operation, the control performance of the system is determined by the long term behavior of the transmission probabilities (7.2). Hence, the following ergodic limits determine the control performance

$$p_i \leq \lim_{t\to\infty} \frac{1}{t} \sum_{l=1}^{t} q_i[l] z_i[l] \prod_{j\neq i} (1 - z_j[l]) \tag{7.10}$$

Likewise, the energy causality constraints (7.4) have a long term behavior determined by the ergodic limits

$$\lim_{t\to\infty}\frac{1}{t}\sum_{l=1}^{t} z_i[l] \leq \lim_{t\to\infty}\frac{1}{t}\sum_{l=1}^{t} e_i[l] \tag{7.11}$$

where, in this case the energy causality constraints (7.4) are satisfied in an ergodic sense. Nonetheless, we will provide conditions ensuring that they are satisfied in a time slot to time slot basis. Furthermore, in order to make an efficient use of the shared medium, we aim to find policies satisfying (7.10) and (7.11) that minimize the number of times the medium is accessed. Due to the ergodic assumption on the system, we can substitute the ergodic limits in (7.10) and (7.11) for their expected value. This allows us to pose the following stochastic optimization problem

$$\begin{aligned}
\underset{z_i\in\mathcal{Z}}{\text{minimize}} \quad & \sum_{i=1}^{M}\mathbb{E}\, z_i && \text{(7.12a)}\\
\text{subject to} \quad & p_i \leq \mathbb{E}\, q_i z_i \prod_{j\neq i}\left(1-z_j\right), i=1,\dots,M && \text{(7.12b)}\\
& \mathbb{E}\, z_i \leq \mathbb{E}\, e_i \quad i=1,\dots,M && \text{(7.12c)}
\end{aligned}$$

where the expectation is taken with respect to the channel realizations $h_i[t]$ and the energy harvesting process $e_i[t]$, and $\mathcal{Z}$ is the set of all functions $\mathbb{R}^+ \to \{0,1\}$. We want that the sensors be able to solve this problem in a distributed manner. However, the optimization problem (7.12) depends on the other sensors scheduling decision by constraint (7.12b). In order to separate the problem in a per sensor basis we take the logarithm of constraint (7.12b) as follows

$$\log(p_i) \leq \log(\mathbb{E}\, q_i z_i) + \sum_{j\neq i}\log\left(1-\mathbb{E}\, z_j\right), \tag{7.13}$$

and introduce the auxiliary variables $r_i = \mathbb{E}\, q_i z_i$ and $s_i = \mathbb{E}\, z_i$. This allows us to rewrite problem (7.12) in the following equivalent form

$$\begin{aligned}
\underset{\substack{z_i\in\mathcal{Z},\\ r_i\in[0,1],\\ s_i\in[0,1]}}{\text{minimize}} \quad & \sum_{i=1}^{M}\mathbb{E}\, z_i && \text{(7.14a)}\\
\text{subject to} \quad & \log(p_i) \leq \log(r_i) + \sum_{j\neq i}\log\left(1-s_j\right), \quad i=1,\dots,M && \text{(7.14b)}\\
& r_i \leq \mathbb{E}\, q_i z_i, \quad i=1,\dots,M && \text{(7.14c)}\\
& s_i \geq \mathbb{E}\, z_i, \quad i=1,\dots,M && \text{(7.14d)}\\
& \mathbb{E}\, z_i \leq \mathbb{E}\, e_i \quad i=1,\dots,M && \text{(7.14e)}
\end{aligned}$$

where the relaxation of the auxiliary variables to an inequality is done without loss of optimality. The optimal solution of (7.14) is equivalent to the optimal solution of

(7.12). Nonetheless, another problem arises due to the fact that the sensors do not have knowledge of the distributions of h_i nor the energy harvesting process e_i (over which the expectation is taken). Nonetheless, they have access to the instantaneous values $h_i[t]$ and $e_i[t]$. Thus, by leveraging stochastic subgradient ascent on the dual domain [70], we will design an algorithm that solves problem (7.14) while satisfying constraints (7.4) for all time slots.

7.3 Stochastic Algorithm

Let us define the vector $\mathbf{z} = \{z_i, r_i, s_i\}$ collecting the primal variables and the vector $\boldsymbol{\lambda} = \{\phi_i, \nu_i, \mu_i, \beta_i\}$ collecting the dual variables. Furthermore, we collect the implicit optimization constraints in the set $\mathcal{C} = \left\{z_i \in \mathcal{Z}, r_i \in [0,1], s_i \in [0,1]\right\}$. We can write the Lagrangian of problem (7.14) as follows

$$\begin{aligned}\mathcal{L}(\mathbf{z}, \boldsymbol{\lambda}) = \sum_{i=1}^{M} \mathbb{E}\, z_i + \sum_{i=1}^{M} \phi_i \left(\log\left(p_i\right) - \log\left(r_i\right) - \sum_{j \neq i} \log\left(1 - s_j\right) \right) \\ + \sum_{i=1}^{M} \nu_i \left(r_i - \mathbb{E}\, q_i z_i\right) + \sum_{i=1}^{M} \mu_i \left(\mathbb{E}\, z_i - s_i\right) + \sum_{i=1}^{M} \beta_i \left(\mathbb{E}\, z_i - \mathbb{E}\, e_i\right)\end{aligned} \tag{7.15}$$

And the Lagrange dual function is then given by

$$g(\boldsymbol{\lambda}) = \max_{\mathbf{z} \in \mathcal{C}} \mathcal{L}(\mathbf{z}, \boldsymbol{\lambda}). \tag{7.16}$$

By approximating the expected values for the instanteneous values and reordering the Lagrangian (7.15), the values of the scheduling variables can be found as the solution to the minimization

$$z_i[t] = \underset{z_i \in \{0,1\}}{\arg\min}\, z_i \left(1 - \nu_i[t] q_i[t] + \mu_i[t] + \beta_i[t]\right). \tag{7.17}$$

Since the scheduling variable $z_i[t]$ acts linearly on the term $1 - \nu_i[t]q_i[t] + \mu_i[t] + \beta_i[t]$, the solution to this minimization problem corresponds to the simple threshold rule given by $z_i[t] = \mathbb{I}\left(\nu_i[t]q_i[t] - \mu_i[t] - \beta_i[t] \geq 1\right)$. In a similar manner, the auxiliary variables are given by the minimizations

$$r_i[t] = \underset{r_i \in [0,1]}{\arg\min} -\phi_i[t] \log(r_i) + \nu_i[t] r_i \tag{7.18}$$

$$s_i[t] = \underset{s_i \in [0,1]}{\arg\min} -\sum_{i=1}^{M} \phi_i[t] \sum_{j \neq i} \log(1 - s_j) - \sum_{i=1}^{M} \mu_i[t] s_i \tag{7.19}$$

Algorithm 7.1 Control-aware scheduling algorithm for energy harvesting sensors.

1: **Initialize:** Initialize the dual variables to $\phi_i[0] := 0$, $\nu_i[0] := 0$, $\mu_i[0] := 0$, and $\beta_i[0] := b_i^{\max} - b_i[0]$.
2: **Step 1:** The sensor decides to access the shared medium according to
3: $z_i[t] := \mathbb{I}\left(\nu_i[t]q_i[t] - \mu_i[t] - \beta_i[t] \geq 1\right)$
4: **Step 2:** The sensor computes the auxiliary variables variables
5: $r_i[t] := \left[\frac{\phi_i[t]}{\nu_i[t]}\right]_0^1$ and $s_i[t] := \left[1 - \frac{\sum_{j\neq i}\phi_i[t]}{\mu_i[t]}\right]_0^1$
6: **Step 3:** The sensor updates the dual variables
7: $\phi_i[t+1] := \left[\phi_i[t] + \log\left(p_i\right) - \log\left(r_i[t]\right) - \sum_{j\neq i}\log\left(1 - s_i[t]\right)\right]^+$
8: $\nu_i[t+1] := \left[\nu_i[t] + r_i[t] - z_i[t]q_i[t]\right]_0^{\nu_i^{\max}}$
9: $\mu_i[t+1] := \left[\mu_i[t] + z_i[t] - s_i[t]\right]^+$
10: $\beta_i[t+1] := \left[\beta_i[t] + z_i[t] - e_i[t]\right]_0^{b_i^{\max}}$
11: **Step 4:** Set $t := t+1$ and go to Step 1.

which have the following closed form solutions

$$r_i[t] = \left[\frac{\phi_i[t]}{\nu_i[t]}\right]_0^1, \qquad s_i[t] = \left[1 - \frac{\sum_{j\neq i}\phi_i[t]}{\mu_i[t]}\right]_0^1, \tag{7.20}$$

Note that the computation of the auxiliary variable $s_i[t]$ requires the dual variables $\phi_i[t]$ of the other sensors. This implies that a certain amount of communication overhead needs to occur to ensure this information exchange takes place. Following, since the dual function (7.16) is concave, we can perform a subgradient ascent on the dual domain. The updates to the dual variables are then given by

$$\phi_i[t+1] = \left[\phi_i[t] + \log\left(p_i\right) - \log\left(r_i[t]\right) - \sum_{j\neq i}\log\left(1 - s_i[t]\right)\right]^+ \tag{7.21}$$

$$\nu_i[t+1] = \left[\nu_i[t] + r_i[t] - z_i[t]q_i[t]\right]_0^{\nu_i^{\max}} \tag{7.22}$$

$$\mu_i[t+1] = \left[\mu_i[t] + z_i[t] - s_i[t]\right]^+ \tag{7.23}$$

$$\beta_i[t+1] = \left[\beta_i[t] + z_i[t] - e_i[t]\right]_0^{b_i^{\max}} \tag{7.24}$$

where for simplicity we have used an unit step size and projected the dual variables to a specific interval. Let us denote by $\nu_i^\star$ and $\beta_i^\star$ the optimal Lagrange multipliers of ν_i and β_i, respectively. Then if $\nu_i^\star \in [0, \nu_i^{\max}]$ and $\beta_i^\star \in [0, \beta_i^{\max}]$, Algorithm 7.1, which summarizes the proposed policy, stabilizes the dynamical systems.

Also, note that due to the use of a unit step size, the dual update (7.24) mimics the battery dynamics (7.3) in a mirrored way, since they can be expressed as $b_i[t] = b_i^{\max} - \beta_i[t]$. This observation leads us to the following proposition, by which we can

choose a battery capacity such that the energy causality constraints (7.4) are satisfied for all time slots.

Proposition 7.2 (Energy Causality)**.** *Let the battery capacity of the i-th sensor satisfy $b_i^{\max} \geq \nu_i^{\max} - 1$. Then Algorithm 7.1 satisfies the energy causality constraints $z_i[t] \leq b_i[t]$ for all t time slots.*

Proof. Assume the battery capacity satisfies $b_i^{\max} \geq \nu_i^{\max} - 1$. Then, to satisfy the energy causality constraints $z_i[t] \leq b_i[t]$ for all t, it suffices to certify that no transmission is scheduled when the sensor has no stored energy, i.e., $z_i[t] = 0$ when $b_i[t] = 0$. When $b_i[t] = 0$, the battery multiplier $\beta_i[t]$ takes the value $\beta_i[t] = b_i^{\max}$. And, by (7.17), we have that the sensor transmits if $\nu_i[t]q_i[t] - \mu_i[t] - \beta_i[t] \geq 1$. Hence, the sensor transmits if $\nu_i[t]q_i[t] - \mu_i[t] - b_i^{\max} \geq 1$. Furthermore, since $q_i[t] \leq 1$ and $\nu_i[t]$ is bounded by the projection to $\nu_i^{\max}$, we can certify that no transmission occurs if $\nu_i^{\max} - b_i^{\max} \leq 1$. This is ensured by the battery capacity assumption $b_i^{\max} \geq \nu_i^{\max} - 1$. ■

7.4 Numerical Results

In this section we study the performance of the proposed random access scheme with energy harvesting sensors. We consider a scalar control system, with $M = 2$ plants sharing the communication medium. The plant dynamics are given by $\mathbf{A}_{o,1} = 1.15$ and $\mathbf{A}_{c,1} = 0.1$ for the first system, and $\mathbf{A}_{o,2} = 1.05$ and $\mathbf{A}_{c,2} = 0.15$ for the second system. Hence, the first system is slightly more unstable than the second one. Further, we consider both systems to be perturbed by i.i.d. zero-mean Gaussian noise. We assume the same control performance requirement for both plants, given by the Lyapunov function $V_i(\mathbf{x}_i[t]) = \mathbf{x}_i^2$ and an expected decrease rate of $\rho_i = 0.8$. By Proposition 7.1 this translates to successful transmission probabilities of $p_1 \approx 0.3981$ and $p_2 \approx 0.2801$, respectively.

Further, we consider the sensors in both systems to be powered by an energy harvesting process of rate $e_i = 1$. The sensors store this energy in batteries of size $b_1^{\max} = 20$ and $b_2^{\max} = 10$ for the first and second sensors, respectively. Since the first system is slightly more unstable, it requires a larger battery capacity as we will see later. Furthermore, the projection of the dual variables ν_i is chosen to be $b_i^{\max} = \nu_i^{\max}$ for both systems, hence satisfying Proposition 7.2. Finally, we consider a communication system where the channel variables $h_i[t]$ are i.i.d. zero-mean Gaussian variables and the decoding probability $q(h_i[t])$ is given by the function shown in Figure 7.2.

In Figure 7.3 we plot the plant state at each time slot. As previously noted, the first system is slightly more unstable than the second system, as can be evidenced by the more pronounced peaks of instability. This instability translates to a higher variance of the energy stored in the batteries, as shown in Figure 7.4. Here, we see that the energy

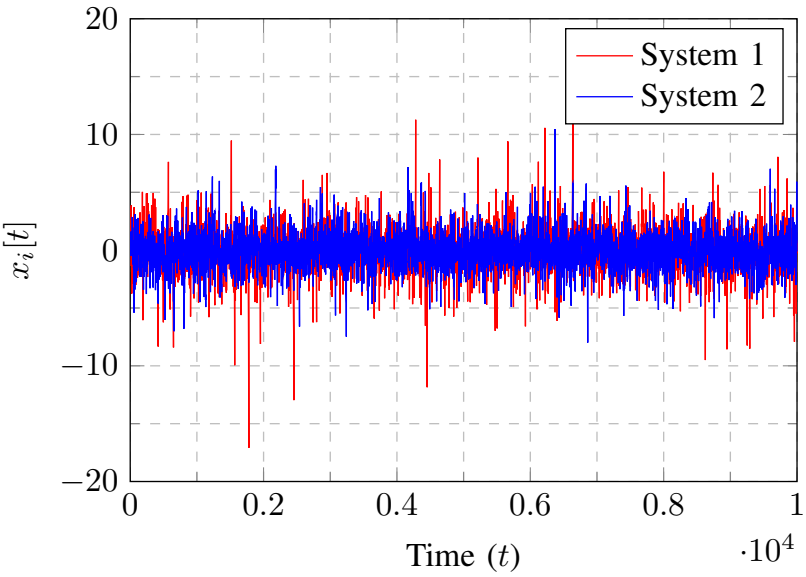

Figure 7.3: Evolution of the plant state at each time slot.

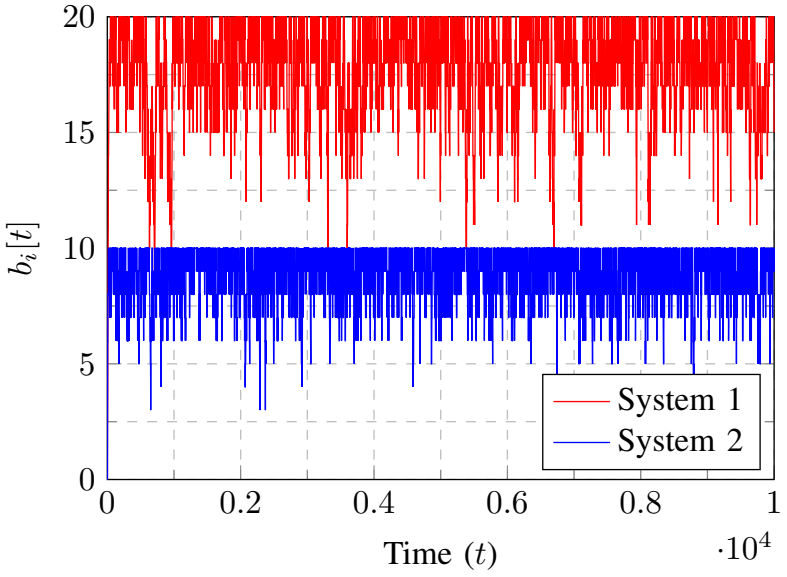

Figure 7.4: Energy stored in the batteries at each time slot.

states vary more drastically in the more unstable system. Also, the battery size chosen for the second system is smaller.

In Figure 7.5 we plot the average value $\frac{1}{t}\sum_{l=0}^{t}\nu_i[l]$ of the ν_i dual variables. The average values of the ν_i multipliers converge to the values $\nu_1^\star \approx 18.2$ and $\nu_2^\star \approx 6.5$, which by Proposition 7.2 evidences the lower battery requirements of System 2. Finally, we show in Figure 7.6 the evolution of the control system performance, where we see that both systems are asymptotically stable.

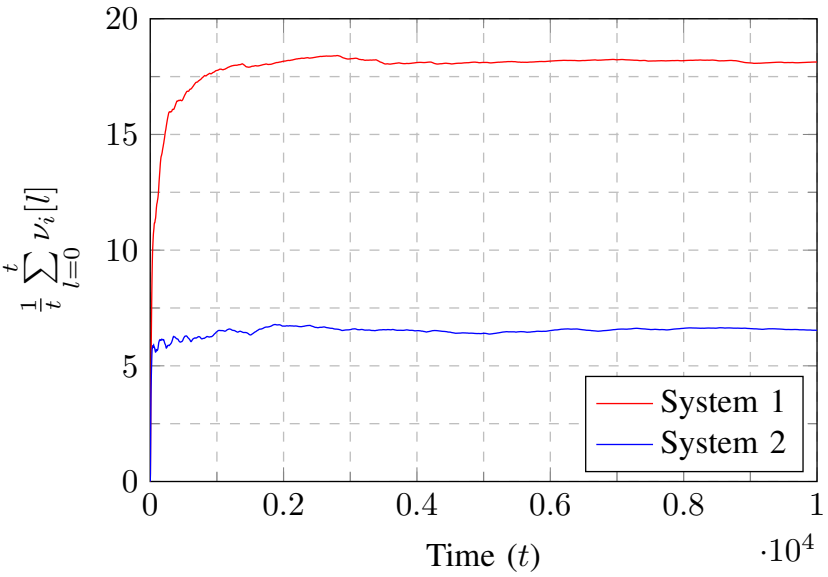

Figure 7.5: Average evolution of the dual variables $\nu_i[t]$ at each time slot.

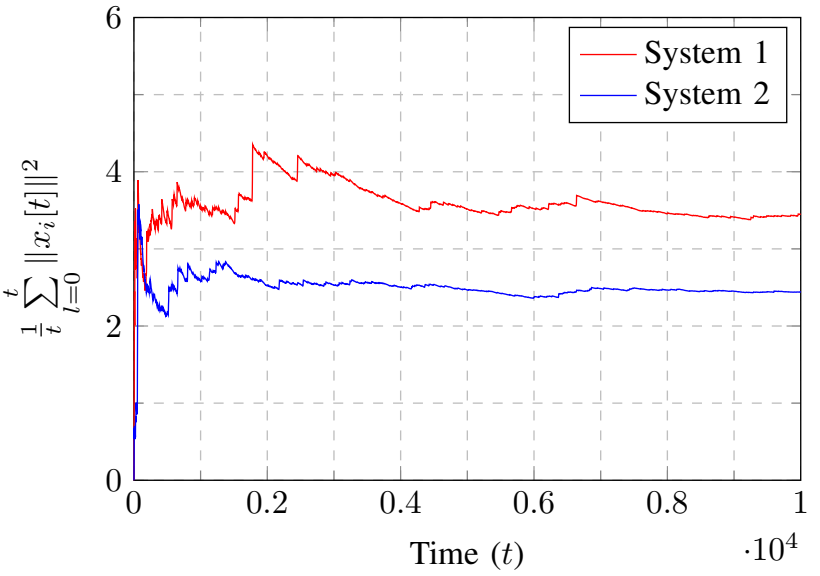

Figure 7.6: Evolution of the control system performance at each time slot.

7.5 Conclusions

In this chapter, we have provided a random access mechanism for energy harvesting sensors in wireless networked control systems. The goal has been to design communication policies such that a required control performance is attained while also satisfying the energy causality requirements imposed by the energy harvesting process. Under ergodic assumptions, we have proposed a decentralized scheduling policy and provided a stochas-

tic dual-based algorithm to compute it. Numerical results have verified the stabilizing properties of the proposed scheme.

Chapter 8

Conclusions and Future Work

8.1 Conclusions

In this thesis, we have studied some problems that arise in wireless communication networks powered by energy harvesting. More specifically, we have addressed problems related to estimation and control. With respect to former, we have studied the estimation of physical phenomena, with a single or multiple sensors. Regarding the latter, we have studied the problem of stabilizing the data queues in an EH-powered network, as well as a general wireless networked control problem. In the following, we summarize in more detail the main results of each problem studied.

In Chapter 4, we have addressed the problem of reconstruction of time-correlated sources with energy harvesting sensors. The scenario that we have considered is that of a point-to-point communication between an energy harvesting sensor and a fusion center. Furthermore, we have considered both the delay-constrained and delay-tolerant cases. For both scenarios, our goal has been the minimization of the average reconstruction distortion at the fusion center. Since the sources are correlated, we have exploited side information in our design of the transmission policies. Then, the problem has been formulated under a convex optimization framework. In order to compute the optimal solution to this problem, we have proposed an iterative subgradient method that exhibits a coupling between a two-dimensional directional waterfilling (for power allocation) and a reverse waterfilling (for rate allocation). The numerical results have illustrated the impact of source correlation in the resulting transmission policies. For the delay-constrained scenario, the results show that in order to minimize the average distortion, the earlier sources need to be encoded more accurately than the latter sources (that is, spending more energy in their transmission). Additionally, the difference in energy expenditure is also more pronounced the higher the correlation is. As expected, this is due to the fact that previous observations might be used as side information for future ones. For the delay-tolerant scenario, the results show that as the delay tolerance increases, the

optimal solution approaches the one for uncorrelated sources. Moreover, we have seen that allowing a higher delay in the reconstructions allows for an overall lower average distortion. Then, we have also compared our policy with a policy not exploiting side information, where the results show that the average distortion can be brought significantly lower when using our scheme (up to an 80% with a delay of $d = 10$ time slots). Also, we have provided a myopic online policy, which has a small performance gap (around 20%) with respect to the offline benchmark policy. Finally, we have studied how individual rates are spread over time slots. The results show that for delay-tolerant scenarios, the higher the correlation, the lower the spread of individual rates over time slots.

In Chapter 5, we have studied the sensor selection problem for energy harvesting sensors. In this way, we have extended some of the ideas of the previous chapter to the case of multiple sensor nodes. The specific scenario that we have studied consists of multiple sensors powered by energy harvesting which acquire distinct measurement from the same source. Then, these measurements need to be transmitted to a fusion center. However, due to the limited availability of wireless channels, only a limited amount of sensors are allowed to transmit at each time slot. Thus, our goal has been to design the joint selection of a subset of sensors and computing their power allocation. However, we have shown this problem to be non-convex. Instead, we have proposed two suboptimal strategies. (i) The joint sensor selection and power allocation (JSS-EH) policy, which is based on an iterative majorization-minimization procedure and has been shown to attain an stationary solution of the original non-convex problem. And (ii) a separate sensor selection and power allocation (SS-EH) policy, which is a heuristic policy that can also be used as an initialization point of the previous one. In this policy, given the selection subset, the resulting optimal power allocation has been shown to follow a directional waterfilling solution. Also as an alternative approach to the problem, we have proposed an sparsity-promoting sensor selection (SSS-EH) scheme. Numerical results have shown that the selected sensors are very similar for both the JSS-EH and SS-EH policies. However, the resulting power allocation over the sensors varies drastically between the two policies. Also, remember that for the JSS-EH policy it is needed to crop the sensor selection vector to the largest K values. We have verified that the effect of doing this procedure and not recomputing the power allocation policy has a negligible impact on the resulting distortion performance. With regard to the distortion performance, the simulations show that both policies attain the lower bound on the distortion with as low as 30% of the sensors selected in the high-SNR case and 50% in the low-SNR case. Furthermore, we have studied how the initialization point of the JSS-EH policy affects its performance. The results show that initializing this policy with the SS-EH solution improves the convergence speed as well as resulting in a lower average distortion. Finally, we have proposed a myopic online version of our proposed policies. In the case of the JSS-EH policy, the gap has been shown to be marginal. For the SS-EH

policy, the gap is higher for a lower number of selected sensors, as conservative power allocation schemes ultimately lead to unspent energy. To alleviate this, we have proposed the use of a sliding window to encourage the early consumption of energy. With regards to the sparse sensor selection policy, the numerical results have shown that by using a log-sum penalty function, the sparse solution approaches the asymptotic distortion with as few as 20% of the sensors selected.

Chapter 6 has been devoted to the problem of routing and scheduling data traffic in an energy harvesting network. In short, the problem that we have studied is that of a network composed of nodes powered by energy harvesting, where each node generates data traffic to be routed to a certain destination in the network. Then, the nodes must collaborate with each other by scheduling and routing the traffic around the network to ensure the delivery of all data packets. To this end, we have relied on stochastic subgradient methods on the dual domain. As such, the routing-scheduling policies that we have proposed act as an energy harvesting generalization of the stochastic family of the backpressure algorithm. Specifically, we have proposed two distinct policies. (i) The Stochastic Backpressure with Energy Harvesting (SBP-EH), a simple policy where the routing-scheduling decision is determined by the difference between a node and its neighbors Lagrange multipliers. And (ii) Stochastic Soft Backpressure with Energy Harvesting (SSBP-EH), a policy with improved convergence guarantees based on a randomized routing-scheduling decision. Furthermore, we have provided energy causality and queue stability guarantees for both SBP-EH and SSBP-EH. Numerical results have shown that given feasible data and energy arrival rates, both SBP-EH and SSBP-EH are capable of stabilizing the data queues in the network. Furthermore, due to its randomized nature, the SSBP-EH policy is capable of stabilizing the queues to a smaller average value. More importantly, while there is a gap between the SBP-EH policy and its non-EH benchmark, the gap between the SSBP-EH policy and its non-EH counterpart seems to vanish asymptotically. Furthermore, we have also verified by simulations that the SSBP-EH policy stabilizes the network faster than the SBP-EH policy. This also relates to the more aggressive use of the available energy in the network by the SSBP-EH policy, a fact also exposed by the numerical results. Finally, we have characterized the delay in the packet delivery of both policies. The simulations show that the more aggressive nature of the SSBP-EH policy pays off, as the average time it takes to deliver a packet to its destination is lower than for the SBP-EH policy.

Finally, in Chapter 7 we have studied networked control systems in which the sensor nodes are powered by energy harvesting. The scenario that we have considered is one of multiple control systems. The sensors of each of these control systems are powered by energy harvesting and must transmit their measurements to their respective controllers in order to satisfy a desired control performance. The sensors share the wireless medium, and therefore, collisions might occur if multiple sensors transmit simultaneously. Our goal

has been to design transmission policies that satisfy all the desired control performances while also satisfying the constraints imposed by the energy harvesting process. To do this, we have used a control performance abstraction to translate the control performance requirements to equivalent successful transmission probabilities. Then, by resorting to a dual subgradient method, we have proposed a random access communication scheme that satisfies the successful transmission probability requirements. Numerical results have shown that the proposed policy is stabilizing while also satisfying the energy harvesting constraints. Furthermore, the simulations have also shown how the battery requirements increase with the instability of the system to be controlled.

8.2 Future Work

There is a vast number of research directions in which the work of this dissertation can be extended. In this section, we provide some ideas and directions that have been identified.

- **More general estimation techniques.** We have devoted Chapters 4 and 5 to some problems of estimation. These results can be readily extended by considering more general models and estimation methods. For example, the time-correlation model used in Chapter 4, including the analysis of delay-constrained and delay-tolerant scenarios, could be incorporated to the multi-sensor problem considered in Chapter 5. In this case, due to the appearance of time-correlation, it is expected that the sensor selection policies would vary substantially when compared to the non-correlated ones. For multi-sensor settings, another extension that can be readily considered is the introduction of correlated noise over sensors. This is often the case when measuring certain physical phenomena, resulting in sensor measurements which are spatially correlated. Such consideration would make the sensor selection and power allocation problem much more challenging. Other extensions that can be considered are, for example, the generalization to non-linear measurement models and the use of more robust estimation techniques (e.g., outlier detection). Also, in a more general sense, the framework we have developed could be used for other techniques of statistical inference, for example, hypothesis testing for signal detection.

- **Actuators powered by energy harvesting.** In Chapter 7 we have considered networked control systems where sensors are powered by energy harvesting. In our scenario, however, actuators are not powered by an energy harvesting process. This scenario is common in systems where the estimation of the system state is done remotely but the actuator has access to the power grid (e.g., industrial applications where the actuator has a high power consumption). However, recent concepts like the IoT also envision large amounts of small actuators that could be powered by

energy harvesting. For such scenarios, there is the need to study how the energy harvesting process affects the design of the controller itself.

- **Joint sensing and actuation with energy harvesting.** When dealing with dynamical systems, it is desirable to deal with scenarios or problems where the principle of separation of estimation and control holds. This principle states that the optimal design of the estimator and controller can be done independently of each other. For example, this is the case of the fundamental Linear-Quadratic-Gaussian (LQG) control problem, which results in a Kalman filter as estimator and a linear-quadratic regulator as controller. However, the introduction of energy harvesting constraints in both the sensors and actuators renders both the estimation and control problems heavily coupled. This motivates the need to study these problems jointly. This is a very challenging endeavor, and the resulting problem formulations are expected to be highly non-convex. However, by making use of the currently available tools and the insight gained throughout this thesis, jointly designed policies could be developed that, while not optimal, greatly outperform their separately designed counterparts. In fact, this would fuse together much of the work done on this thesis, leading to a joint theory of estimation and control of energy harvesting networks.

Bibliography

[1] M. Calvo-Fullana, J. Matamoros, and C. Antón-Haro, "Reconstruction of correlated sources with energy harvesting constraints in delay-constrained and delay-tolerant communication scenarios," *IEEE Transactions on Wireless Communications*, vol. 16, no. 3, pp. 1974–1986, 2017.

[2] ——, "Reconstruction of correlated sources with energy harvesting constraints," in *European Wireless 2015; 21th European Wireless Conference; Proceedings of.* VDE, 2015, pp. 1–6.

[3] ——, "Sensor selection and power allocation strategies for energy harvesting wireless sensor networks," *IEEE Journal on Selected Areas in Communications*, vol. 34, no. 12, pp. 3685–3695, 2016.

[4] ——, "Decentralized sparsity-promoting sensor selection in energy harvesting wireless sensor networks," in *Signal Processing Conference (EUSIPCO), 2016 24th European.* IEEE, 2016, pp. 582–586.

[5] M. Calvo-Fullana, J. Matamoros, C. Antón-Haro, and S. M. Fosson, "Sparsity-promoting sensor selection with energy harvesting constraints," in *Acoustics, Speech and Signal Processing (ICASSP), 2016 IEEE International Conference on.* IEEE, 2016, pp. 3766–3770.

[6] M. Calvo-Fullana, J. Matamoros, and C. Antón-Haro, "Sensor selection in energy harvesting wireless sensor networks," in *Signal and Information Processing (GlobalSIP), 2015 IEEE Global Conference on.* IEEE, 2015, pp. 43–47.

[7] M. Calvo-Fullana, C. Antón-Haro, J. Matamoros, and A. Ribeiro, "Stochastic routing and scheduling policies for energy harvesting communication networks," 2017.

[8] M. Calvo-Fullana, J. Matamoros, C. Antón-Haro, and A. Ribeiro, "Stochastic backpressure in energy harvesting networks," in *Acoustics, Speech and Signal Processing (ICASSP). 2017 IEEE International Conference on*, March 2017.

[9] M. Calvo-Fullana, C. Antón-Haro, J. Matamoros, and A. Ribeiro, "Random access communication for wireless control systems with energy harvesting sensors," 2017.

[10] ——, "Random access policies for wireless networked control systems with energy harvesting sensors," in *American Control Conference (ACC)*, May 2017.

[11] J. Matamoros, M. Calvo-Fullana, and C. Antón-Haro, "On the impact of correlated sampling processes in wsns with energy-neutral operation," in *2015 IEEE International Conference on Communications (ICC)*. IEEE, 2015, pp. 258–263.

[12] J. M. Rabaey, M. J. Ammer, J. L. Da Silva, D. Patel, and S. Roundy, "Picoradio supports ad hoc ultra-low power wireless networking," *Computer*, vol. 33, no. 7, pp. 42–48, 2000.

[13] S. Roundy, D. Steingart, L. Frechette, P. Wright, and J. Rabaey, "Power sources for wireless sensor networks," *Wireless sensor networks*, pp. 1–17, 2004.

[14] E. M. Yeatman, "Advances in power sources for wireless sensor nodes," in *Proc. Int'l Workshop Wearable and Implantable Body Sensor Networks*, 2004, pp. 20–21.

[15] R. J. Vullers, R. Schaijk, H. J. Visser, J. Penders, and C. V. Hoof, "Energy harvesting for autonomous wireless sensor networks," *IEEE Solid-State Circuits Magazine*, vol. 2, no. 2, pp. 29–38, 2010.

[16] J. W. Stevens, "Optimized thermal design of small δt thermoelectric generators," SAE Technical Paper, Tech. Rep., 1999.

[17] P. Mitcheson, T. Green, E. Yeatman, and A. Holmes, "Analysis of optimized microgenerator architectures for self-powered ubiquitous computers," in *Adjunct Proc. UBICOMP 2002, 4th Int. Conf. Ubiquitous Computing*, 2002, pp. 5–6.

[18] S. Roundy, P. K. Wright, and K. S. Pister, "Micro-electrostatic vibration-to-electricity converters," in *ASME 2002 International Mechanical Engineering Congress and Exposition*. American Society of Mechanical Engineers, 2002, pp. 487–496.

[19] A. S. Holmes, G. Hong, K. R. Pullen, and K. R. Buffard, "Axial-flow microturbine with electromagnetic generator: design, cfd simulation, and prototype demonstration," in *Micro Electro Mechanical Systems, 2004. 17th IEEE International Conference on.(MEMS)*. IEEE, 2004, pp. 568–571.

[20] J. A. Paradiso and M. Feldmeier, "A compact, wireless, self-powered pushbutton controller," in *International Conference on Ubiquitous Computing*. Springer, 2001, pp. 299–304.

[21] J. A. Paradiso and T. E. Starner, "Human-generated power for mobile electronics," in *Low-power electronics design*. CRC Press, 2004, pp. 45–1.

[22] N. S. Shenck and J. A. Paradiso, "Energy scavenging with shoe-mounted piezoelectrics," *IEEE micro*, vol. 21, no. 3, pp. 30–42, 2001.

[23] J. A. Paradiso and T. Starner, "Energy scavenging for mobile and wireless electronics," *IEEE Pervasive computing*, vol. 4, no. 1, pp. 18–27, 2005.

[24] Z. Popovic, "Cut the cord: Low-power far-field wireless powering," *IEEE Microwave Magazine*, vol. 14, no. 2, pp. 55–62, 2013.

[25] L. R. Varshney, "Transporting information and energy simultaneously," in *Information Theory, 2008. ISIT 2008. IEEE International Symposium on*. IEEE, 2008, pp. 1612–1616.

[26] R. Vullers, H. Visser, B. O. het Veld, and V. Pop, "Rf harvesting using antenna structures on foil," *Proc. of PowerMEMS*, pp. 209–212, 2008.

[27] T. Ungan and L. Reindl, "Harvesting low ambient rf-sources for autonomous measurement systems," in *Instrumentation and Measurement Technology Conference Proceedings, 2008. IMTC 2008. IEEE*. IEEE, 2008, pp. 62–65.

[28] V. Leonov and P. Fiorini, "Thermal matching of a thermoelectric energy scavenger with the ambience," in *Proceedings of the European Conference on Thermoelectrics*, 2007, pp. 129–133.

[29] J. Taneja, J. Jeong, and D. Culler, "Design, modeling, and capacity planning for micro-solar power sensor networks," in *Proceedings of the 7th international conference on Information processing in sensor networks*. IEEE Computer Society, 2008, pp. 407–418.

[30] N. Sharma, J. Gummeson, D. Irwin, and P. Shenoy, "Cloudy computing: Leveraging weather forecasts in energy harvesting sensor systems," in *Sensor Mesh and Ad Hoc Communications and Networks (SECON), 2010 7th Annual IEEE Communications Society Conference on*. IEEE, 2010, pp. 1–9.

[31] A. Kansal, J. Hsu, S. Zahedi, and M. B. Srivastava, "Power management in energy harvesting sensor networks," *ACM Transactions on Embedded Computing Systems (TECS)*, vol. 6, no. 4, p. 32, 2007.

[32] M. Gorlatova, A. Wallwater, and G. Zussman, "Networking low-power energy harvesting devices: Measurements and algorithms," *IEEE Transactions on Mobile Computing*, vol. 12, no. 9, pp. 1853–1865, 2013.

[33] M. Gorlatova, J. Sarik, G. Grebla, M. Cong, I. Kymissis, and G. Zussman, "Movers and shakers: Kinetic energy harvesting for the internet of things," *IEEE Journal on Selected Areas in Communications*, vol. 33, no. 8, pp. 1624–1639, 2015.

[34] A. Seyedi and B. Sikdar, "Modeling and analysis of energy harvesting nodes in wireless sensor networks," in *Communication, Control, and Computing, 2008 46th Annual Allerton Conference on*. IEEE, 2008, pp. 67–71.

[35] C. K. Ho, P. D. Khoa, and P. C. Ming, "Markovian models for harvested energy in wireless communications," in *Communication Systems (ICCS), 2010 IEEE International Conference on*. IEEE, 2010, pp. 311–315.

[36] S. Ulukus, A. Yener, E. Erkip, O. Simeone, M. Zorzi, P. Grover, and K. Huang, "Energy harvesting wireless communications: A review of recent advances," *IEEE Journal on Selected Areas in Communications*, vol. PP, no. 99, pp. 1–1, 2015.

[37] D. Gunduz, K. Stamatiou, N. Michelusi, and M. Zorzi, "Designing intelligent energy harvesting communication systems," *IEEE Communications Magazine*, vol. 52, no. 1, pp. 210–216, 2014.

[38] O. Ozel and S. Ulukus, "Achieving awgn capacity under stochastic energy harvesting," *IEEE Transactions on Information Theory*, vol. 58, no. 10, pp. 6471–6483, 2012.

[39] R. A. Raghuvir, D. Rajan, and M. D. Srinath, "Capacity of the multiple access channel in energy harvesting wireless networks," in *Wireless Communications and Networking Conference (WCNC), 2012 IEEE*. IEEE, 2012, pp. 898–902.

[40] R. Rajesh, P. Deekshith, and V. Sharma, "Capacity of a gaussian mac with energy harvesting transmit nodes," in *Information Theory and Applications Workshop (ITA), 2012*. IEEE, 2012, pp. 338–343.

[41] O. Ozel and S. Ulukus, "Awgn channel under time-varying amplitude constraints with causal information at the transmitter," in *Signals, Systems and Computers (ASILOMAR), 2011 Conference Record of the Forty Fifth Asilomar Conference on*. IEEE, 2011, pp. 373–377.

[42] J. G. Smith, "The information capacity of amplitude-and variance-constrained sclar gaussian channels," *Information and Control*, vol. 18, no. 3, pp. 203–219, 1971.

[43] O. Ozel and S. Ulukus, "On the capacity region of the gaussian mac with batteryless energy harvesting transmitters," in *Global Communications Conference (GLOBECOM), 2012 IEEE*. IEEE, 2012, pp. 2385–2390.

[44] K. Tutuncuoglu, O. Ozel, A. Yener, and S. Ulukus, "Binary energy harvesting channel with finite energy storage," in *Information Theory Proceedings (ISIT), 2013 IEEE International Symposium on.* IEEE, 2013, pp. 1591–1595.

[45] V. Anantharam and S. Verdu, "Bits through queues," *IEEE Transactions on Information Theory*, vol. 42, no. 1, pp. 4–18, 1996.

[46] W. Mao and B. Hassibi, "On the capacity of a communication system with energy harvesting and a limited battery," in *Information Theory Proceedings (ISIT), 2013 IEEE International Symposium on.* IEEE, 2013, pp. 1789–1793.

[47] D. Shaviv, P.-M. Nguyen, and A. Özgür, "Capacity of the energy-harvesting channel with a finite battery," *IEEE Transactions on Information Theory*, vol. 62, no. 11, pp. 6436–6458, 2016.

[48] J. Yang and S. Ulukus, "Optimal packet scheduling in an energy harvesting communication system," *IEEE Transactions on Communications*, vol. 60, no. 1, pp. 220–230, 2012.

[49] K. Tutuncuoglu and A. Yener, "Optimum transmission policies for battery limited energy harvesting nodes," *IEEE Transactions on Wireless Communications*, vol. 11, no. 3, pp. 1180–1189, 2012.

[50] M. A. Zafer and E. Modiano, "A calculus approach to energy-efficient data transmission with quality-of-service constraints," *IEEE/ACM Transactions on Networking*, vol. 17, no. 3, pp. 898–911, 2009.

[51] B. Devillers and D. Gündüz, "A general framework for the optimization of energy harvesting communication systems with battery imperfections," *IEEE Journal of Communications and Networks*, vol. 14, no. 2, pp. 130–139, 2012.

[52] O. Ozel, K. Tutuncuoglu, J. Yang, S. Ulukus, and A. Yener, "Transmission with energy harvesting nodes in fading wireless channels: Optimal policies," *IEEE Journal on Selected Areas in Communications*, vol. 29, no. 8, pp. 1732–1743, 2011.

[53] O. Orhan, D. Gunduz, and E. Erkip, "Throughput maximization for an energy harvesting communication system with processing cost," in *Information Theory Workshop (ITW), 2012 IEEE.* IEEE, 2012, pp. 84–88.

[54] J. Yang, O. Ozel, and S. Ulukus, "Broadcasting with an energy harvesting rechargeable transmitter," *IEEE Transactions on Wireless Communications*, vol. 11, no. 2, pp. 571–583, 2012.

[55] O. Ozel, J. Yang, and S. Ulukus, "Optimal broadcast scheduling for an energy harvesting rechargeable transmitter with a finite capacity battery," *IEEE Transactions on Wireless Communications*, vol. 11, no. 6, pp. 2193–2203, 2012.

[56] J. Yang and S. Ulukus, "Optimal packet scheduling in a multiple access channel with energy harvesting transmitters," *Communications and Networks, Journal of*, vol. 14, no. 2, pp. 140–150, 2012.

[57] O. Kaya and S. Ulukus, "Achieving the capacity region boundary of fading cdma channels via generalized iterative waterfilling," *IEEE Transactions on Wireless Communications*, vol. 5, no. 11, 2006.

[58] Z. Wang, V. Aggarwal, and X. Wang, "Iterative dynamic water-filling for fading multiple-access channels with energy harvesting," *IEEE Journal on Selected Areas in Communications*, vol. 33, no. 3, pp. 382–395, 2015.

[59] W. Yu, W. Rhee, S. Boyd, and J. M. Cioffi, "Iterative water-filling for gaussian vector multiple-access channels," *IEEE Transactions on Information Theory*, vol. 50, no. 1, pp. 145–152, 2004.

[60] K. Tutuncuoglu and A. Yener, "Sum-rate optimal power policies for energy harvesting transmitters in an interference channel," *Journal of Communications and Networks*, vol. 14, no. 2, pp. 151–161, April 2012.

[61] D. Gündüz and B. Devillers, "Two-hop communication with energy harvesting," in *Computational Advances in Multi-Sensor Adaptive Processing (CAMSAP), 2011 4th IEEE International Workshop on*. IEEE, 2011, pp. 201–204.

[62] O. Orhan and E. Erkip, "Energy harvesting two-hop communication networks," *IEEE Journal on Selected Areas in Communications*, vol. 33, no. 12, pp. 2658–2670, 2015.

[63] N. Michelusi, K. Stamatiou, and M. Zorzi, "On optimal transmission policies for energy harvesting devices," in *Information Theory and Applications Workshop (ITA), 2012*. IEEE, 2012, pp. 249–254.

[64] ——, "Transmission policies for energy harvesting sensors with time-correlated energy supply," *IEEE Transactions on Communications*, vol. 61, no. 7, pp. 2988–3001, 2013.

[65] N. Michelusi, K. Stamatiou, L. Badia, and M. Zorzi, "Operation policies for energy harvesting devices with imperfect state-of-charge knowledge," in *Communications (ICC), 2012 IEEE International Conference on*. IEEE, 2012, pp. 5782–5787.

[66] N. Michelusi, L. Badia, R. Carli, K. Stamatiou, and M. Zorzi, "Correlated energy generation and imperfect state-of-charge knowledge in energy harvesting devices," in *Wireless Communications and Mobile Computing Conference (IWCMC), 2012 8th International*. IEEE, 2012, pp. 401–406.

[67] S. Boyd and L. Vandenberghe, *Convex Optimization*. Cambridge University Press, 2009.

[68] D. P. Bertsekas, *Nonlinear Programming*. Athena Scientific, 1999.

[69] D. R. Hunter and K. Lange, "A tutorial on mm algorithms," *The American Statistician*, vol. 58, no. 1, pp. 30–37, 2004.

[70] A. Ribeiro, "Ergodic stochastic optimization algorithms for wireless communication and networking," *IEEE Transactions on Signal Processing*, vol. 58, no. 12, pp. 6369–6386, 2010.

[71] Y. Hu and A. Ribeiro, "Optimal wireless communications with imperfect channel state information," *IEEE Transactions on Signal Processing*, vol. 61, no. 11, pp. 2751–2766, 2013.

[72] A. G. Marques, X. Wang, and G. B. Giannakis, "Dynamic resource management for cognitive radios using limited-rate feedback," *IEEE Transactions on Signal Processing*, vol. 57, no. 9, pp. 3651–3666, 2009.

[73] N. Gatsis and A. G. Marques, "A stochastic approximation approach to load shedding inpower networks," in *Acoustics, Speech and Signal Processing (ICASSP), 2014 IEEE International Conference on*. IEEE, 2014, pp. 6464–6468.

[74] S. Cui, J.-J. Xiao, A. J. Goldsmith, Z.-Q. Luo, and H. V. Poor, "Estimation diversity and energy efficiency in distributed sensing," *IEEE Transactions on Signal Processing*, vol. 55, no. 9, pp. 4683–4695, 2007.

[75] S. C. Draper and G. W. Wornell, "Side information aware coding strategies for sensor networks," *IEEE Journal on Selected Areas in Communications*, vol. 22, no. 6, pp. 966–976, 2004.

[76] A. D. Wyner and J. Ziv, "The rate-distortion function for source coding with side information at the decoder," *IEEE Transactions on Information Theory*, vol. 22, no. 1, pp. 1–10, 1976.

[77] P. Castiglione, O. Simeone, E. Erkip, and T. Zemen, "Energy management policies for energy-neutral source-channel coding," *Communications, IEEE Transactions on*, vol. 60, no. 9, pp. 2668–2678, 2012.

[78] P. Castiglione and G. Matz, "Energy-neutral source-channel coding with battery and memory size constraints," *IEEE Transactions on Communications*, vol. 62, no. 4, pp. 1373–1381, April 2014.

[79] C. Tapparello, O. Simeone, and M. Rossi, "Dynamic compression-transmission for energy-harvesting multihop networks with correlated sources," *IEEE/ACM Transactions on Networking*, vol. 22, no. 6, pp. 1729–1741, Dec 2012.

[80] O. Orhan, D. Gündüz, and E. Erkip, "Delay-constrained distortion minimization for energy harvesting transmission over a fading channel," in *IEEE International Symposium on Information Theory Proceedings (ISIT)*, Istanbul, Turkey, July 2013, pp. 1794–1798.

[81] R. Puri, A. Majumdar, P. Ishwar, and K. Ramchandran, "Distributed video coding in wireless sensor networks," *IEEE Signal Processing Magazine*, vol. 23, no. 4, pp. 94–106, 2006.

[82] P. Ishwar and K. Ramchandran, "On decoder-latency versus performance tradeoffs in differential predictive coding," in *IEEE International Conference on Image Processing (ICIP)*, Singapore, October 2004, pp. 1097–1100.

[83] N. Ma and P. Ishwar, "On delayed sequential coding of correlated sources," *IEEE Transactions on Information Theory*, vol. 57, no. 6, pp. 3763–3782, 2011.

[84] E.-H. Yang, L. Zheng, D.-K. He, and Z. Zhang, "Rate distortion theory for causal video coding: Characterization, computation algorithm, and comparison," *IEEE Transactions on Information Theory*, vol. 57, no. 8, pp. 5258–5280, 2011.

[85] T. M. Cover and J. A. Thomas, *Elements of Information Theory*. John Wiley & Sons, 2012.

[86] J. Xu and R. Zhang, "Throughput optimal policies for energy harvesting wireless transmitters with non-ideal circuit power," *IEEE Journal on Selected Areas in Communications*, vol. 32, no. 2, pp. 322–332, 2014.

[87] O. Orhan, D. Gündüz, and E. Erkip, "Optimal packet scheduling for an energy harvesting transmitter with processing cost," in *IEEE International Conference on Communications (ICC)*, Budapest, Hungary, June 2013, pp. 3110–3114.

[88] S. Cui, A. J. Goldsmith, and A. Bahai, "Energy-constrained modulation optimization," *IEEE Transactions on Wireless Communications*, vol. 4, no. 5, pp. 2349–2360, 2005.

[89] Z. Wei, X. Zhu, S. Sun, Y. Huang, L. Dong, and Y. Jiang, "Full-duplex versus half-duplex amplify-and-forward relaying: Which is more energy efficient in 60-ghz dual-hop indoor wireless systems?" *IEEE Journal on Selected Areas in Communications*, vol. 33, no. 12, pp. 2936–2947, 2015.

[90] P. Ishwar, R. Puri, K. Ramchandran, and S. S. Pradhan, "On rate-constrained distributed estimation in unreliable sensor networks," *IEEE Journal on Selected Areas in Communications*, vol. 23, no. 4, pp. 765–775, 2005.

[91] D. P. Bertsekas, A. Nedic, and A. E. Ozdaglar, *Convex analysis and optimization.* Athena Scientific, 2003.

[92] A. Schrijver, *Theory of Linear and Integer Programming.* John Wiley & Sons, 1998.

[93] H. Li, J. Xu, R. Zhang, and S. Cui, "A general utility optimization framework for energy-harvesting-based wireless communications," *IEEE Communications Magazine*, vol. 53, no. 4, pp. 79–85, 2015.

[94] S. M. Kay, *Fundamentals of Statistical Signal Processing, Volume I: Estimation Theory.* Prentice Hall, 1993.

[95] S. Joshi and S. Boyd, "Sensor selection via convex optimization," *IEEE Transactions on Signal Processing*, vol. 57, no. 2, pp. 451–462, February 2009.

[96] H. Jamali-Rad, A. Simonetto, and G. Leus, "Sparsity-aware sensor selection: Centralized and distributed algorithms," *IEEE Signal Processing Letters*, vol. 21, no. 2, pp. 217–220, February 2014.

[97] S. P. Chepuri and G. Leus, "Sparsity-promoting sensor selection for non-linear measurement models," *IEEE Transactions on Signal Processing*, vol. 63, no. 3, pp. 684–698, February 2015.

[98] S. Liu, S. P. Chepuri, M. Fardad, E. Maşazade, G. Leus, and P. K. Varshney, "Sensor selection for estimation with correlated measurement noise," *IEEE Transactions on Signal Processing*, vol. 64, no. 13, pp. 3509–3522, 2016.

[99] S. Liu, A. Vempaty, M. Fardad, E. Masazade, and P. K. Varshney, "Energy-aware sensor selection in field reconstruction," *IEEE Signal Processing Letters*, vol. 21, no. 12, pp. 1476–1480, December 2014.

[100] S. Liu, M. Fardad, P. Varshney, and E. Masazade, "Optimal periodic sensor scheduling in networks of dynamical systems," *IEEE Transactions on Signal Processing*, vol. 62, no. 12, pp. 3055–3068, June 2014.

[101] K. Lange, D. R. Hunter, and I. Yang, "Optimization transfer using surrogate objective functions," *Journal of computational and graphical statistics*, vol. 9, no. 1, pp. 1–20, 2000.

[102] O. Orhan, D. Gunduz, and E. Erkip, "Source-channel coding under energy, delay, and buffer constraints," *IEEE Transactions on Wireless Communications*, vol. 14, no. 7, pp. 3836–3849, July 2015.

[103] P. M. Narendra and K. Fukunaga, "A branch and bound algorithm for feature subset selection," *IEEE Transactions on Computers*, vol. 100, no. 9, pp. 917–922, September 1977.

[104] K. J. Arrow, L. Hurwicz, and H. Uzawa, *Studies in linear and non-linear programming*. Cambridge University Press, 1958.

[105] J. H. Bramble, J. E. Pasciak, and A. T. Vassilev, "Analysis of the inexact uzawa algorithm for saddle point problems," *SIAM Journal on Numerical Analysis*, vol. 34, no. 3, pp. 1072–1092, 1997.

[106] R. Tibshirani, "Regression shrinkage and selection via the lasso," *Journal of the Royal Statistical Society. Series B (Methodological)*, pp. 267–288, 1996.

[107] E. J. Candes, M. B. Wakin, and S. P. Boyd, "Enhancing sparsity by reweighted ℓ_1 minimization," *Journal of Fourier analysis and applications*, vol. 14, no. 5-6, pp. 877–905, 2008.

[108] H. Zou, "The adaptive lasso and its oracle properties," *Journal of the American statistical association*, vol. 101, no. 476, pp. 1418–1429, 2006.

[109] C. Tapparello, O. Simeone, and M. Rossi, "Dynamic compression-transmission for energy-harvesting multihop networks with correlated sources," *IEEE/ACM Transactions on Networking (TON)*, vol. 22, no. 6, pp. 1729–1741, 2014.

[110] L. Lin, N. B. Shroff, and R. Srikant, "Asymptotically optimal energy-aware routing for multihop wireless networks with renewable energy sources," *IEEE/ACM Transactions on networking*, vol. 15, no. 5, pp. 1021–1034, 2007.

[111] M. Gatzianas, L. Georgiadis, and L. Tassiulas, "Control of wireless networks with rechargeable batteries," *IEEE Transactions on Wireless Communications*, vol. 9, no. 2, pp. 581–593, 2010.

[112] L. Huang and M. J. Neely, "Utility optimal scheduling in energy-harvesting networks," *IEEE/ACM Transactions on Networking (TON)*, vol. 21, no. 4, pp. 1117–1130, 2013.

[113] L. Tassiulas and A. Ephremides, "Stability properties of constrained queueing systems and scheduling policies for maximum throughput in multihop radio networks," *IEEE Transactions on Automatic Control*, vol. 37, no. 12, pp. 1936–1948, 1992.

[114] R. Durrett, *Probability: theory and examples.* Cambridge university press, 2010.

[115] L. Huang and M. J. Neely, "Delay reduction via lagrange multipliers in stochastic network optimization," *IEEE Transactions on Automatic Control*, vol. 56, no. 4, pp. 842–857, 2011.

[116] A. Ribeiro, "Stochastic soft backpressure algorithms for routing and scheduling in wireless ad-hoc networks," in *Computational Advances in Multi-Sensor Adaptive Processing (CAMSAP), 2009 3rd IEEE International Workshop on.* IEEE, 2009, pp. 137–140.

[117] D. P. Bertsekas, *Convex optimization algorithms.* Athena Scientific, 2015.

[118] W. Zhang, M. S. Branicky, and S. M. Phillips, "Stability of networked control systems," *IEEE Control Systems*, vol. 21, no. 1, pp. 84–99, 2001.

[119] D. Hristu-Varsakelis, "Feedback control systems as users of a shared network: Communication sequences that guarantee stability," in *Decision and Control, 2001. Proceedings of the 40th IEEE Conference on*, vol. 4. IEEE, 2001, pp. 3631–3636.

[120] G. C. Walsh, H. Ye, and L. G. Bushnell, "Stability analysis of networked control systems," *IEEE transactions on control systems technology*, vol. 10, no. 3, pp. 438–446, 2002.

[121] K. Gatsis, M. Pajic, A. Ribeiro, and G. J. Pappas, "Opportunistic control over shared wireless channels," *IEEE Transactions on Automatic Control*, vol. 60, no. 12, pp. 3140–3155, 2015.

[122] K. Gatsis, A. Ribeiro, and G. J. Pappas, "Random access design for wireless control systems," *arXiv preprint arXiv:1605.00627*, 2016.

[123] A. Goldsmith, *Wireless communications.* Cambridge University Press, 2005.